UNIVERSITY OF TECHNOLOGY SYDNEY

Exploiting Bacterial Lifestyles for the Treatment of *Pseudomonas aeruginosa* Biofilms

Giulia Ballerin

Thesis submitted to
the University of Technology Sydney, Faculty of Science
in fulfilment of the requirements for the degree of
Doctor of Philosophy

October 2018

Certificate of Original Authorship

I, Giulia Ballerin, declare that this Thesis, submitted in fulfilment of the requirements for the award of the degree of Doctor of Philosophy, in the ithree institute/School of Life Sciences/Faculty of Science at the University of Technology Sydney.

This Thesis is wholly my own work unless otherwise referenced or acknowledged. In addition, I certify that all information sources and literature used are indicated in the Thesis.

This document has not been submitted for qualifications at any other academic institution.

Signature of Student: Production Note:
Signature removed prior to publication.

Date: 08/10/2018

Acknowledgments

My first big thank you goes to my primary supervisor Cynthia Whitchurch, who has guided me through these years to become a good scientist and increased my passion for Science. I will always be very grateful.

Thanks to my supervisor Rosalia Cavaliere who taught me all the laboratory practices, supported me through the hardest times and helped me to be a good scientist.

The experiments of Chapter 5 of this Thesis were conducted at the Woolcock Institute of Medical Research, therefore my gratitude also goes to my other supervisors Daniela Traini and Paul Young, whose both scientific and moral support meant a lot to me. A special thanks to Daniela, who believed in my abilities as a scientist immediately after completing my Master's Degree research project in 2013 and pushed me in coming back to Australia for starting my PhD. Thanks also to Roberto and Michele who helped me in designing a new tool for my project and outlining the development of the nasal formulation. It has been exciting to brainstorm ideas with you guys.

A special thanks also to Lynne Turnbull who made me love microscopy and taught me a lot about it; to Christopher Evenhuis who helped me in writing a script for analysing the large bulk of microscopy images, your patience and help are extremely appreciated. To Sarah who made my work in the 37 warm room less “baleful” with nice and interesting conversations; to James who made the coffee brakes always an interesting and fun time between intellectual and funny conversations; to all the past and present members of the Whitchurch group, Davide, Erin, Laura McC and Joyce for guiding me over the years and for your patience, encouragement and for always be there if I needed help. A massive thanks to Michael Johnson for assisting me in the Microbial Imaging Facility. To Judy, Wing, Hui Xin (YY), Sandra, Maliheh, Maree and all the amazing people of the RespiTec group at the Woolcock Institute that I met. You always made me feel welcome. In particular, to Judy, who was next to me during the hard times of my first year and gave me the strength to never give up. A big thanks to Lyn Moir, who trained me in using some of the equipment and for the laughs when calling me “the stranger”.

To my fellow students and in particular, Amelia, David, Larissa, Michele, Eby and Ibrahim. Your friendship, support and understanding over these years has meant so much to me. You always made me laugh and were present if I needed a shoulder to despair on. I hope that our friendship will last for many years.

To my whole family back home in Italy, who supported my decision of leaving home and beginning a new adventure. I will always be grateful for having such a supportive and loving family to count on. Words cannot explain my gratitude. Thank you.

I'd like to specially dedicate this Thesis to my grandfather Mario "Ciano" Berti who passed away last year and to my mum Renata, my dad Guido and my brother Simone. Your unconditional love and support over these years was everything for me. Thank you.

To my best friends Chiara dC, Chiara V, Ilaria, Silvia T. and Giovanna: I've been missing you so much and thanks for being there for me, even from the other side of the world.

And finally, Roberto, my partner in love and Science. I couldn't image being able to complete this PhD without you by my side, always ready to support me when things were difficult, to push me in never giving up in front of challenges, in listening to my brainstorm of ideas, questions and doubts and for loving me even when I was difficult to deal with. Thank you for all of this.

The course of life is like quantum entanglement:
No matter where you are,
Who you are or have become,
What you did, do and will do.
Everything will always be shared and connected
With the ones you had a strong connection.

Table of Contents

List of Figures

List of Tables

List of Equations

List of Abbreviations

°	Degree
°C	Degree Celsius
3D	Three-dimensional
5x	Five times
AIDS	Acquired immune deficiency syndrome
ALI	Air liquid interface
AM1-43	Acetoxymethyl
AMPs	Antimicrobial peptides
AMR	Antimicrobial resistance
ASM	Artificial sputum medium
ATCC	American Type Cell Culture Collection
BE	Bronchiectasis
C-1	Carbon in position 1
$CaCl_2.2H_2O$	Calcium chloride dihydrate
CaMHB	Cation-adjusted Mueller Hinton Broth
CDC	Centers for Disease Control and Prevention
$Cells/cm^2$	Cells per centimetres squared
Cells/mL	Cells per millilitre
CF	Cystic Fibrosis
CFTR	Transmembrane conductance regulator gene
CFU/mL	Colony forming units per millilitre
cm^2	Centimetres squared
CO_2	Carbon dioxide
COPD	Chronic obstructive pulmonary disease
CRS	Chronic rhinosinusitis
CWD	Cell wall deficient
Da	Dalton
d_{ae}	Aerodynamic diameter

dH_2O	Deionised water
DNA	Deoxyribonucleic acid
DTPA	Diethylenetriaminepenta acetic acid
Dv_{50}	Volume median diameter
eDNA	Extracellular deoxyribonucleic acid
EMA	European Medicines Agency
EPS	Extracellular polysaccharide
EtHD-III	Ethidium homodimer three
EtOH	Ethanol
FBS	Fetal bovine serum
FDA	Food and Drug Administration
FISH	Fluorescent *in situ* hybridisation
Flu-Na	Sodium fluorescein
Fps	Frames per second
g	Grams
g/cm^2	Grams per centimetre square
g/L	Grams per litre
g/mol	Grams per mole
h	Hour(s)
HAP	Hospital acquired pneumonia
HBSS	Hanks's balanced salt solution
HS-LBA	High salt Luria Bretani agar
HSL	Homoserine lactone
ICH	International Council for Harmonisation
KCl	Potassium chloride
KH_2PO_4	Monopotassium phosphate
kPa	Kilo Pascal
L	Litre
LBA	Luria Bretani agar
LCC	Liquid Cover Culture

LDH	Lactate dehydrogenase
LPS	Lipopolysaccharide
M	Molar
m^2	Meters squared
MBEC	Minimal biofilm eradication concentration
MEM	Minimum Essential Medium
mg	Milligrams
mg/mL	Milligram per millilitre
$MgSO_4.7H_2O$	Magnesium sulphate heptahydrate
MIC	Minimal inhibitory concentration
Min	Minute(s)
mL	Millilitre
mM	Millimolar
mm	Millimetres
Na_2HPO_4	Disodium phosphate
NaCl	Sodium chloride
NaOH	Sodium hydroxide
NH_4Cl	Ammonium chloride
nm	Nanometre
Ø	Diameter
P_{app}	Permeation coefficient
PBPs	Penicillin binding proteins
PBS	Phosphate buffered saline
PI	Propidium iodide
PNA	Pneumonia
RO	Reverse osmosis
rpm	Revolution per minute
rRNA	Ribosomal ribonucleic acid
R&D	Research and development
SEM	Standard error mean

StDev	Standard deviation
TEER	Transepithelial electrical resistance
URTIs	Upper respiratory tract infections
UV	Ultra violet
v/v	Volume per volume
VAP	Ventilator associated pneumonia
w/v	Weight per volume
WHO	World Health Organisation
β	Beta
λ	Lambda (wavelength)
μg	Microgram
μg/mL	Microgram per millilitre
μL	Microliter
μL/min	Microliters per minutes
μm	Micrometre
μM	Micromolar

Abstract

Pseudomonas aeruginosa is a Gram-negative opportunistic pathogen commonly associated with respiratory infections. *P. aeruginosa* has mechanisms of both intrinsic and adaptive resistance that render this bacterium very difficult to eradicate. The formation of biofilms, which is considered a mechanism of adaptive resistance, is the cause of refractory chronic infections of both the upper and lower respiratory tract. *P. aeruginosa* infections have now become a serious global health concern due to the variety of mechanisms of resistance to the most commonly used antibiotics. This highlights the importance of developing new antibiotics and alternative strategies to combat these infections.

It has been previously shown in the Whitchurch laboratory that *P. aeruginosa* modifies its lifestyle to survive exposure to β-lactam antibiotics. Upon exposure to this class of antibiotics, planktonic rod-shaped cells transition to a viable cell wall deficient (CWD) spherical morphotype that lack a functional cell wall and has a disrupted outer membrane. This transition can be rapidly reversed after antibiotic removal, indicating that this response may be an alternative mechanism of antibiotic tolerance that enables *P. aeruginosa* to survive exposure to β-lactam antibiotics.

The CWD morphological structure lacks the presence of the outer membrane and this can be exploited to induce cell lysis by compounds that induce pores in the cytoplasmic membrane. In fact, it has been shown that the addition of antimicrobial peptides, such as LL-37 and nisin, rapidly and efficiently kills planktonic β-lactam-induced CWD cells of *P. aeruginosa*. However, as *P. aeruginosa* infections are primarily associated with biofilms, it is essential to investigate whether the CWD morphotype can be exploited as an alternative strategy for the treatment of *P. aeruginosa* biofilms.

This Thesis therefore aims to determine whether the CWD spherical morphotype could be induced in *P. aeruginosa* biofilms by the β-lactam antibiotic meropenem and whether the addition of the antimicrobial peptide nisin could efficiently lyse these CWD cells in the biofilm. Moreover, given the need to develop novel strategies to

specifically target upper respiratory tract infections caused by *P. aeruginosa*, a combination of meropenem with nisin was formulated as a nasal spray treatment.

This Thesis demonstrates that the CWD spherical morphotype could also occur in both static and flow cell biofilms after exposure to 5x MIC meropenem. The combination treatment of meropenem with nisin showed efficacy in eradicating static biofilms and significantly decreased biofilm viability. This Thesis also demonstrates that the combination of meropenem and nisin was suitable for nasal delivery and effective in reducing the viability of biofilms when used in a nasal spray form.

Overall the results presented in this Thesis demonstrate that it is possible to exploit the transition to the CWD spherical morphotype to treat *P. aeruginosa* biofilms that form in the nasal cavity and opens a new perspective for the development of alternative strategies to defeat antibiotic-resistant bacteria.

Chapter 1

General Introduction

1 General Introduction

1.1 The respiratory system

The respiratory system is divided into two parts: the upper respiratory tract and the lower respiratory tract. The upper respiratory tract includes the nose, paranasal cavities or sinuses, pharynx and part of the oral cavity, while the lower tract includes the trachea, bronchi, bronchioles and lungs. The upper airways are implicated in filtering foreign agents that could cause infections as well as warming the air that enters in the respiratory tract (*1*). The nasal cavity has a total surface area of about 150 cm^2 and has a volume of 15 mL (*2*). It is divided into three regions: the vestibule, the respiratory region and the olfactory region. The nasal turbinates, located on the lateral walls of the nasal cavity, increase the surface area of the nasal cavity allowing more inhaled air to come in contact with the cavity walls. The turbinates are covered by a pseudostratified columnar epithelium, which is composed of various types of cells: goblet cells which produce mucus, basal cells that drive homeostasis of the normal epithelium and its regeneration after injury (*3*) and ciliated cells. Ciliated cells are equipped with motile cilia which are hair-like projections responsible for mucus transport and mucociliary clearance towards the nasopharynx (Figure 1-1). The mucus is a thin layer of fluid that covers the luminal surface and it is comprised of 95 % water, 2 % glycoproteins, albumin, immunoglobulins, lysozyme, lactoferin, 1 % inorganic salts and less than 1 % of lipids (*2*, *4*). It traps foreign particles between 2-8 µm which are then propelled towards the nasopharynx by the cilia (*1*).

The lungs are the functional units that pass oxygen into the body and carbon dioxide out of the body. The muscles work together as a pump, pushing air into and out of the lungs during breathing. During normal resting state, humans breathe 12-15 times per minute and 500 mL of air per breath is inspired and expired. The regions of the airways that are responsible for gas exchange are the respiratory bronchioles and the alveoli. The human adult lung has over 300 million alveoli with a total surface area of approximately 100 m^2 (*5*). At the inferior end of the trachea, the airway splits into left

and right branches, called bronchi, which are connected to the lungs before branching off into the secondary bronchi. These carry air into the lobes of the lung and then split into many smaller tertiary bronchi within each lobe. These tertiary bronchi split into many smaller bronchioles, which then divide into many smaller branches less than a millimetre in diameter, known as terminal bronchioles. Finally, the millions of tiny terminal bronchioles conduct air to the alveoli of the lungs. The respiratory tract is covered with an epithelium composed of varied cells along the respiratory tract. From the nose to the bronchi, pseudostratified columnar ciliated epithelial cells cover most of the epithelium. The cilia beat in one direction, moving mucus towards the throat, where it is then swallowed. Further down the bronchioles, the cells remain ciliated but more cuboidal (*6*).

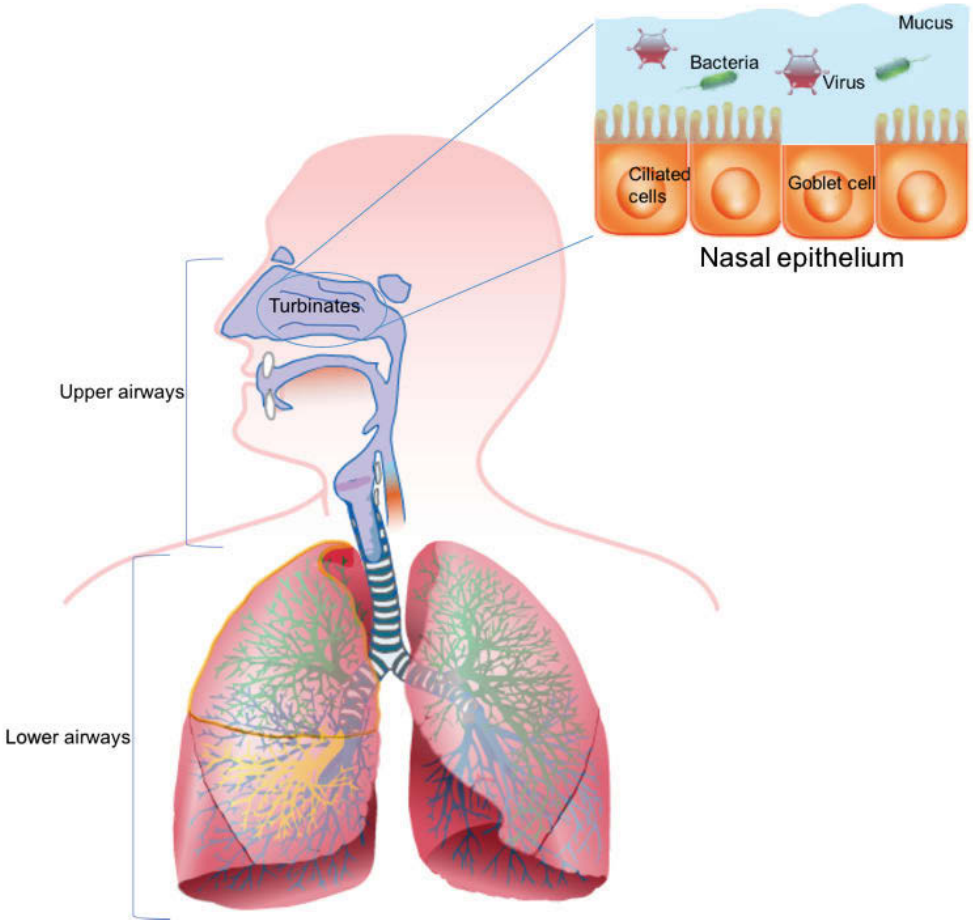

Figure 1-1: Respiratory system. The nasal epithelium is composed of ciliated cells, which transport and clear the airways of the mucus produced by the goblet cells.

In healthy conditions, specialised mechanisms of defence take place to defend the respiratory tract from pathogens. Inhaled foreign agents are cleared out by the mucociliary clearance and the immune system. However, in the case of a failure in clearing the airways from microorganisms, inflammation and infection can occur (*7*).

1.2 Biofilms in respiratory infections

Pulmonary infections and inflammation can cause significant morbidity and mortality in patients suffering from chronic pulmonary diseases, such as cystic fibrosis (CF), bronchiectasis (BE), chronic obstructive pulmonary disease (COPD), pneumonia (PNA) and chronic rhinosinusitis (CRS). These diseases are associated with similar characteristics in terms of hypersecretion and/or accumulation of mucus in the airways, causing a cycle of inflammation and infection (*8*). During this cycle, bacteria easily grow in the thick layer of mucus and start to colonise the airway, eventually leading to biofilm formation. The secretion of mucus in the airways is a normal way to defend the respiratory tract from pathogen agents and it is an important part of the innate immunity system (*9*). The mucus is a viscoelastic gel and in healthy individuals is comprised of 97 % water and 3 % of lipids, proteins, mucins, salts and cellular debris (*10*). It is formed by two layers: the upper layer is a gel film that floats above a lower layer made of more watery periciliary liquid. The gel layer traps particles that are then moved to the tips of the cilia from which they are eliminated by mucociliary clearance. In mucus hyper-secretion diseases, the production of mucus is abnormally high, producing a thicker, more tenacious and less penetrable mucus. This results in a reduced mucociliary clearance.

CF is an autosomal recessive disease caused by mutations in the CF transmembrane conductance regulator gene (CFTR). The CFTR is present not only in mucus-producing cells but also in epithelia that lack those cells, such as sweat ducts and kidney. The CTFR regulates salt transport, ion concentrations and fluid flow across the epithelia. In the specific case of mucus-secreting cells of the respiratory epithelium, the water

content, composition and volume of mucus are regulated by the secretion and absorption of ions, such as Na^+ and Cl^-. In healthy individuals, there is a normal balance of chloride ions between the inside and outside of the cell, while in CF patients the transport of Cl^- and water is altered. This gene encodes a transmembrane channel that allows the transport of chloride for mucus-producing cells. These ions have the capability to help and control the movement of water in tissues and to produce a thin layer of mucus. The abnormal production of mucus can obstruct the airways, causing severe problems with breathing and bacterial infections in the lungs (*11*). In fact, CF is characterised by an increased airways wall thickness and a decreased luminal diameter. The inability to clear pathogens from the airways induces a strong inflammatory response, which causes lung tissue damage and bacterial colonisation (*12*, *13*). *Pseudomonas aeruginosa* is the major pathogen that cause chronic infections in patients with CF. In fact, it has been demonstrated that up to 80 % of patients with CF are eventually infected with this pathogen (*14*), which leads to pulmonary exacerbation and increased morbidity (*15*).

COPD is characterised by a chronic inflammation of the pulmonary tissue. It is caused by a variety of individual risk reasons (such as enzymatic deficiencies) and environmental exposures (such as cigarette smoking). Other risk factors may include air pollution, childhood infections, heredity, advanced age, airway hyper-responsiveness and occupational exposures (*16*). COPD is a progressive disease and studies have shown that 4 to 15 % of patients presented *P. aeruginosa* isolates. The role of *P. aeruginosa* has not been clarified yet and is more likely to appear in patients who require hospitalisation, have exacerbation or require mechanical ventilation (*17*).

Bronchiectasis is an uncommon disease of the bronchi and bronchioles involving inflammation and infection cycles with dilation in one or more of the airways, in which the extra mucus promotes establishment of infection. The widened portions of the airways are damaged and inflamed. This causes extra mucus to accumulate, which is harder to clear. These portions of the airways are also softer and liable to collapse inwards which may affect airflow through the affected airways (*18*). The severity of

symptoms depends on how severely the airways are affected. Bronchiectasis can be developed from conditions that affect or damage the airways, such as: severe lung infections such as tuberculosis; deficiencies of the immune system; ciliary dyskinesia that affects the correct beat of cilia to clear the mucus and some diseases that cause inflammation in the bronchi. *P. aeruginosa* appears in the 12 to 27 % of the cases and it is associated with increased exacerbation and mortality (*19*).

Chronic rhinosinusitis is usually described as a cycle of inflammation and infection of the nose and paranasal sinuses which is ongoing for at least 12 weeks (*20*) and it has been associated with the formation of biofilms (*21–25*). *P. aeruginosa* is one of the most frequent species found in mucus and tissue samples together with *Haemophilus, Staphylococcus, Streptococcus, Citrobacter and Propionibacterium* genera (*26*).
Finding an optimal therapy for the treatment of *P. aeruginosa* in respiratory infections appears to be difficult due to the vast mechanisms of resistance that this bacterium possesses especially when it forms biofilms, where cells acquire different phenotypes and genotypes leading to an increased resistance or tolerance to antibiotics (*27*). In the last decade, researchers have found new biological targets for the development of new drugs and promising results were demonstrated *in vitro* (*28–31*). However, therapies against this bacterium still fail (*32*) and more research is needed to better understand and address a correct treatment for biofilm infections.

1.3 *Pseudomonas aeruginosa*

P. aeruginosa is a Gram-negative, rod-shaped bacterium found in soil and aquatic environments and infects many organisms including insects, animals and plants (*33*). *P. aeruginosa* is also a human opportunistic pathogen that causes nosocomial infections and is associated with infections of open wounds, burns, eyes and ears (*11*, *34–36*). It is also found in infections related with implanted medical devices and catheters as well as in immunocompromised individuals, as those suffering from cancer and AIDS. Acute and chronic infections with *P. aeruginosa* are often found in individuals with

respiratory diseases such as pneumonia, (community-acquired and ventilator-associated pneumonia), cystic fibrosis, chronic obstructive pulmonary disease, bronchiectasis and chronic rhinosinusitis. This bacterium is successful in various settings due to the production of numerous virulence factors, metabolic versatility, production of efflux pumps, production of antibiotic-degrading enzymes, low membrane permeability and its ability to grow as multi-cellular communities, known as biofilms.

1.3.1 Biofilm development

Biofilms are described as a complex community of multicellular bacteria embedded into a polymeric matrix composed of polysaccharides, proteins, peptides and extracellular DNA (eDNA). A biofilm is an adherent organised group of microorganisms with a dynamic structure that may include single or multiple microbial species, which are able to survive in hostile environments. Bacteria within a biofilm are also able to disperse and colonise other niches (*37*). Its formation is a process that involves the expression of different genes and begins with the transition of bacteria from the planktonic form to the attached form (Figure 1-2). Different steps comprise this process: conditioning, contact, adhesion, growth, production of extracellular products, attachment and eventual dispersion. During the conditioning phase, a surface exposed to an aqueous medium is covered with a conditioning film of organic molecules (e.g. macromolecules and nutrients present in aqueous environment that tend to accumulate to surfaces (*38*)) and macromolecules that alter the characteristic of the substratum (*39*). Bacteria come in contact with abiotic (inert materials) or biotic surfaces (living cells or tissues) using different mechanisms (*40*). Some bacteria adhere to the substrate through active adhesion by secreting extracellular polysaccharide (EPS) that binds the surface using physical forces, such as van der Waals forces, steric and electrostatic interactions. Other bacteria can adhere to a surface by using cellular appendages such as pili or flagella to consolidate the adhesion (*41–43*).

After bacteria have adhered to the surface, they begin to irreversibly bind onto the surface with initial weak interactions characterised by low specificity. Subsequently, bacteria consolidate their attachment by an irreversible and high specific interaction, producing exopolysaccharides, which binds materials on the surface or receptor-specific ligands (*43*). Following this, secondary colonising cells attach to the existing community and they increase biofilm volume due to replication (*44*).

A mature biofilm has a mushroom-like structure characterised by many water channels between different micro-colonies, which distribute nutrients and signalling molecules, helping the development of a resistant structure. The development of a biofilm is an important process that allows cells to resist the effect of antibiotic therapy and environmental changes (*45*). An increased synthesis of EPS, increased range of genetic exchange and the production of secondary metabolites characterise this process. The maturation of the biofilm continues even though its potential growth is limited by the availability of nutrients, the diffusion of these nutrients to the cells within the biofilm and the removal of waste (*43*).

P. aeruginosa biofilms can rapidly adapt to environmental changes due to signalling pathways, such as the Gac/Rsm cascade pathway that regulates the lifestyle and infection strategy initiation from the planktonic state to the formation of biofilms (*46*, *47*). Furthermore, the formation of biofilms allows this pathogen to grow within a host without being detected by the immune system. The different types of interactions allow biofilms to attach and grow on different surfaces, especially on medical devices and inert surfaces or tissues. In situations of depletion of nutrients or other environmental changes, bacteria can detach from the biofilm. The dispersion of a biofilm is due to sessile cells that diffuse from it and allows the colonisation of new niches and formation of a new biofilm (*48*, *49*).

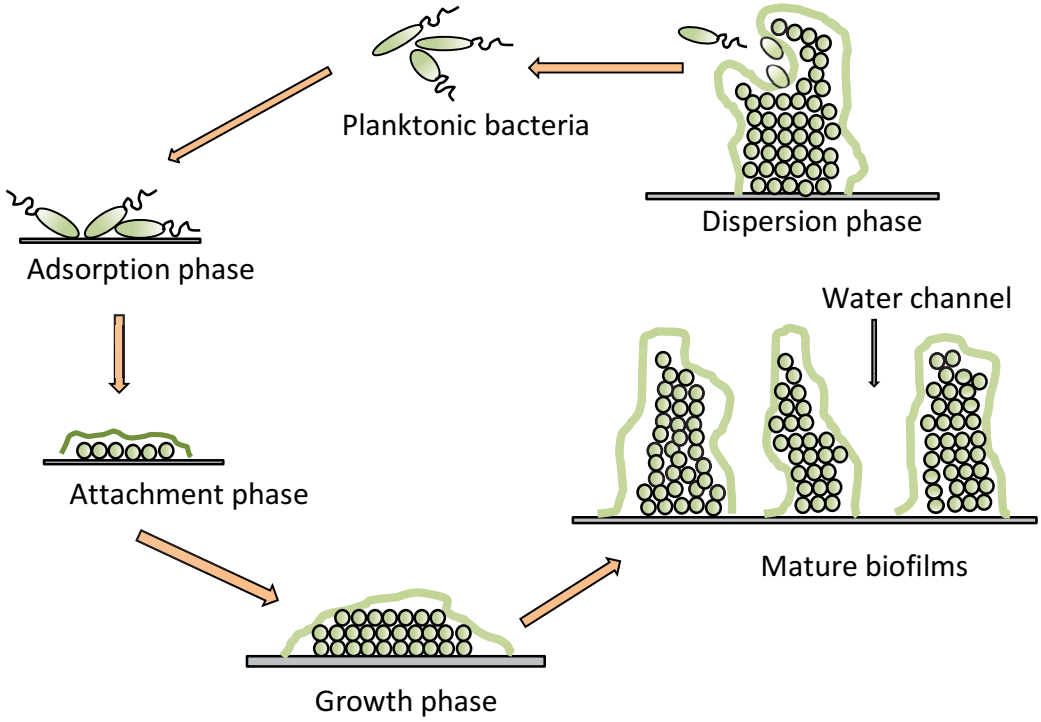

Figure 1-2: Biofilm development. Planktonic bacteria firstly come into contact with a surface to then irreversibly attach and begin to grow and develop into mature biofilms. Once the biofilm is formed, cells may disperse from the microcolonies and colonise other areas.

1.3.2 Antibiotic resistance in *P. aeruginosa* biofilms

Chronic bacterial infections are mostly caused by the formation of biofilms, which have a very high resistance against antibiotic treatments up to 1,000 times that of planktonic cells (*50*, *51*). Because of this, chronic infections are still a major problem and cause a high rate of death especially those caused by *P. aeruginosa*. In fact, in 2017, the World Health Organisation (WHO) released a list of bacteria for which new therapeutical strategies and new antibiotics are urgently needed (*52*). *P. aeruginosa* is ranked as second in the Category 1 "Critical priority" due to its high resistance to the most commonly used antibiotics, such as carbapenems.

P. aeruginosa infections are typically treated with β-lactam antibiotics such as carbapenems, cephalosporins and monobactams; aminoglycosides; quinolones and polymyxins (*53*). However, Jeukens *et al.* have demonstrated that antibiotic resistance

developed rapidly in clinical multi-drug resistant strains of *P. aeruginosa* leading to therapies failure (*54*).

Antibiotic resistance occurs when a bacterial species is no longer susceptible to the activity of antibiotics and is often due to a permanent change in the bacteria, such as a genetic transfer of resistance genes via plasmids and/or a mutation of target genes (*55*). The main mechanisms of resistance include a low permeability of the cell wall due to the presence of the outer membrane, the production of enzymes that disrupt the molecular structure of antibiotics, mutations or resistance acquired through horizontal gene transfer, the up-regulation of multi-drug efflux pumps and the alteration of the drug target (*56*).

P. aeruginosa has a variety of resistance mechanisms that can be intrinsic, acquired or adaptive. Intrinsic resistance is the ability to survive the antibiotic activity due to structural or functional features (Figure 1-3), such as the presence of the outer membrane which limits or blocks antibiotic penetration (*57*), multi-drug efflux pumps (*58*) and drug-inactivating enzymes (*59*). Acquired resistance instead arises when the bacteria express chromosomal gene mutations (*60*, *61*) or acquisition of resistance genes after exposure to antibiotics (*62*). Whereas, adaptive resistance depends on growth conditions that trigger regulatory events in the cells and susceptibility usually reverts when the inducing conditions are removed. This mechanism of resistance is becoming progressively recognised as a clinically important mechanism of resistance (*63*).

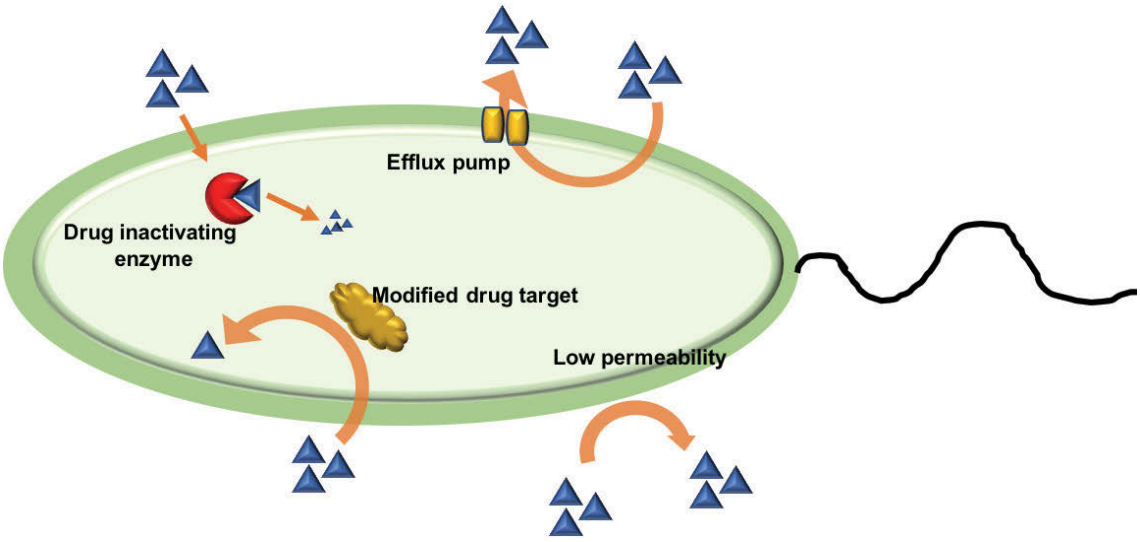

Figure 1-3: Mechanisms of resistance in planktonic *P. aeruginosa*. The presence of an outer membrane renders the cell envelope less penetrable to antibiotics; chromosomal gene mutations can modify the drug target; drugs can be inactivated by enzymes that disrupt the molecular structure or be expelled out of the cell by efflux pumps.

Antibiotic resistance in biofilms is more complex when compared to bacteria growing in the planktonic state and it is a result of intrinsic, acquired or adaptive mechanisms (Figure 1-4). This makes them up to 1,000 times more resistant or tolerant to antibiotics than planktonic cells (*64*). Biofilm cells are not physiologically identical to the planktonic cells and different mechanisms take place in order to protect them from the attack of antibiotics (*65*). In addition to the mechanisms of resistance described above, cells that form biofilms are embedded in the extracellular polymeric substance (EPS). The EPS plays a role in maintaining the integrity of the biofilm preventing desiccation and acting as a diffusion barrier (*66*). It is the major component of a biofilm, constituting about 80-85 % of the total volume and only 15-20 % is comprised of bacterial cells. EPS contributes to bacterial tolerance to antimicrobials by acting as a barrier and limiting exposure to high antimicrobial concentrations (*44*).

Moreover, the cell population of biofilms is heterogeneous meaning that distinct metabolic pathways are expressed due to various gradients of nutrients, oxygen and metabolic waste products. (*67*). Such chemical heterogeneity leads bacterial cells to

exhibit different rates of growth and metabolic activity. In fact, cells in the outer part of the biofilms are more metabolically active than those in the inner part (*68*, *69*). The cells located in the interior of the biofilm have a slow growth rate due to the depletion of nutrients. Such cells, known as persisters, have multi-drug tolerance mechanisms due to their non-growing or slow-growing state that makes them refractory to antimicrobial activity (*70*), while active growing cells do not survive when treated with a bactericidal antibiotic (*71*). Antibiotics generally target metabolically active cells and for this reason the dormant persister cells are not susceptible to such antibiotics. Their presence within a bacterial cell population is determined by environmental conditions or they can pre-exist.

Due to these wide variety of mechanisms of resistance, *P. aeruginosa* biofilms are very difficult to eradicate therefore, it is imperative to research and develop new strategies to treat such infections (*56*).

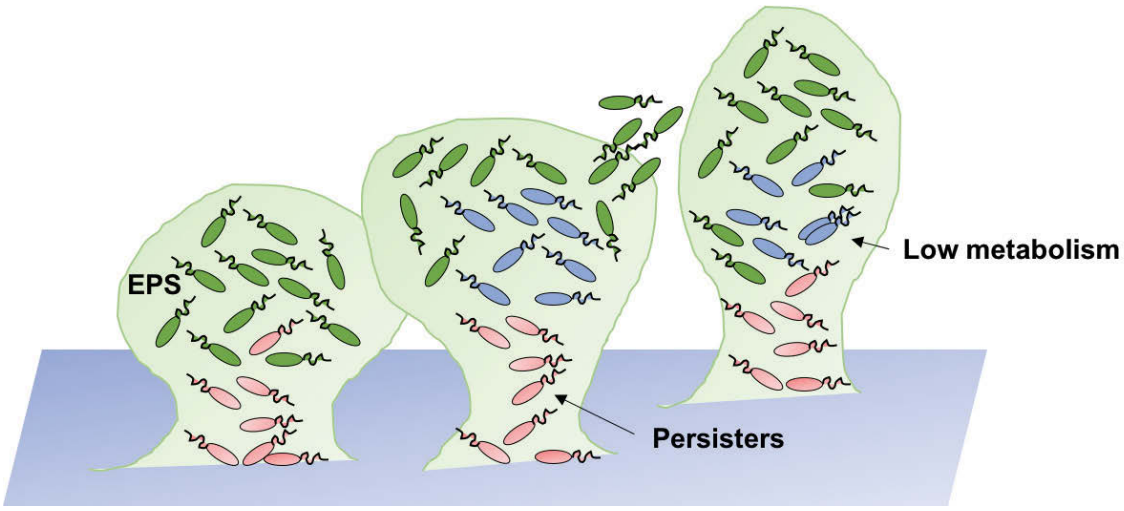

Figure 1-4: Antibiotic resistance in *P. aeruginosa* biofilms. Representation of *P. aeruginosa* microcolonies showing cells with different growth rate: normal growth (green), low metabolism (light blue) and dormant persister cells (pink). The light green shading represents the EPS.

1.3.3 *In vitro* biofilm models

In vitro models for growing and analysing biofilms have been developed to closely reflect biofilms formed in natural and clinical settings (*72*). Such models can be differentiated in closed and open systems. An example of a closed system is the use of microtiter plates, which are widely used for screening antimicrobial compounds, such as for the determination of the minimum biofilm eradication concentration (MBEC). This assay allows the determination of the minimal concentration of a compound required to eradicate biofilms. Biofilms grown using this model develop in static conditions where the environment changes during the experiment, as there is no flow into and out of the wells unless the growth medium is regularly replaced. Assays performed using this model have advantages as the use of reagents is cheap (small volumes are required) and it is possible to perform high-throughput screening assays for the identification of active compounds (*73*). Whereas the flow cell technology is an example of an open system, where biofilms grow under a continuous flow of fresh nutrients. The advantage of using this system is the analysis of biofilms without the interference of planktonic cells which are washed away by the flow. Moreover, the continuous supply of fresh nutrients by flow displaces the used media and waste products. In addition, this system allows analyses of biofilms in real-time using microscopy for the characterisation of the effect of antimicrobials and different biofilm features such as biomass, thickness, roughness coefficient and others (*74*, *75*). The flow cell system is labour intensive but it is the gold-standard method for the investigation of biofilms down to the single-cell level (*76*, *77*).

1.4 Treatment of upper respiratory tract infections

Currently, patients suffering from *P. aeruginosa* respiratory infections are treated with two-drug combination therapy such as a β-lactam with an aminoglycoside or a β-lactamase inhibitor. For example, a combination of ceftazidime/avibactam (Avycaz), a β-lactam with a β-lactamase inhibitor, was FDA-approved in 2015 and showed a good clinical response in patients with complicated intra-abdominal infections and complicated urinary tract infection. Future studies are aiming to expand the use of this drug combination also to hospitalised adults with ventilator-associated pneumonia and cystic fibrosis associated with resistant *P. aeruginosa* infection (*78*).

It has been shown that before colonising the lower respiratory tract, *P. aeruginosa* colonises the paranasal sinuses and from there it is aspirated to the lung (*79*, *80*). Antibiotics for the treatment of upper respiratory tract infections (URTIs) are administered orally or intravenously. However, systemic administration may cause side effects and the dose of the drug may not reach the target site with the adequate concentration due to its pharmacokinetic and pharmacodynamic profile. On the other hand, some inhaled antibiotics have shown good results in the treatment of CF even though there is still no evidence that this treatment is effective also for URTIs. Antimicrobial peptides (AMPs) represent an alternative strategy to treat respiratory infections and their use as inhaled antibiotics seems promising (*81*, *82*). Additional studies are required to further investigate the efficacy of inhaled antibiotics for the treatment of upper respiratory tract infections and to assess the best drug of choice, dosage, duration of treatment and device for drug administration (*83*).

1.5 β-lactam antibiotics

β-lactam antibiotics are characterised by a β-lactam ring fused to a saturated five-membered ring. Different ring molecular structures determine a range of antibiotic sub-classes (Figure 1-5). This class of antibiotics target the synthesis of the bacterial cell wall by binding to the penicillin-binding proteins (PBPs), which are essential for the synthesis of the peptidoglycan layer (*84*). Carbapenems are a sub-class of the β-lactam

group and are characterised by the fusion of the lactam ring with a double bond between C-2 and C-3 and the substitution of carbon for sulphur at C-1. The stereochemistry of the hydroxyethyl side chain is important for the antibiotic activity and is a key feature of carbapenems (*85*). This class has a broad spectrum of action, has shown resistance to hydrolysis by the majority of the β-lactamases and is widely used for the treatment of respiratory infections. However, with the emergence of antibiotic resistance, carbapenems alone are no longer effective in the treatment of chronic infections, especially those with *P. aeruginosa* colonisation (*86–89*).

Usually, *Pseudomonas* infections are treated with a combination of a β-lactam with an aminoglycoside and carbapenems are commonly administrated in combination with the polymyxin colistin or quinolones. An ongoing study conducted by Dickstein *et al.* is evaluating whether a combination therapy of meropenem with colistin is effective in treating patients suffering from ventilator associated pneumonia (VAP) and hospital acquired pneumonia (HAP) caused by multi-resistant Gram-negative bacteria, including *P. aeruginosa* (*90*). Meropenem is also administered intravenously for the treatment of critically ill patients with a dose of 1 g every 8 h (*91*) and combination therapies showed promising results (*92–94*) in treating *P. aeruginosa* infections. However, more research is needed to guarantee optimal efficacy of the treatment and avoid the development of new mechanisms of resistance (*95*, *96*).

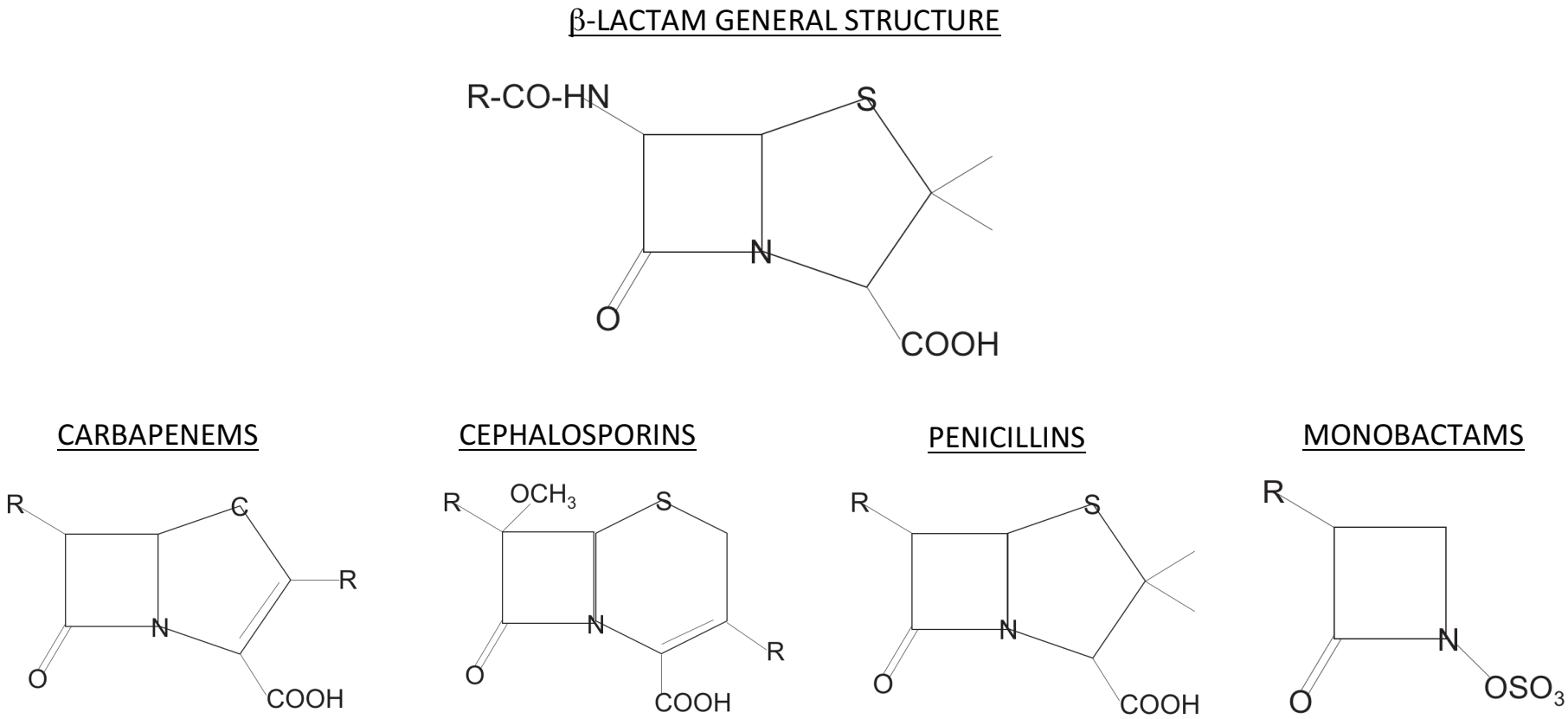

Figure 1-5: β-lactam antibiotics classification. General chemical structures for each class of β-lactam antibiotics where "R" denotes functional groups. Functional groups are specific substituents within the molecule and determine the chemical reactions of the molecule.

1.6 Antimicrobial peptides

The production of antimicrobial peptides (AMPs) is a widespread phenomenon among many forms of life, from multicellular organisms to bacterial cells. Bacteriocins are the main group of antimicrobial peptides produced by bacteria. Gram-negative bacteria, specifically *E. coli*, produce most microcins and colicins. Furthermore, Gram-positive bacteria produce lantibiotics, which contain unusual amino acids (*97*, *98*). Defensins are another type of host defence peptides produced by multicellular organisms. Unlike other antimicrobial peptides that typically form amphiphilic helices, defensins have a β-sheet structure (*99*). There are different types of antimicrobial peptides and cationic peptides have been demonstrated to be the best candidate to target bacterial membranes. Cationic peptides are all characterised by a net positive charge given by arginine and lysine residues; they are amphipathic molecules and formed from 11 to 50 amino acid residues. They have enhanced activity, working in synergy with classical antibiotics and have an anti-endotoxin activity binding to the lipopolysaccharide (LPS) compound in the bacterial membrane of Gram-negative bacteria. Cationic peptides are able to create channels in the cytoplasmic membrane of both Gram-negative and Gram-positive bacteria, via the interaction between positive and negative charges in the membrane. The channels originate from the aggregation of peptides in clusters, which disrupt the membrane integrity eventually lysing the bacterial cell (*100*). In particular, nisin, a lantibiotic peptide (class I bacteriocins, Figure 1-6) produced by certain strains of *Lactococcus lactis*, causes cell death via two mechanisms which have been well characterised (Figure 1-7); nisin binds to lipid II (*101*), a component of the cell wall biosynthesis, causing the formation of pores which lead to cell death. Nisin also interferes with the synthesis of the peptidoglycan layer by relocating lipid II into patches outside their functional location and this mechanism is independent of the pore-forming machinery (*98*). Nisin has a rare modified amino acid composition compared to other cationic peptides. It includes lanthionine, 3-methyllanthionine, dehydroalanine and dehydrobutyrine, and has an important role in food products as a preservative (*102*). In the last few years, the applications of nisin are expanding from

its use as a food preservative and studies proved its efficacy as antimicrobial agent against Gram-positive pathogens (*103*), especially when used in combination with conventional drugs such as meropenem, polymyxin E and doxycycline (*104*).

The reason why antimicrobial peptides are specifically targeting bacterial cells instead of host cells is due to the compositions of the bacterial membrane (*105*). The bacterial membrane has a large transmembrane gradient potential, high content of negatively charged lipids on the surface of the cytoplasmic membrane and a lack of cholesterol (*106*). The difference in the membrane composition of bacterial and human cells renders AMPs selective in targeting pathogenic bacteria in the human body. The selectivity and the various mode of actions of AMPs highlights their clinically positive properties and they may represent a novel way to avoid antibiotic resistance when used as a treatment (*107*).

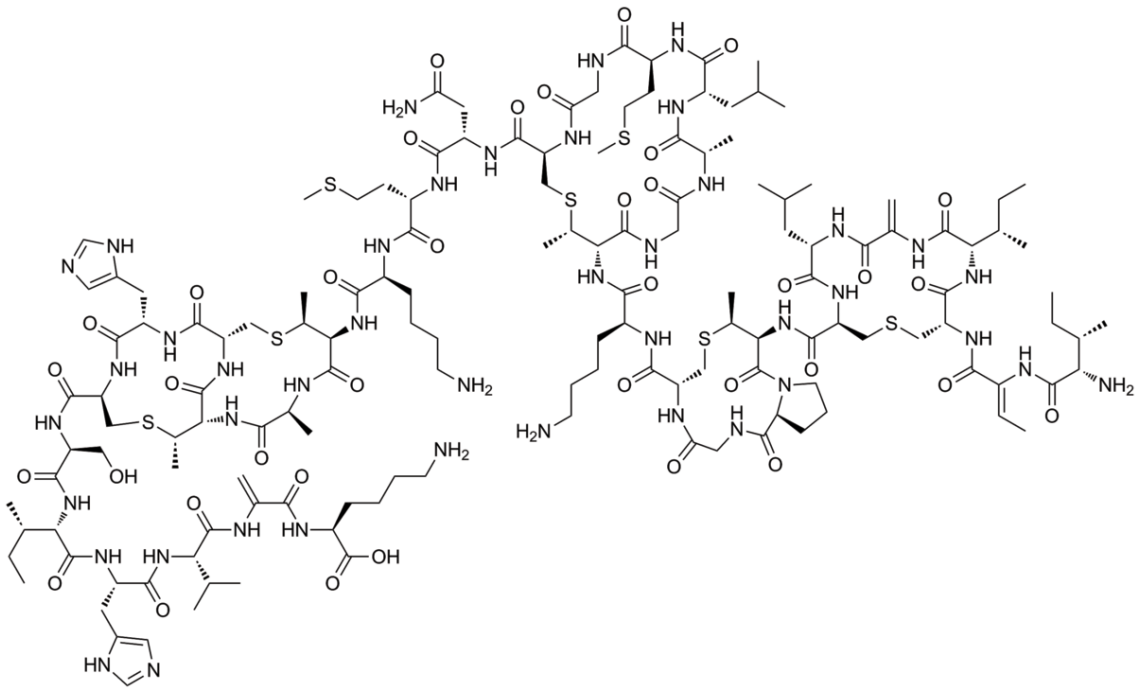

Figure 1-6: Nisin chemical structure. Nisin is a hydrophobic macromolecule with a molecular weight of 3,354 g/mol with 34 amino acid residues and it is unable to cross the outer membrane of Gram-negative bacteria (*108*).

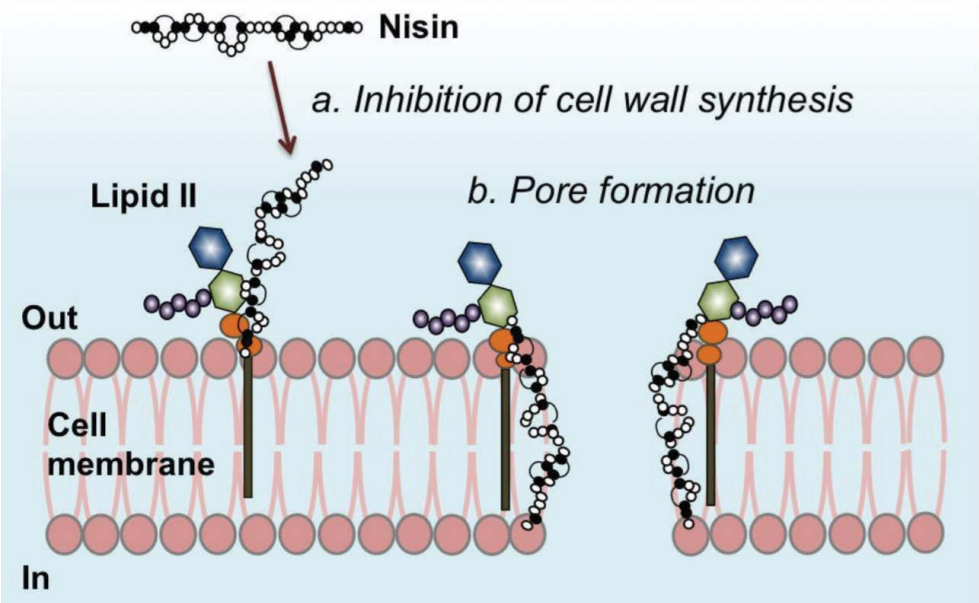

Figure 1-7: Nisin dual mode of action. A) Inhibition of cell wall synthesis via relocation of lipid II and B) pore formation via binding with lipid II (*109*).

1.7 Nasal drug delivery and absorption mechanisms

Over the past decades nasal delivery has been proven to be more advantageous for specific molecules and indications over other routes of delivery (*110*). Drugs delivered to the nose are efficiently absorbed due to the large surface area of the nose and the highly vascularised epithelium. Moreover, the drug enters the systemic circulation directly without being metabolised by the liver first. This may allow the delivery of lower doses to the site of infection. In addition, the delivery to the nose offers a quick onset of pharmacology activity, less side effects and both a local or systemic effect (*111*, *112*). Also, it is a safe and non-invasive route of administration. However, there are some limitations such as the complex geometry of the nose, low volume of liquid available for drug dissolution, impaired drug absorption due to nasal congestion and the mucociliary clearance mechanism (*113*). Nevertheless, it represents a promising and effective solution for the delivery of the vaccines, treatment of allergy, nasal congestion and infection.

The absorption of drugs takes place primarily in the respiratory region and part of the nasal septum. The absorption through the nasal mucosa can occur via two main pathways, depending on the chemical and physical properties of the drug: transcellularly and paracellularly. Lipophilic drugs are transported transcellularly by a passive diffusion process while polar drugs cross the mucosa paracellularly through the tight junctions, which are gaps between cells. The tight junctions can open and close but drugs larger than ~ 1000 Da will not be able to be transported via this pathway. The nasal absorption of lipophilic drugs can reach almost 100 % of bioavailability which is comparable to the intravenous administration (*110*, *114*). The permeability of the mucosa instead is usually low for polar drugs, large molecular weight peptides and proteins, where the bioavailability is less than 10 % (*115*). The absorption of polar drugs and peptides can be enhanced using surfactants, phospholipids, sodium salts and cyclodextrins (*116*, *117*); indeed nasal products containing absorption enhancers are already present in the market (*118*, *119*).

1.7.1 Commercial nasal technologies

Drugs for nasal delivery can be administered as liquid solutions or suspensions, dry powders and emulsions. Liquid formulations are generally aqueous solutions delivered with metered-dose spray pumps (Figure 1-8, A). These formulations usually contain a thickening agent to increase the stability of suspensions and prolong the residence of the formulation in the nasal cavity. The addition of thickening agents also increases the viscosity of the formulation leading to a reduction of the dripping out effect.

Nasal spray pumps are used for a local effect and are comprised of a container, a pump equipped with the valve and the actuator. The pumps typically deliver between 25 μL and 250 μL per spray actuation, offering high reproducibility of the dose delivered (*120*). Liquid formulations usually contain preservatives in order to avoid the growth of microorganisms although pump manufacturers have developed new spray systems that avoid the use of preservatives (*121*) and the acidification of saline-based sprays, which also supports the stability and longer shelf life of some drugs (*122*).

Drugs for local action are also delivered by pressurised metered-dose inhalers that produce aerosols due to the presence and the expansion of propellants such as hydrofluoroalkanes. Two of these products were marketed in USA to deliver corticosteroids locally (*123*, *124*). The advantages of this new type of nasal formulation are the quick evaporation of the propellant which limits the dripping effect and the high velocity of the plume emission that helps the deposition of the formulation (*125*). Dry powder dosage forms (Figure 1-8, B) convey various advantages such as high dose delivery, improved chemical stability, lack of preservatives, decreased clearance rate, improved absorption rate and enhanced residence time on the nasal mucosa (*126*, *127*). However, this form is less frequently used compared to liquid formulations due to a variety of aspects detailed in a review by Fasiolo *et al.* (*128*). A review by Djupesland (*125*) investigates a number of liquid and powder delivery devices in clinical development as well as in use on the market.

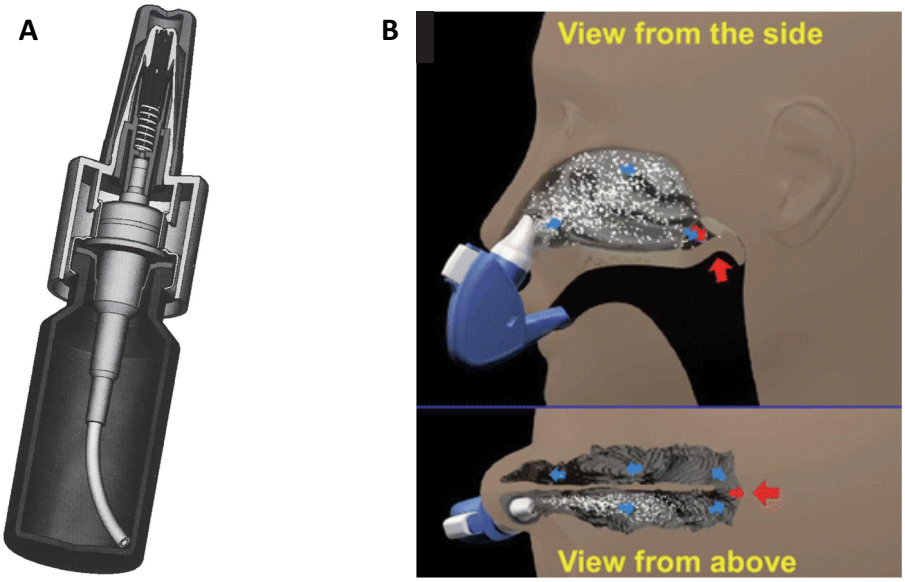

Figure 1-8: Examples of nasal devices. A) Metered-dose spray pump (preservative-free, Pfeiffer, Radolfezell, Germany) (*120*) and B) dry powder dosage device (Optinose) (*125*).

1.8 Nasal formulations characterisation

The complexity of the nasal cavity needs to be taken into consideration during the development of products for nasal delivery. The Food and Drug Administration (FDA) and the European Medicines Agency (EMA) have published guidelines listing analytical tests of physicochemical properties for assessing the quality of nasal products (*129*, *130*). However, during the development of a novel product, the deposition and the effect of drug absorption still need to be considered. In fact, several studies indicated that the *in vitro* tests suggested by the guidelines discriminated between different nasal products but such differences were not relevant when applied *in vivo* (*131–134*). This has encouraged the development of various deposition and absorption models (*135*). A number of factors need to be considered when developing a nasal formulation for ensuring optimal deposition and absorption of the drug. The main factors that influence the deposition and permeation of the formulation in the nasal cavity are: the droplet size, droplet size distribution and the spray plume characteristics. Particles above 10 μm deposit in the nasal cavity, while smaller particles may pass through the nasal cavity and deposit in the throat or lungs.

In order to understand and describe the motion of particles, it is necessary to introduce the concept of the aerodynamic diameter (d_{ae}), which is a measure of the diameter of a hypothetical spherical particle with standard density (1 g/cm^2) that settles with the same velocity as the particle of interest (*136*). The aerodynamic diameter is commonly applied to inhaled drugs or particulate pollutants to predict where they will deposit in the respiratory tract (Figure 1-9). Particles <1 μm are likely to reach the peripheral airways and alveoli or be exhaled. Particles between 1 μm and 5 μm will deposit in the large and conducting airways, while particles between 5 μm and 10 μm will predominately deposit in the oropharynx and particles above 10 μm will generally deposit in the nasal cavity (*137*).

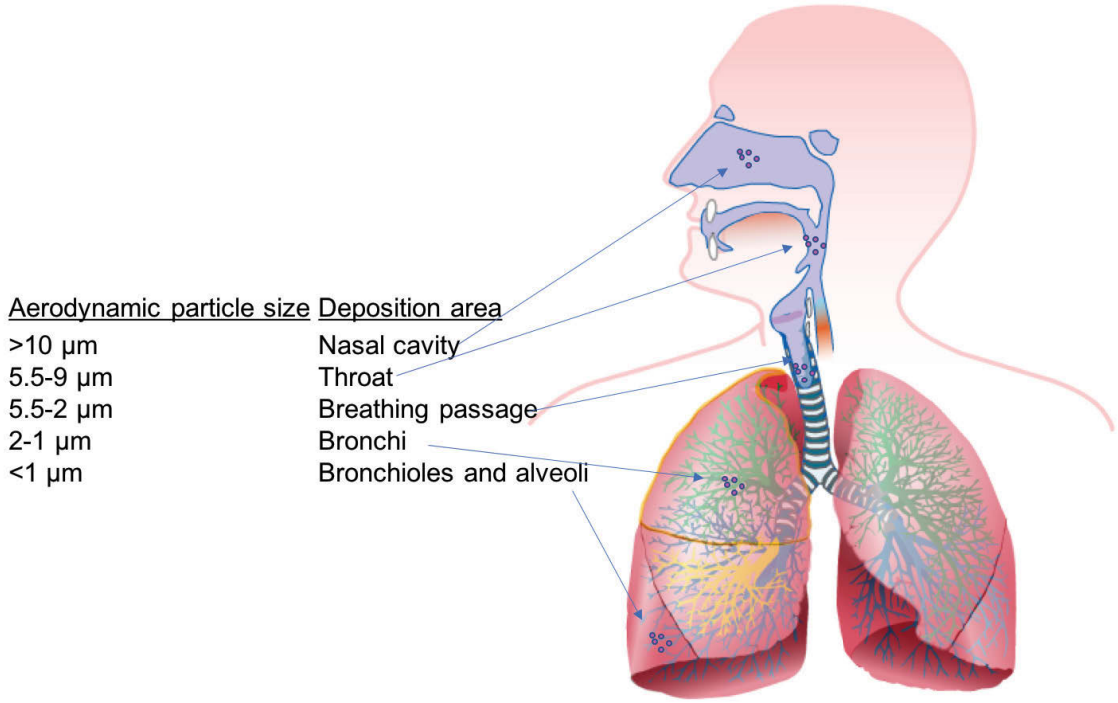

Figure 1-9: Particles deposition into the respiratory tract. Particles with an aerodynamic size between 1 µm and 10 µm will respectively deposit in the areas reported in the figure. However, there is no 1:1 linkage between particle size and deposition area as particle deposition also depends on particle density and shape, lung anatomy, presence of disease, inhalation flow rate and breath hold.

In order to simplify the measurement process of aerodynamic particles, the particle size is defined by the diameter of an equivalent sphere having the same volume as the particle in examination. Whereas the particle size distribution is characterised by the volume distribution, span and percentage less than 10 µm (% V< 10 µm). The measurement of the particle size distribution is based on the maximum particle size for a given percentage volume of the sample. The most common percentiles are the Dv_{10}, Dv_{50} and Dv_{90}. The Dv_{50} value indicates that 50 % of the mass distribution is contained in particles that are smaller than this value. Similarly, the Dv_{10} and Dv_{90} values indicate that 10 % and 90 %, respectively, of the distribution are contained in particles that are

smaller than these values. The span indicates the spread of the particle size distribution and it is calculated by using the following equation:

$$Span = \frac{Dv90 - Dv10}{Dv50}$$

Equation 1-1: Span calculation.

The percentage less than 10 µm is the cumulative volume of the particles with size less than 10 µm. This fraction provides a risk estimate of mass of particles from nasal sprays that may be inhaled into the lung (*138*).

The characterisation of the spray plume allows prediction of the deposition performance and a better understanding of the bioavailability of the drug exiting the device. The emitted plume is analysed using laser diffraction (such as the Spraytec system, Malvern) that offers the analysis of the plume development, which is comprised of three phases: formation, stable and dissipation. As per FDA guidelines, the plume is characterised during the stable phase, where a relatively constant droplet size is delivered (*139*).

1.8.1 *In vitro* models for nasal deposition

Assessment of the drug deposition is a crucial parameter to ensure optimal drug delivery to the nasal cavity. Various *in vitro* models have been developed in order to investigate how nasal formulations deposit in the nose. The two main ones are the cascade impactor equipped with an expansion chamber and the nasal casts. The cascade impactors are most commonly used to assess the deposition of drugs for delivery to the lungs but they can be equipped with an expansion chamber for investigating the deposition on the nasal cavity (Figure 1-10, A and B) (*130*, *140*). Such impactors are comprised of stages assembled in a stack or row in order of decreasing particle size and sealed with O-rings. The impactor includes a series of nozzles or jets

through which the sample laden air is drawn, directing any airborne particles towards the surface of the collection plate for that particular stage. Whether a particular particle impacts on that stage is dependent on its aerodynamic diameter. Particles having sufficient inertia will impact on that particular stage, whilst smaller particles will remain entrained in the air stream and pass to the next stage where the process is repeated.

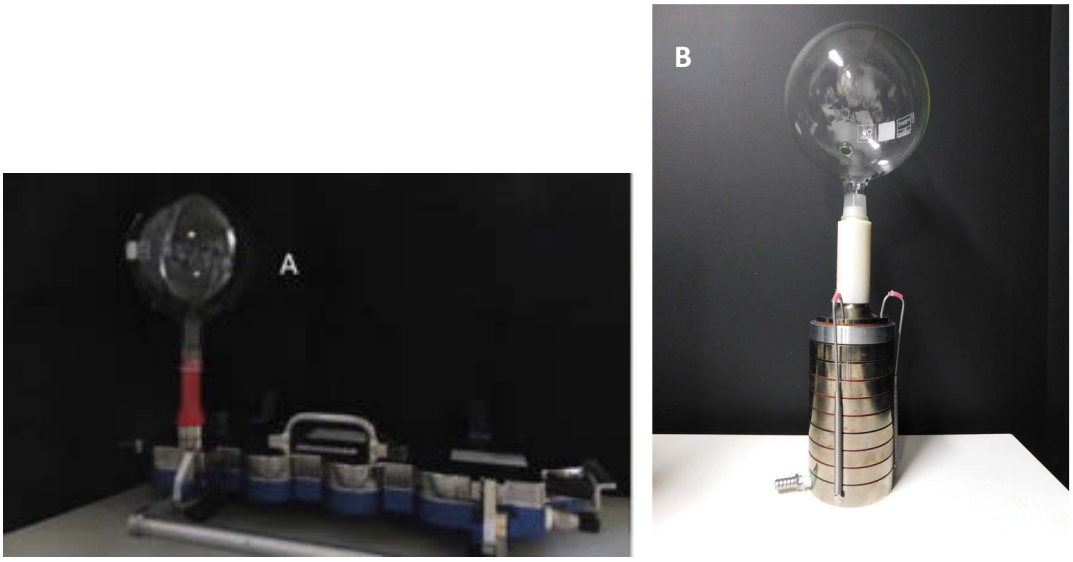

Figure 1-10: Examples of Cascade impactors equipped with 2 L expansion chamber. A) Next Generation impactor (*141*) and B) Andersen Cascade impactor.

A physically realistic representation of the nose is achieved through a nasal cast (*142–144*). Nasal geometric casts are obtained from human cadavers, like the Koken cast (Koken LM-005, Japan), which was obtained from a Japanese male cadaver. Even though this model does not represent the general population and is not anatomically correct, it is still one of the most used models as it allows imaging of the drug deposition due to its transparency.

The measurement of the nasal geometry and the production of the nasal models became more accurate with the improvement of imaging techniques such as magnetic resonance imaging and computed tomography (*145*, *146*).

1.8.2 Cell culture models for nasal drug permeation study

Primary cells or cell lines of human nasal epithelium are used to investigate the drug permeation in the nose. Primary cell models were obtained from harvesting nasal cells from the turbinates using surgery or nasal brushing and such cells were cultured as Liquid Cover Culture (LCC), where cells are seeded and subsequently covered with liquid media or as Air Liquid Interface (ALI), where the apical surface of the cells is exposed to air after seeding (*147–149*). This model represents a useful tool for *in vitro* transport studies with the advantages of production of viable cilia, mucus, tight junctions and inflammatory mediators. However, primary cell models present a number of disadvantages such as low reproducibility, expensive culture conditions and the invasive sampling procedure (*150*, *151*).

Immortalised cell lines offer another approach for studying drug permeation. These cells present advantageous aspects compared to the primary cell lines as the cost of the culturing is lower, they grow faster, they can be used for multiple passages without losing their features and there is less variability (*151*, *152*). A relatively recent cell line has been widely used in *in vitro* nasal drug permeation and transport studies. The RPMI 2650 cell line was originated from a cell carcinoma of the nasal septum (*153*) and has shown suitability as a model of the nasal mucosa. Generally, drug permeation models consist of culturing cells in ALI conditions using Transwell™ or Snapwell™ cell culture inserts and it is important to monitor that the cell layer is maintained intact. Therefore, the measurement of the transepithelial electrical resistance (TEER) is required to ensure cell layer integrity and permeability (*154*). Studies have demonstrated that RPMI 2650 cells cultured in ALI conditions were able to differentiate and form a continuous monolayer, showing also TEER values similar to those of the nasal mucosa (*141*, *155–157*). However, Reichl *et al.* have shown that culturing conditions, such as differences in cell inserts characteristics (membrane porosity and polymer) and media supplements, affected the tightness of the model (*155*). Despite this, the RPMI 2650 cell line represents a promising model for studying

drug transport and permeation and opens opportunities to further investigate and optimise it as a model of the nasal mucosa.

1.9 Exploiting bacterial lifestyles as a novel therapy for the treatment of *P. aeruginosa* infections

An additional aspect that may play a role in antibiotic resistance is the shape that the bacteria assume in the environment. Bacteria are classified into 5 groups according to their shape: coccus, coccobacillus, bacillus and vibrio, existing as single, pairs, chains or clusters (*158*). Some bacteria can assume different shapes based on the surrounding environment, moving between growth phases and life cycles, passing through a host and/or the development of specialised structures (*159*).

Some bacterial cells are able to modify their morphology upon external stressors, such as antimicrobial exposure. For example, it has been shown that rod-shaped bacteria can undergo elongation or filamentation upon inhibition or disruption of the peptidoglycan synthesis induced by antibiotic treatment (*160*, *161*). Moreover, it has been shown that Gram-positive and Gram-negative bacteria are able to switch into a cell wall-deficient form after inhibition of the peptidoglycan (PG) precursor synthesis due to the activity of cell wall synthesis-inhibiting antibiotics (*162*).

Bacteria are protected from the outside environment by the cell wall. In Gram-negative bacteria, the cell wall is formed by a thin layer of peptidoglycan that is surrounded by the outer membrane, which contains lipopolysaccharide (LPS). The outer membrane is considered to be leakier than the cytoplasmic membrane due to the presence of pore-forming proteins called porins (*163*) that allow hydrophilic solutes to diffuse and therefore might play a role in antibiotic resistance (*164*). A very important finding has been described in a study conducted in the Whitchurch laboratory by Monahan *et al.* where planktonic *P. aeruginosa* cells were treated with the carbapenems meropenem and imipenem, which are commonly used antibiotics for *P. aeruginosa* infections (*165*). They found that *P. aeruginosa* morphology changed when cells were exposed to these antibiotics at concentrations at or higher than the

minimum inhibitory concentration (MIC). A rapid change in morphology was observed just after 1 h of meropenem treatment, where the cells switched from a rod shape to a spherical morphology. The entire population of cells completed the transition after 24 h (Figure 1-11) and fluorescence microscopy determined that the majority of the spherical cells were viable (Figure 1-12). This behaviour has also been reported in previous studies and it represents a novel mechanism of tolerance against β-lactam antibiotics (*165–171*).

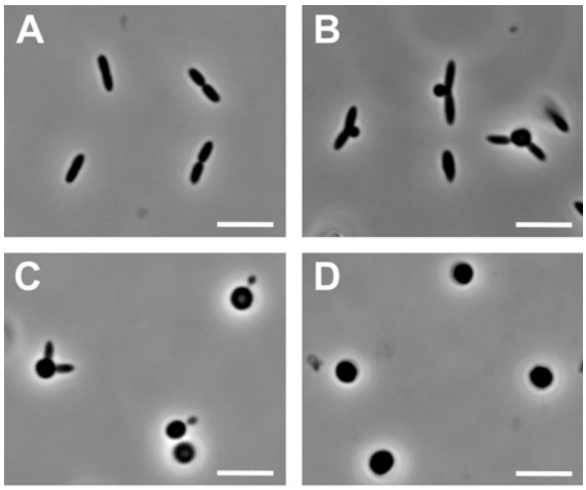

Figure 1-11: Morphological transition of planktonic *P. aeruginosa* cells. A) Prior to meropenem addition, B) 1 h, C) 4 h and D) 24 h after drug exposure. Scale bar = 5 μm. (*165*).

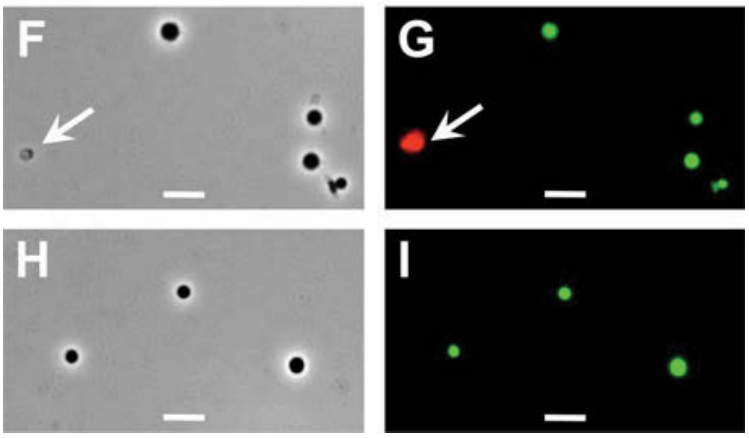

Figure 1-12: Live/Dead viability staining of meropenem-treated cells after 24 h grown in CaMHB (F and G) and in CaMHB supplemented with 0.5 M sucrose (H and I). Scale bar= 5 μm. (*165*).

Moreover, Monahan *et al.* showed that these spherical cells lack an intact cell wall, which is an important feature for the cell structure and acts as a barrier from the external environment. Therefore, these spherical cells were identified as a cell wall deficient (CWD) spherical morphotype (Figure 1-13). Also, they showed for the first time that the formation of the CWD cells was reversible after antibiotic removal and occurred under physiological conditions (Figure 1-14). They speculated that this morphological transition could lead to recurrent or prolonged infection by allowing survival over the course of β-lactam antibiotic and reversion of the bacterium shape to the rod form after antibiotic treatment termination.

Monahan *et al.* hypothesised that the altered structure of the cell membrane rendered these cells more susceptible to membrane-active agents such as antimicrobial peptides (AMPs) (Figure 1-15). They confirmed this hypothesis by treating meropenem-induced spherical cells of *P. aeruginosa* with the two AMPs, nisin and LL-37. As described in section 1.6, AMPs are able to interact directly with membrane lipids inducing cell death via the formation of pores in the cytoplasmic membrane of cells (*172*). The viability of the meropenem induced spherical cells treated with the peptides started to decrease significantly after 1 h of LL-37 treatment and 8 h of nisin treatment, whereas these AMPs alone had no effect on cell viability. In conclusion, this study has showed that carbapenems in combination with antimicrobial peptides induced a rapid and effective killing of planktonic *P. aeruginosa* cells. Therefore, this combination could be a new approach to treat *P. aeruginosa* infections.

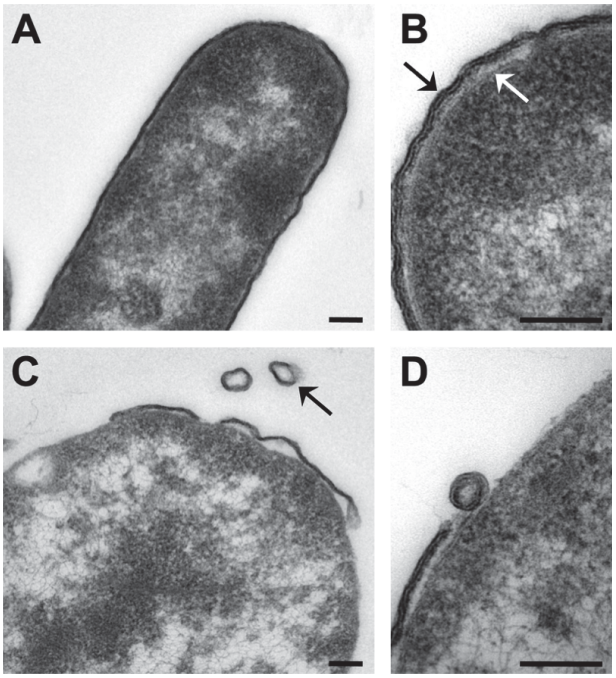

Figure 1-13: *P.* aeruginosa cell structure. Transmission electron microscopy images A) prior and C) after meropenem treatment. B and D are high magnification images to show the envelop structure of the cell. Arrows in B indicate outer membrane (black) and the inner membrane (white). Arrow in C indicates a vesicle formed from the detached outer membrane. Scale bar = 100 nm. (*165*).

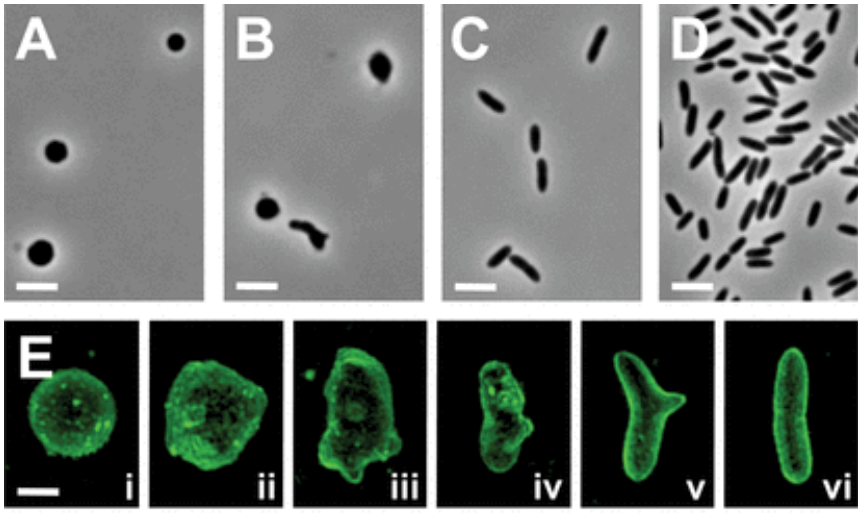

Figure 1-14: Meropenem-induced CWD cells reversion. Top panel shows phase contrast microscopy images of CWD cells reversion after A) 0 h, B) 2 h, C) 6 h and D) 24 h of antibiotic removal. E) 3D-SIM images of membrane-stained cells transitioning from i) the CWD form to vi) the normal rod shape. Scale bars, 5 μm (A through D) and 1 μm (E). (*165*).

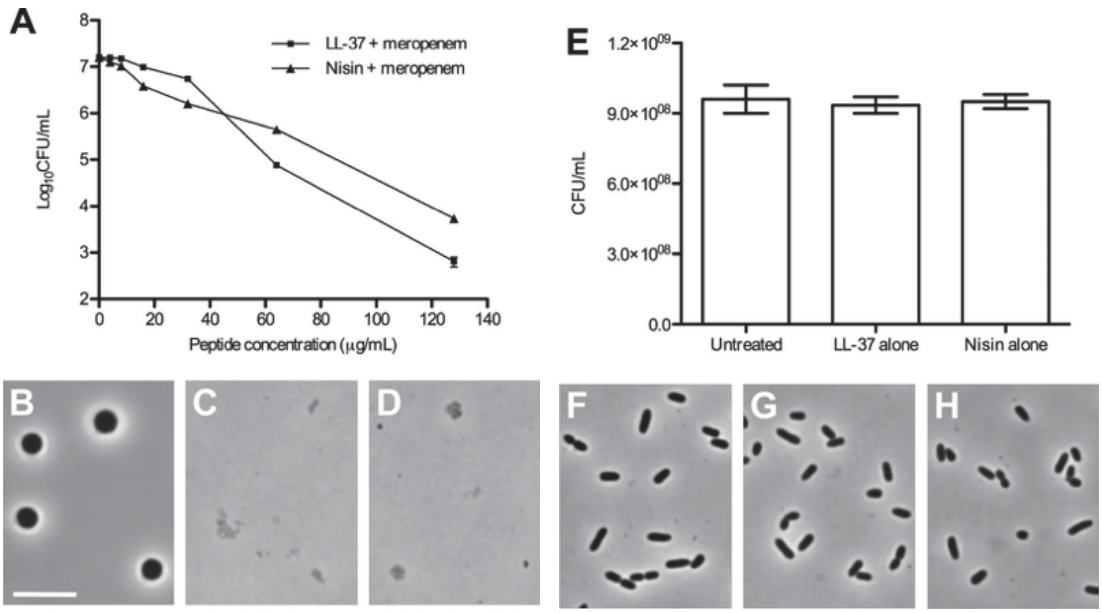

Figure 1-15: Antibiotic combination effect. A) Cell viability after combination treatments, B) meropenem-treated cells, C) meropenem+LL-37 treated cells and D) meropenem+nisin treated cells. E) Cell viability after AMPs treatment. F) Untreated cells, G) LL-37 treated cells and H) nisin treated cells. Scale bar = 5 μm. (*165*).

P. aeruginosa is not the only pathogen that has shown this behaviour as a tolerance response to β-lactam antibiotics. In fact, a study by Dörr *et al.* (*173*) has demonstrated that the bacterium *Vibrio cholerae* responded with a morphological change when exposed to a wide range of β-lactams and other antibiotics. They exposed mid- to late exponential phase cultures of *V. cholerae* to penicillin G, ampicillin, fosfomycin, D-cycloserine, cefsulodine (100 μg/mL, 20x MIC) and meropenem (10 μg/mL, 100x MIC), which are antibiotics targeting the cell wall synthesis that usually prevents *V. cholerae* proliferation. These spherical cells were also found to have a defective cell wall which had a highly susceptibility to membrane-acting agents, such as triton X-100 and polymyxin B (*173*). Furthermore, other pathogens such as *Staphylococcus aureus* (*174*), *Bacillus subtilis* (*175*) and *E. coli* (*176*) appear to tolerate the activity of β-lactams by transitioning into CWD cells and hence are also likely to be susceptible to membrane-acting agents.

1.10 Thesis aims

Bacterial infections have become a serious public health threat due to the increase in antimicrobial resistance. The Centers for Disease Control and Prevention (CDC) stated that in the United States at least 23,000 people die each year due to bacterial infections and if no measures are taken, the global deaths will increase from 700,000 to 10 million per year by 2050 (*177*). In 2017, the World Health Organisation (WHO) released a list of priority pathogens for which research and discovery of new antibiotics are needed and *P. aeruginosa* was classified as second in the Category 1 "critical priority" list (*52*).

P. aeruginosa infections are very difficult to treat due to a vast variety of mechanisms of tolerance and resistance. Previous research conducted in the Whitchurch laboratory demonstrated that planktonic *P. aeruginosa* cells survive the exposure to β-lactams, the most commonly used antibiotics, by transitioning to a CWD spherical morphotype. Also, they revealed that the CWD form reverts back to the original rod shape after antibiotic removal, indicating that this response may act as a mechanism of drug tolerance (*165*). However, bacteria are normally found as biofilms in infections and those are up to 1,000 times more resistant to antibiotics than their planktonic counterpart.

The aim of this Thesis is to investigate whether it is possible to exploit the CWD spherical morphotype to develop a novel antibiotic combination strategy for the treatment of *P. aeruginosa* respiratory infections, in particular for the eradication of biofilms in chronic rhinosinusitis. Chapter 2 details the materials and methods used to address the aims of this Thesis. Chapter 3 of this Thesis explores whether the CWD morphotype also occurs in static and flow cell biofilms after exposure to meropenem. Also, the development of a method for visualising CWD cells in clinical samples is described. Chapter 4 examines the viability of static biofilms after treatment with a range of combined concentrations of meropenem with nisin. The viability of static and flow cell biofilms is then assessed after exposure to a combination treatment of meropenem with nisin using microscopy and the colony forming unit (CFU) assay.

Furthermore, the characterisation of flow biofilm structural changes upon single and combined antibiotic treatment is explored. Chapter 5 identifies whether this combination treatment is suitable for nasal delivery via the analysis of the plume emitted by the combined formulation and demonstrates the effectiveness of the nasal spray combination on biofilms. Chapter 6 discusses the overall results of this Thesis, proposes a final conclusion and future directions in this research field.

Chapter 2

Materials and Methods

2 Materials and Methods

2.1 Materials

2.1.1 Media, buffers and antibiotic solutions

2.1.1.1 Cation-Adjusted Mueller-Hinton Broth (CaMHB)

Twenty-two g/L of cation-adjusted Mueller-Hinton broth powder (Oxoid) was dissolved in dH_2O with constant stirring and sterilised by autoclaving at 121°C and 15 kPA for 20 min (unless otherwise stated, all autoclave settings are the same as those stated here). The solution was stored at room temperature.

2.1.1.2 10x M9 salts solution

The following amount of salts was dissolved in 900 mL of $MilliQH_2O$: 32 g of Na_2HPO_4 (Amresco, Solon, USA), 27 g of KH_2PO_4 (Amresco, Solon, USA), 4.2 g of NaCl (ChemSupply, Port Adelaide, Australia) and 8.66 g of NH_4Cl (Sigma Aldrich, St. Louis, USA). The pH of the solution was adjusted to 7 with 1 M NaOH and autoclaved to sterilise. The solution was stored at room temperature.

2.1.1.3 1 M Magnesium Sulfate solution

The solution was prepared by dissolving 12.37 g of $MgSO_4.\ 7H_2O$ (Sigma-Aldrich) in 50 mL of $MilliQH_2O$ and autoclave to sterilise. The solution was stored at room temperature.

2.1.1.4 0.1 M Calcium Chloride solution

The solution was prepared by dissolving 0.735 g of $CaCl_2.\ 2H_2O$ (Mallinkrodt) in 50 mL of $MilliQH_2O$ and autoclave to sterilise. The solution was stored at room temperature.

2.1.1.5 20 % w/v D-glucose solution

Eight g of D-glucose (Sigma-Aldrich) was dissolved in 50 mL of MilliQH_2O and filter sterilised using a 0.22 µm syringe filter (Sartorius) and a 50 mL syringe. The solution was stored at room temperature.

2.1.1.6 M9 minimal media

Ninety mL of 10x M9 salts solution were diluted in 802 mL of sterile MilliQH_2O. The pH was adjusted to 7.25 and 0.9 mL of 0.1 M $CaCl_2$, 1.8 mL of 1 M $MgSO_4$ and 4.5 mL of 20 % D-glucose were added to the media after autoclaving. The media was made a day prior use and stored at 37°C.

2.1.1.7 Artificial sputum media (ASM)

The following compounds were dissolved in 1 L of dH_2O: 5 g of mucin from porcine stomach type II (Sigma), 4 g of DNA from salmon sperm (Sigma), 5.9 mg diethylenetriaminepenta acetic acid (DTPA, Sigma), 5 g NaCl (ChemSupply), 2.2 g KCl (AnalaR, Merk), 5 mL yolk egg emulsion (Oxoid) and 5 g casamino acids (Difco). The solution was filter sterilised using a vacuum sterile filter (Stericup, Merck, Millipore) and stored at 4°C.

2.1.1.8 Cell culture medium and buffers

Minimum essential medium (MEM) supplemented with non-essential amino acids solution (100x), fetal bovine serum (FBS) and L-glutamine (200 mM) were purchased from Gibco, Invitrogen (Sydney, Australia). Hanks's balanced salt solution (HBSS) was purchased from Gibco, Invitrogen (Sydney, Australia) and used for washing passages in cell work. CellLytic™ buffer and Tryptan blue solution were purchased from Sigma-Aldrich (Sydney, Australia) and used to perform cell counting.

2.1.1.9 Phosphate buffer saline

Phosphate buffer saline (PBS, Astral Scientific, Sweden) was prepared by dissolving 1 PBS tablet per 100 mL of dH_2O. The solution was sterilised by autoclaving and stored at room temperature.

2.1.1.10 0.9 % (w/v) Sodium chloride solution

Nine g of sodium chloride (NaCl, ACS reagent grade, ICN Biomedicals, Inc., Ohio) were dissolved in 1 L of RO water and stored at room temperature. The solution was sterilised by autoclaving when required or filtered for analytical analysis.

2.1.1.11 Luria-Bertani (LBA) and High Salt Luria-Bertani Agar (HS-LBA)

Luria-Bertani agar (LBA) plates were prepared by dissolving 4 g of tryptone (Oxoid), 2 g of yeast extract (Oxoid), 2 g of NaCl and 6 g of bacteriological grade agar (1.5 % w/v, Oxoid) in 400 mL of dH_2O. High Salt LBA plates were made by dissolving 4 g of tryptone (Oxoid), 2 g of yeast extract (Oxoid), 4 g of NaCl and 6.4 g of bacteriological grade agar (1.5 % w/v, Oxoid) in 400 mL of dH_2O. Twenty mL of agar was poured into Petri dishes, solidified at room temperature and stored at 4°C.

2.1.1.12 Acetic acid solution (33 % v/v)

Thirty-three % (v/v) acetic acid solution was diluted in RO water from glacial acetic acid and stored at room temperature.

2.1.1.13 Crystal violet (0.2 % v/v)

Crystal violet solution was prepared at 0.2 % (v/v) by diluting 20 mL crystal violet in 1,980 mL RO water and filter sterilised using a paper filter. The solution was stored at room temperature.

2.1.1.14 Fluorescent dyes

AM1-43 is a lipophilic styryl compound which binds to cell membranes and lipids and has an excitation/emission wavelength of 472/580 nm. One mg of AM1-43 (Jomar Life Research, Biotium) was dissolved in 1 mL of sterile MilliQH_2O and stored in aliquots at -20°C. The stock solution (1 mg/mL) was diluted in PBS to a final working concentration of 2 mM. Ethidium homodimer III (EthD-III) is a cell-impermeable DNA stain that binds to extracellular DNA and DNA of cells with compromised membranes. The stock solution (2 mM, Jomar Life Research, Biotium) was stored in aliquots at - 20 °C and diluted in PBS to a final working concentration of 4 µM.

2.1.1.15 Meropenem stock solution

Meropenem trihydrate (Hangzhou ICH Biofarm, China, CAS 119478-56-7) 5.12 mg/mL stock solution was prepared by dissolving the drug in sterile MilliQH_2O, filtered using a 0.22 µm nylon filter, aliquoted and stored at -20°C.

2.1.1.16 Nisin stock solution

Nisin from *Lactococcus lactis* (2.5 % w/w, Hangzhou ICH Biofarm, China, CAS 1414-45-5) 1 mg/mL stock solution was prepared by dissolving the drug in sterile MilliQH_2O, filtered using a 0.22 µm nylon filter, aliquoted and stored at -20°C.

2.1.1.17 FISH probes, hybridisation buffer and washing solution

The probes EUB338 (5'/5cy3/GCT GCC TCC CGT AGG AGT-3', Integrated DNA Technologies) and PsearA (5'/5cy5/GGT AAC CGT CCC CCT TGC-3', Integrated DNA Technologies), which are directed against the 16s rRNA genes, were used to perform fluorescence *in situ* hybridisation (FISH). The hybridisation buffer was prepared as follows: 180 µL of 5 M NaCl, 20 µL of 1 M Tris-HCl (pH 7.6), 2 µL of 5 % (w/v) SDS, 150 µL of 15 % formamide up to 1 mL of MilliQH_2O. The solution was then filter sterilised. FISH washing buffer was prepared by adding 840 µL of 5 M NaCl, 1 mL of 1 M Tris-HCl

(pH 7.6), 500 µL of 0.5 M EDTA (pH 7.2), 100 µL of 5 % (w/v) SDS up to 50 mL of MilliQH_2O. The solution was then filter sterilised.

2.2 Methods

2.2.1 Bacterial culture conditions

2.2.1.1 Reviving bacteria

Bacteria were revived by culturing part of the frozen glycerol stock cultures onto a LBA plate and incubating at 37°C overnight.

2.2.1.2 *P. aeruginosa* planktonic culture conditions

The bacterial strain used in this study was *Pseudomonas aeruginosa* PAO1 (ATCC 15692, infected wound) and was cultured in 2 mL of CaMHB in 14 mL round-bottom loosely capped polypropylene tubes (BD Falcon®) at 37 °C overnight in an orbital shaker at 250 rpm.

2.2.2 Minimum inhibitory concentration assay

Sensitivity of planktonic *P. aeruginosa* cells to meropenem (Hangzhou, 0.031 µg/mL to 8 µg/mL) and nisin (Hangzhou, 0.125 µg/mL to 256 µg/mL) as single compounds was assessed by determining the minimum inhibitory concentration (MIC). The MIC was determined with the microtitre broth dilution method. Briefly, the overnight cultures were diluted 1:100 in fresh CaMHB. Two-fold dilutions of 100 µL of antibiotics were setup in triplicate in a 96-well microtitre plate (Falcon, Corning Inc., USA). Five µL of diluted cells were added to each well and incubated for 24 h at 37 °C covering the plate with Aeraseal™ (Interpath Services, Australia). The MIC corresponded to the concentration in which there was no visible growth. Turbid cultures were marked as "+++ to ++++", moderate turbidity as "++", slightly turbid as "+" and no visible growth as "-".

2.2.3 Antibiotic-induced CWD spherical cells

Overnight cultures were diluted 1:100 in 2 mL of CaMHB and incubated for 2 h 37°C with shaking at 250 rpm in an orbital shaker. Logarithmic phase cultures were then diluted 1:100 in either CaMHB or ASM, treated with 5x MIC (10 µg/mL) meropenem and incubated at 37°C in static conditions overnight to induce the morphological change.

2.2.4 Effect of 8 % SDS on CWD cells

Meropenem-induced CWD cells were prepared in ASM as described in section 2.2.3. CWD cells were then fixed in 4 % paraformaldehyde overnight at 4 °C with slow rotation. Cells were then washed, re-suspended in 8 % SDS and incubated overnight at 37°C with slow rotation. Cells were then washed in PBS and 65 µL of the cell culture was placed on a microscope slide equipped with a gene frame (ThermoFisher Scientific, Australia). Cells were imaged with phase contrast microscopy (Delta Vision Elite microscope, GE Healthcare).

2.2.5 Preparation of acrylamide hydrogels with embedded cells

Hydrogel blocks were prepared by mixing 148 µL of 40 % (v/v) acrylamide: bis-acrylamide solution (BioRad), 5 µL of ammonium persulfate (APS, BioRad), 1 µL of TEMED (BioRad) to 846 µL of MilliQH_2O. Meropenem-induced CWD cells were prepared in ASM as described in section 2.2.3. Two-hundred and fifty µL of rod and CWD cells was added to 500 µL of acrylamide: bis-acrylamide solution, separately. One-hundred and twenty-five µL of rod and CWD cells was mixed in a 1.5 mL centrifuge tube and the mixture was then added to 500 µL of acrylamide: bis-acrylamide solution. Microscope slides were ethanol sterilised and two 125 µL gene frames (ThermoFisher Scientific, Australia) were attached on top of each other on the slide. One-hundred and thirty µL of the cell suspension was placed into the gene frame chamber and covered with the coverslips provided with the gene frame kit. The

hydrogels were left to harden at room temperature for 24 h. Afterward, the hydrogels were carefully removed from the gene frame chamber and clarified in 2 mL of 8 % SDS for 5 days at 37°C with slow rotation.

2.2.6 Biofilm antibiotic susceptibility assays

2.2.6.1 Minimum biofilm eradication concentration

The minimum biofilm eradication concentration (MBEC) was calculated for biofilms grown on 96-well microtitre plates. The MBEC is defined as the minimal concentration of a compound required to eradicate biofilms. The overnight cultures were diluted 1:100 in fresh CaMHB and 100 µL of the diluted culture was setup on a 96-well microtitre plate. Plates were covered with Aeraseal (Interpath Services, Australia) and biofilms were grown for 24 h at 37 °C in static conditions. The established biofilms were then treated with 150 µL of meropenem (2.5 µg/mL to 20 µg/mL) and nisin (0.125 µg/mL to 256 µg/mL) as single compounds and in combination for 24 h at 37 °C in static conditions. After the treatments, plates were washed three times with PBS using the plate washer (BioTek ELx405) and stained with crystal violet (0.2 % w/v) for 1 h at room temperature on an orbital shaker. The crystal violet was extracted using 33 % (v/v) acetic acid at room temperature for 30 min on an orbital shaker. The absorbance was measured at 600 nm using a plate reader (BioTek) and the value was used as relative biofilm biomass.

2.2.6.2 Fluoro dish static biofilm assay

The effect of meropenem and nisin in combination and as single compounds was examined by growing biofilms in glass-bottom fluoro dishes (Figure 2-1, dish ø 35 mm, glass ø 23.5 mm, World Precision Instruments, Inc.). Overnight cultures were diluted 1:100 in 2 mL of CaMHB and incubated for 2 h 37°C with shaking at 250 rpm in an orbital shaker. Logarithmic phase cultures were then diluted 1:100 in M9 minimal media and 2 mL added to each dish. The dishes were statically incubated for 24 h at 37 °C.

Figure 2-1: Glass bottom (No 1.5) fluoro dish. Static biofilms were grown for microscopy investigation of biofilm cells morphology and viability.

2.2.6.3 Flow cell biofilm assay

PAO1 biofilms were grown for 3 days in M9 minimal medium with continuous flow in a warm room at 37°C. Plastic coverslips (No. 1.5, 170 ± 5 µm thick, ibidi®, Munich, Germany) were glued (Clone FX glue, Barners) on in-house manufactured flow cells with channel dimensions of 1 mm x 4 mm x 40 mm (Figure 2-2 A). The system was set up as previously described (*178*) (Figure 2-2 B). The flow cell apparatus was sterilised by flowing 1 % hypochlorite solution through the apparatus and was then rinsed with sterile MilliQH_2O. Flow of sterile M9 minimal medium was then established in each channel. Overnight cultures were diluted 1:100 in 2 mL of CaMHB and incubated for 2 h at 37°C with shaking at 250 rpm in an orbital shaker. Logarithmic phase cultures were then diluted 1:100 in M9 minimal medium and the flow cells were inoculated with bacteria by reversing the flow at 200 µL/min. After the inoculation, the flow was stopped for 1 h to allow bacterial attachment and then started at a flow rate of 50 µL/min.

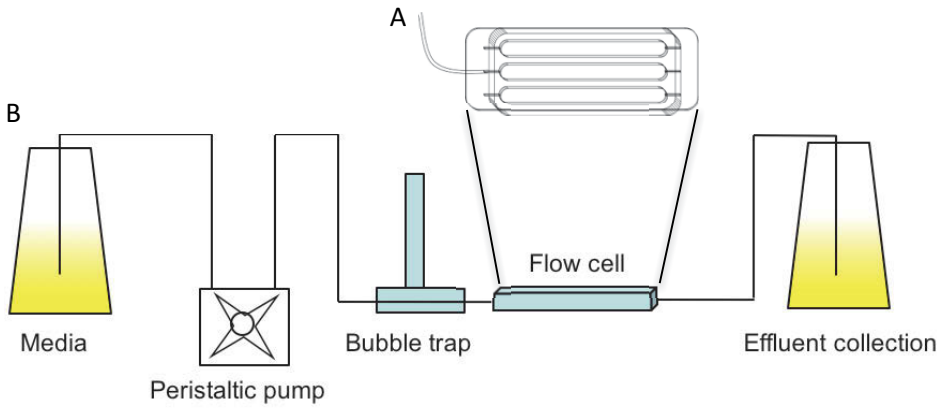

Figure 2-2: Flow cell apparatus. A) Three-channels flow cell for biofilm growth. B) Flow cell system showing the flow of the medium from left to right. The system is equipped with a peristaltic pump that allows forward and backward flow and a bubble trap to avoid the formation of air bubbles.

2.2.6.4 Antibiotic treatment of fluoro dish static biofilms

Sterile solutions of meropenem at 10 µg/mL and/or nisin at 64 µg/mL were prepared by diluting antibiotic stock solutions in M9 minimal media. After 24 h of biofilm growth, the planktonic cells were carefully removed by pipetting and biofilms were rinsed with sterile PBS. The biofilms were then re-submerged in the following solutions and incubated statically for 24 h at 37 °C: M9 minimal media for the control, meropenem at 5x the MIC and/or nisin at 64 µg/mL.

2.2.6.5 Antibiotic treatments of flow cell biofilms

Sterile solutions of meropenem at 10 µg/mL and/or nisin at 64 µg/mL were prepared by diluting antibiotic stock solutions in M9 minimal media. After 72 h of biofilm growth, the bottles containing media were replaced with media containing the antibiotics in sterile conditions. Biofilms were treated with the antibiotics as single treatments and in combination for 24 h.

2.2.6.6 Colony forming unit (CFU) assay of antibiotic treated flow cell biofilms

Following treatments, the flow cell coverslips were carefully removed and placed into separate 9 cm Petri dishes. The coverslips were scraped with a 25 cm cell scraper (Sarstedt, Newton, USA) to detach the biofilms and then submerged in 1 mL of PBS. The Petri dishes were sealed with parafilm and cells harvested after 10 min incubation in a water bath sonicator (50 Hz, Unisonics, Australia) at room temperature. Petri dishes were then placed on an orbital shaker for 10 min at 250 rpm at room temperature. Sonication and shaking steps were repeated twice. Thereafter, the bacterial suspension was collected from each Petri dish and placed separately into 1.5 mL centrifuge tubes. Twenty µL of bacterial suspension was collected from each centrifuge tube, placed into a 96-well plate and serially diluted in 180 µL of PBS, in triplicate. Twenty µL of each dilution was plated on a 1.6 % HS-LBA plates. Once dried, the plates were incubated at 37 °C overnight. The number of CFU/mL was then calculated using the following equation:

$$\mathrm{CFU/mL} = \frac{Number\ of\ colonies \times dilution\ factor}{Volume}$$

Equation 2-1: Colony forming unit per mL.

2.2.7 Microscopy analyses

2.2.7.1 Sample preparation of antibiotic-treated static biofilms

Following treatments, the planktonic cells were carefully removed by pipetting and the biofilms were then rinsed with sterile PBS. In order to determine biofilm biomass, biofilms were stained with 2 mM AM1-43/ 4 µM EthD-III (membrane/cell death dye mixture) for 30 min at room temperature in the dark. The stained biofilms were then washed once in 2 mL of PBS to remove excess stain.

2.2.7.2 Sample preparation of antibiotic-treated flow cell biofilms

Antibiotic-treated biofilms were stained with 2 mM AM1-43 to determine bacterial morphology and total biofilm biomass, and 4 µM EthD-III to determine dead biomass. The fluorescent dye mixture was prepared in PBS and injected into the flow cells for 15 min. The flow was then stopped and biofilms were stained in static conditions for 45 min. Subsequently, the excess stain was removed by washing the flow cells with PBS for 15 min.

2.2.7.3 Microscopy of antibiotic-treated static and flow cell biofilms

Live fluorescence images were acquired using wide-field fluorescence microscopy (Delta Vision Elite microscope, GE Healthcare Life Sciences) with Z-series images taken in 1 µm slices for biomass quantification and 0.1 µm for visual analysis. Twenty images were acquired for each biofilm sample. Prior to analyses, images were deconvolved using SoftWoRx software (GE Healthcare Life Sciences). Biofilms were volume-rendered using Imaris® Image analysis software (Bitplane) and COMSTAT analyses were performed (*74*).

2.2.7.4 Sample preparation and microscopy of planktonic CWD cells

Cultures of planktonic CWD cells were stained with 2 mM AM1-43 for 30 min at room temperature in the dark to determine cell morphology. Microscope slides and coverslips were ethanol sterilised and a 65 µL gene frame was placed on the slides. Cultures were then washed with PBS and 65 µL aliquots were placed on the microscope slides. Planktonic CWD cells were imaged using wide-field fluorescence microscopy (Delta Vision Elite microscope, GE Healthcare Life Sciences). Prior to analyses, images were deconvolved using SoftWoRx software (GE Healthcare Life Sciences).

2.2.7.5 Fluorescence *in situ* hybridisation of CWD cells hydrogels

Hydrogel blocks were prepared and cells were embedded in the hydrogels as detailed in section 2.2.5. After clearing, the hydrogels were washed in PBS and FISH was performed. The FISH probes used were EUB338 (Integrated DNA Technologies) which is a universal bacterial probe, in combination with PsearA (Integrated DNA Technologies) which is specific for *Pseudomonas*. Small squares were cut from the hydrogel block and placed into a 1.5 mL centrifuge tube. Five-hundred µL of the hybridisation buffer (see section 2.1.1.17) and 5.5 µL of EUB338 and PsearA were added to the tube which was then incubated at 46°C in a rotating incubator at 100 rpm overnight. The hydrogels were then washed in 1 mL of FISH washing buffer at 48°C for 6 h. The hydrogels were then placed on a large fluoro dish (World Instrument Precision) and visualised with wide-field fluorescence microscopy (Delta Vision Elite microscope, GE Healthcare).

2.2.8 Microscopy images analyses

2.2.8.1 COMSTAT analysis of biofilms

Fluorescent images of biofilms were processed with a customised IJ1 Macro, Fiji software for COMSTAT analysis (*74*). Images were analysed for biofilm biomass ($\mu m^3/\mu m^2$), roughness coefficient, maximum thickness (µm) and area distribution of microcolonies at the substratum (%). The AM1-43 (green, indicating total biofilm biomass) and the EthD-III (orange, indicating dead biofilm biomass) fluorescence were quantified to determine biofilm viability, while only the green fluorescence was quantified for determining the other parameters.

2.2.8.2 Imaris analysis of biofilms

Fluorescent images of biofilms were visualised with Imaris software (v 9.0, Bitplane) which allows the visualisation of 3D images. This software was used to investigate cells

morphology and measure cells diameter. Images are presented in this Thesis as volume reconstruction, cross sections of XY, XZ and YZ planes or as single slices.

2.2.9 UV spectroscopy method for drug quantification

The UV spectroscopy analysis was performed using the Shimadzu UV-1280 spectrophotometer and a 10 mm quartz cuvette (Shimadzu quartz spectrophotometer cell, Cat. N. Z27672-3, spectra range 170-2700 nm). Fifteen mg of meropenem was weighed and dissolved into a 100 mL volumetric flask in 0.9 % NaCl to obtain a final stock concentration of 150 μg/mL. The stock solution was sonicated for 5 min at room temperature. Standard solutions were prepared by dilution of the stock concentration in 0.9 % NaCl (*179*, *180*). The maximum absorbance for meropenem was determined at the concentration of 100 μg/mL between 200 and 400 nm. The method was validated between the concentration range of 1.5 – 75 μg/mL at 298 nm in terms of linearity, precision, accuracy, and limit of detection and of quantification according to the ICH Q2 (R1) guidelines for the validation of analytical procedures and in accordance with a previous study (*181*, *182*). The content of meropenem was quantified by correlation with the daily made calibration curve and using 0.9 % NaCl as blank. About 700 μL of each sample was inserted into the quartz cuvette and the absorbance was recorded at a wavelength of 298 nm.

2.2.10 Nasal formulation characterisation

2.2.10.1 Nasal spray solutions preparation

Meropenem nasal formulation was prepared as a spray solution by dissolving 60 mg of the raw drug in 20 mL of 0.9 % NaCl for a final concentration of 3 mg/mL. This concentration was chosen based on other nasal spray antimicrobials for the treatment of chronic rhinosinusitis (*183*). The drug was dissolved and sonicated for 5 min at room temperature to ensure complete dissolution. Nisin nasal formulation was prepared as a spray solution by dissolving 800 mg of the powder corresponding to 20 mg of nisin in

20 mL of 0.9 % NaCl for a final concentration of 1 mg/mL. The drug was dissolved and sonicated for 5 min at room temperature to ensure complete dissolution. Sodium fluorescein (Flu-Na) was dissolved in 0.9 % NaCl for a final concentration of 0.25 mg/mL. The solutions were then transferred into the Aptar nasal spray pump system using a 50 μL VP7 valve and a 20 mL canister (Aptar Pharma, Aptargroup, Milton Keynes, UK). All formulations were prepared fresh before conducting the experiments and filtered using a 20 mL syringe with a 0.45 μm nylon filter (Sartorius).

2.2.10.2 Spraytec system for nasal spray characterisation

Analyses of the droplet size, size distribution and obscuration profile were assessed using laser diffraction (Spraytec, Malvern Instrument, Malvern, UK). The device was placed at 5 cm from the centre of the laser and the actuation was manually performed. Prior to measurement, five actuations were manually performed to prime the pump of the spray system. Five measurements were taken for each formulation tested. Droplet size measurements were analysed for droplet size (Dv_{10}, Dv_{50}, Dv_{90}) and distribution. The obscuration profile was determined to characterise the plume emission of the formulations by evaluating the stable phase, were relatively constant particle size is delivered by the device.

2.2.10.3 Plume angle measurements

Plume angle measurements were assessed recording the spray plume with a high-speed camera (Phantom Mico C-210, Vision Research, USA) at 1800 fps (frames per second) and video processed with the Vision Research Phantom software (Ametek, USA). The angle of the spray plume was measured using the measuring tool in the Vision Research Phantom software.

2.2.10.4 Aerosol characterisation through cascade impaction

In order to characterise the aerosol particle size distribution and the respirable fraction of the nasal spray formulations, a British Pharmacopoeia Apparatus D: Andersen

Cascade Impactor (Copley) was used. The impactor was used in conjunction with a 2 L glass chamber (Figure 2-3) to measure the droplets deposition and distribution. The 7-stage cascade impactor was assembled following the manufacturer's instructions and connected to a rotary pump (Westech Scientific Instruments, Upper Stondon, UK) setting the flow rate at 28.3 L/min with a calibrated flow meter (Model 4040, TSI Precision Measurement Instruments, Aachen, Germany). The nasal spray was primed 5 times before each impaction study and the shot weight was recorded to ensure a spray volume of 50 ± 5 μL each time. Three shots were performed delivering a theoretical total dose of 450 μg to the chamber. The chamber, throat, all the impactor stages and the filter were washed with 0.9 % saline solution, separately. Samples were collected and quantified by UV spectrophotometry (Shimadzu UV-1280, Shimadzu, Australia) at 298 nm. The experiment was performed in triplicate.

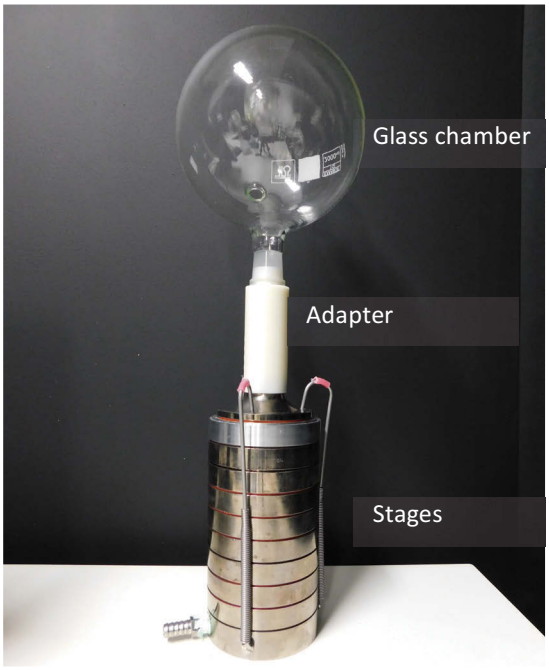

Figure 2-3: Andersen Cascade impactor equipped with 2 L glass chamber. The glass chamber represents the nasal cavity, the adapter represents the pharynx and the stages symbolise the lower respiratory tract from the trachea and primary bronchi to the alveoli.

2.2.11 Cell culture nasal cell line

2.2.11.1 Cultivation of RPMI 2650 nasal cell line

The RPMI 2650 human nasal cell line was purchased from the American Type Cell Culture Collection (ATCC, Manassas, VA, USA). Cells between passage 16-30 were grown in 75 cm^2 flasks using complete Minimum Essential Medium (MEM) containing 10 % (v/v) fetal bovine serum, 1 % (v/v) non-essential amino acid solution and 2 mM L-glutamine, incubated at 37°C, 5 % CO_2 and 95 % humidity. Cells were sub-cultured by removing the medium from the flask and incubated in 4 mL of Cell/Lytic™ solution for 10-15 min to detach cells from the flask. Six mL of complete MEM was added to inactivate the lytic solution and cells were agitated by gentle pipetting. Cell counting was performed combining 100 µL of cells with 100 µL of Tryptan blue. Subsequently, cells were seeded into a new flask with 10 mL of fresh pre-warmed MEM for a final seeding density of 3.5 x 10^6 cells/cm^2. Cells were fed in 10 mL of fresh pre-warmed MEM every 2 days (*153*).

2.2.11.2 RPMI 2650 air-liquid interface model

Snapwell™ cell inserts (1.13 cm^2, 0.4 µm pore size, Corning Costar, USA) were used to establish the air-liquid interface (ALI, Figure 2-4) model (*148*). The inserts were coated with 250 µL of 1 µg/mL collagen solution in PBS (rat collagen type 1 in PBS, BD Biosciences, Australia) overnight at 37°C to increase cell attachment to the insert membrane. Two hundred µL of cell suspension was then seeded in the cell inserts at a density of 2.5 x 10^6 cells/mL and after 24 h, the medium was removed from the apical compartment establishing the ALI conditions. The medium in the basolateral compartment was replaced every 2 days and the cells were left to grow in the ALI conditions up to 21 days before using the model for transport studies.

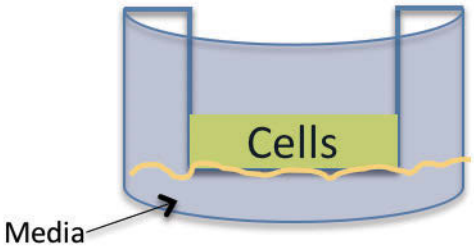

Figure 2-4: Schematic representation of the air liquid interface (ALI) model. Cells were grown on Snapwell™ cell inserts for 21 days.

2.2.12 Development and validation of a novel drug deposition apparatus for nasal formulations

2.2.12.1 Development of the novel apparatus

The apparatus was designed using SolidWorks design software (Dassault Systemes) and printed with the Form2 3D printer (Formlabs, USA) using a mixture of methacrylic acid esters and photoinitiator (clear photoreactive resin, Formlabs, USA), a non-porous material, as a cylindrical body for a total volume of 1 L. The body (Figure 2-5, A) is equipped with a removable cap (Figure 2-5, B) provided with an aperture (Figure 2-5, B, arrow) for allowing delivery of the spray (Figure 2-5, F). A disk (Figure 2-5, D) was designed to hold three cell culture inserts and was then placed inside the cylinder (Figure 2-5, E). The disk is maintained at the correct distance from the cylinder aperture by a spacer (Figure 2-5, C) and it can be removed after drug administration with forceps using the insertion at the top (arrow figure 2-5, D, arrow). The spacer can be easily modified to study drug transport at different distances, although for the purpose of this Thesis, it was maintained at 5 cm from the aperture. The body is also equipped with a protrusion to place the apparatus at a desired angle, set a 45° for the purpose of this Thesis (Figure 2-5, E and F).

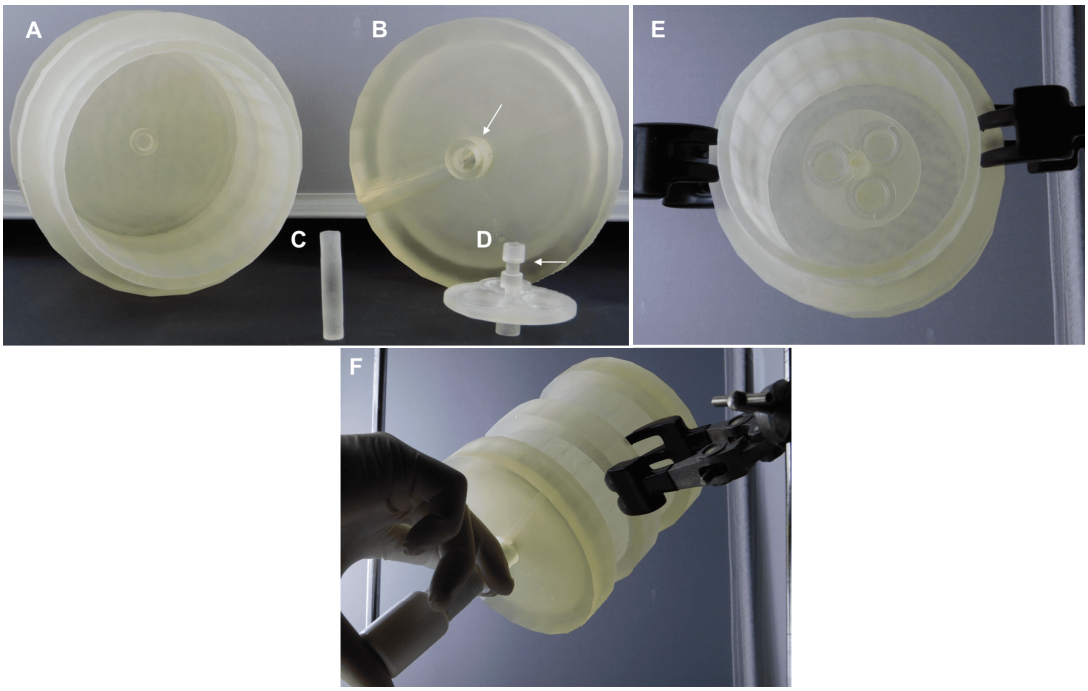

Figure 2-5: Novel nasal apparatus design. A) apparatus body, B) removable cup where the arrow indicates the insertion aperture for the nasal spray pump, C) spacer to place the disk D) at 5 cm from the aperture. Arrow in D indicates the insertion for the removal of the disk. E) shows the three Snapwells inserted into the disk which is hold by the spacer and attached to the body of the apparatus. F) The formulation is delivered to the Snapwells maintaining the apparatus at 45° from the working plane.

2.2.12.2 Characterisation of the novel nasal apparatus

2.2.12.2.1 Nasal delivery quantification on Snapwells™

The apparatus was assembled with a disk distance of 5 cm and three empty Snapwell™ cell inserts were placed into the disk. A solution of 0.25 mg/mL Flu-Na was prepared in PBS and dispensed into the Aptar device. After three shots, the membrane of the inserts was carefully removed from each insert using a cutter and washed with 2 mL of PBS. In addition, insert rings were washed with 2 mL of PBS. The body of the apparatus was then washed with 50 mL of PBS to collect the Flu-Na that may have deposited on the chamber. Two hundred µL aliquots of the samples were dispensed into a black 96 - well plate (Corning, Sigma-Aldrich, Sydney, Australia). The absorbance was quantified

using the plate reader SpectraMax M2 (Molecular device CA, USA) at excitation and emission wavelength of 485 nm and 535 nm, respectively. The quantification of the solution was expressed as recovery (%). Images of the deposition of Flu-Na solution after three shots were obtained using a Nikon Coolpix-B500 and a 25w blue spectra LED lamp.

2.2.12.2.2 Barrier integrity of nasal cell model

Flu-Na was used to evaluate the cell layer integrity after spray deposition. The device was assembled with three cell inserts containing cells cultivated in ALI conditions after 14 days of seeding. The cell inserts were gently rinsed with pre-warmed HBSS and placed into the disk. The cell layer integrity was assessed after one and three shots of PBS using the Aptar VP7 nasal pump. Cell inserts were then placed into a 6-well plate with 1.5 mL of pre-warmed HBSS into the basolateral chamber and 250 µL of Flu-Na 2.5 mg/mL was added to the apical chamber. Aliquots of 200 µL were collected from the basolateral chamber every 30 min up to 4 h after the administration. The same amount of warmed HBSS was replaced after the sampling. Samples were dispensed into a black 96-well plate and the fluorescence of Flu-Na was recorded as described above (2.2.11.2.1). The calibration curve was determined by preparing standards in a concentration range between 0.0125 and 1.25 µg/mL with a linearity of 0.999. Flu-Na absorbance values were used to calculate the permeation coefficient (P_{app}) according to the following:

$$\mathrm{Papp} = \frac{\mathrm{dQ}}{dt \cdot C_o \cdot A}$$

dQ/dt = flux across cell layer (µg/s)

C_0 = initial basolateral chamber concentration (µg/mL)

A = surface area (cm^2)

Equation 2-2: Permeation coefficient.

2.2.12.2.3 Flu-Na quantification

A stock solution of Flu-Na was prepared at a concentration of 2.5 mg/mL and standards were prepared by dilution of the stock solution in PBS with a concentration range between 1.25 and 0.0125 µg/mL. Samples were quantified using the plate reader SpectraMax M2 (Molecular device CA, USA) at excitation and emission wavelengths of 485 nm and 535 nm, respectively.

2.2.13 Meropenem transport through RPMI 2650 cell line

To estimate the transport of meropenem nasal spray solution on RPMI 2650 nasal cells, the novel apparatus was used using a similar methodology previously described and validated by Pozzoli *et al.* (*141*). Cells were used after 14 days from seeding on Snapwells™. Three inserts were washed with pre-warmed HBSS buffer and placed into the disk of the nasal apparatus. One and three shots of 3 mg/mL meropenem were delivered to the cells using the Aptar spray pump. Cell inserts were transferred into a 6-well plate containing 1.5 mL of pre-warmed HBSS. The plate was incubated at 37°C, 5 % CO_2 and 95 % humidity, aliquots of the basolateral compartment were analysed every hour and cell inserts were moved into a new well with 1.5 mL of fresh pre-warmed HBSS. After 4 h, the apical compartment was washed 3 times with 300 µL of HBSS to estimate the remaining amount of drug on the cell surface. Cells were then scraped from the insert membrane and lysed with 1 mL of HBSS/CellLytic™ buffer, 1:1 ratio to quantify the amount of drug inside the cells. A control experiment with a solution containing no drug was also performed to account for any interference due to the cell lysate. Meropenem concentration in the unknown samples was quantified using UV spectrophotometry at 298 nm and the experiment was performed in triplicate.

2.2.14 Cytotoxicity assays

2.2.14.1 Lactate dehydrogenase (LDH) assay

The toxicity of meropenem and nisin was evaluated on RPMI 2650 nasal cells. The cytotoxicity test was performed measuring the lactate dehydrogenase (LDH) released upon cell damage using the RayBio® LDH-Cytotoxicity Assay Kit II (RayBiotech, Inc.). One hundred µL of 2.5 x 10^5 cells/mL were added to the wells of a 96-well plate and incubated at 37°C, 5 % CO_2 and 95 % humidity overnight. Stock concentrations of meropenem and nisin were prepared in 0.9 % NaCl and serially diluted in complete MEM. One hundred µL of different concentrations of meropenem (3 mg/mL to 0.01 mg/mL) and nisin (1 mg/mL to 0.06 mg/mL) were added to the cells and incubated for 24 h. One hundred µL of 1 % (v/v) of Triton®X-100 was used as positive control. After treatments, 10 µL of the supernatant was withdrawn and transferred to a new plate. One-hundred µL of the LDH Reaction Mix was added to each well and incubated for 30 min in the dark. Absorbance values were obtained using the SpectraMax plate reader at 450 nm and the LDH release (%) was calculated according to with the following equation.

$$LDH\ \% = \frac{(Test\ Sample - Negative\ Control)}{(Positive\ control - Negative\ control)} * 100$$

Equation 2-3: LDH release percentage.

2.2.14.2 Flow cytometry assay

The cytotoxicity of meropenem and nisin was evaluated using Propidium Iodide (PI), a dye that stains nucleic acids when the cellular membrane integrity had been damaged. Briefly, cells were seeded in a 24-well plate (Falcon, Corning Inc., USA) at density of 2.5 x 10^5 cells/mL and allowed to attach and grow overnight at 37°C, 5 % CO_2 and 95 % humidity. Stock concentrations of meropenem and nisin were prepared in 0.9 % NaCl and serially diluted in complete MEM. One mL of different concentrations of meropenem (3 mg/mL to 0.01 mg/mL) and nisin (1 mg/mL to 0.06 mg/mL) were added

to the cells and incubated for 24 h. One mL of 0.3 % Hydrogen Peroxide (H_2O_2, Gold Cross, Biotech Pharmaceutical) was used as a positive control. After 24 h cells were washed with PBS and detached using CellLytic™ buffer. The cells that may have lifted during the incubation were included in the analysis. Cells were re-suspended in PBS and stained with 50 µg/mL PI for 10 min in the dark at room temperature. Cell toxicity was evaluated using BD Accuri C6 (BD Accuri) using the fluorescent channel 2 (FL2 detector). Measurements were carried out in triplicate and 10,000 events were acquired per sample. Toxicity is expressed as the percentage of cells stained by the PI dye and a treatment was considered toxic to the cells if the cell viability percentage was below 80%.

2.2.15 Nasal spray formulation delivery on *P. aeruginosa* biofilm

A PAO1 logarithmic phase culture was diluted 1:100 in M9 minimal media and 350 µL of the culture was dispensed into the Snapwell™ cell culture inserts. Two mL of pre-warmed M9 was added to the basolateral compartment of a 6-well plate, plates were covered with Aeroseal and incubated for 24 h at 37°C in static conditions (Figure 2-6). Three mg/mL meropenem and 1 mg/mL nisin were prepared as detailed in section 2.2.10.1. The novel nasal apparatus was cleaned with 95 % (v/v) EtOH, let air-dry, dried and sterilised using the UV light. The nasal apparatus was then assembled in a Biosafety cabinet at 45°angle. Three cell inserts were placed into the disk after 24 h of biofilm growth. The nasal spray formulations were delivered to the biofilms by spraying three shots. Snapwells™ were then removed from the disk, placed into a clean 6-well plate with 2 mL of 0.9 % NaCl in the basolateral compartment. Plates were covered with Aeroseal and incubated for 24 h at 37°C. After 24 h, the membrane of each cell culture insert was carefully removed using a sterile surgical blade (Livingston International, Australia) and placed into the wells of a 6-well plate, individually. The biofilms were detached from the membranes with a 25 cm cell scraper and then the membrane was submerged in 1 mL of 0.9 % NaCl. The 6-well plates were sealed with parafilm and cells harvested for 5 min in a water bath sonicator at room temperature.

Plates were then placed on an orbital shaker for 5 min at 250 rpm at room temperature. Sonication and shaking steps were repeated twice. Thereafter, 20 µL of bacterial suspension was collected from each well of the 6 well plate and placed into a 96-well plate. Samples were serially diluted in 180 µL of 0.9 % NaCl, in triplicate. Twenty µL of each dilution was plated on 1.6 % HS-LBA plates. Once dried, the plates were incubated at 37 °C overnight and the number of CFU/mL was then calculated.

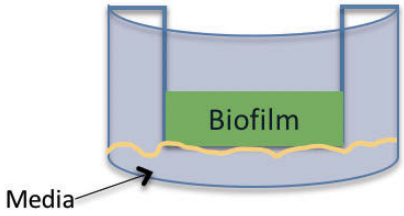

Figure 2-6: Schematic representation of biofilms grown on Snapwell™ cell culture inserts.

2.2.15.1 Microscopy of biofilm harvested cells

After 24 h of treatment, harvested biofilm cells were stained with 2 mM AM1-43 alone or in a mixture with 4 µM EthD-III for 15 min at room temperature in the dark to visualise cell morphology and cell viability. Glass microscope slides and coverslips were sterilised with 95 % (v/v) EtOH and let air-dry. Sixty-five µL aliquots were then placed onto the microscope slide using a 65 µL gene frame (Life Technologies, Australia) and a No. 1.5 coverslip was set on top. Fluorescence images were acquired using wide-field microscopy (Delta Vision Elite microscope, GE Healthcare Life Sciences). Five images were acquired for each sample and the experiment was performed in triplicate, including technical replicates. Images were processed using Fiji-ImageJ (version 2.0.0).

2.2.16 Statistical Analyses

Group comparisons were performed using Kruskal-Wallis test followed by Dunn's multiple comparisons test (One-way ANOVA, nonparametric) and Unpaired t-test with Welch's correction in GraphPad Prism 7.

Chapter 3

Morphological Analyses of Biofilm Cells Exposed to the Carbapenem Antibiotic Meropenem

3 Morphological Analyses of Biofilm Cells Exposed to the Carbapenem Antibiotic Meropenem

3.1 Introduction

β - lactam antibiotics perform their activity by binding to the penicillin-binding proteins (PBP) causing inhibition of the synthesis of the peptidoglycan layer of the cell wall.

P. aeruginosa has a variety of mechanisms to survive the penetration of such antibiotics. Interestingly, previous studies have demonstrated that *P. aeruginosa* planktonic cells undergo a morphological transition to a cell wall deficient (CWD) spherical morphotype when exposed to β - lactam antibiotics, such as carbapenems, as a novel mechanism of antibiotic tolerance (*165*, *170*, *171*). This class of antibiotic is unique in that it is relatively resistant to hydrolysis by most β - lactamases thus is still able to target PBPs. In fact, this morphological change to CWD form is associated with a higher affinity of carbapenems to PBP2 (*184*).

P. aeruginosa has an innate resistance to antibiotics, mainly due to the low permeability of the cell wall, the production of β - lactamases and the use of efflux pumps (*62*, *185*). Furthermore, bacterial cells often aggregate and grow as biofilms in the environment and clinical settings.

Biofilms like those produced by *P. aeruginosa* are comprised of bacterial cells embedded in an extracellular polymeric matrix, which is a mixture of polysaccharides, extracellular DNA, proteins, lipids and membrane vesicles (*34*). Bacterial cells in a biofilm lifestyle can survive stressful conditions more than planktonic cells. This ability is due to the presence of the biofilm matrix that functions as a shield to protect the cells (*186*). Moreover, physiological alterations arise within the bacterial community and new mechanisms of resistance can take place (*187*). It is well documented that antibiotics generally penetrate cells in biofilms with less efficiency than when targeting planktonic cells (*50*, *187*, *188*). In the specific case of carbapenems, studies have shown that this class of antibiotics is still able to penetrate the biofilm and bind to the PBPs due to its ability to resist to the activity of β -lactamases in comparison to other

sub-classes of β-lactams, which are more easily hydrolysed (*85*). So far, the morphological change due to β - lactam exposure has been documented only for planktonic cells and has not been explored in biofilms. We hypothesise that the morphological change to CWD spherical morphotype could also occur in *P. aeruginosa* biofilms. Therefore, this Thesis Chapter focuses on investigating the effect of the carbapenems such as meropenem on the morphology of biofilm cells. We investigated the effect of meropenem on established *P. aeruginosa* PAO1 biofilms to determine whether CWD spherical morphotypes are present in meropenem-treated biofilms. The minimum inhibitory concentration (MIC) as well as the minimum biofilm eradication concentration (MBEC) were first determined. Studies looking at cell diameters following meropenem exposure were also conducted in order to characterise differences between planktonic and biofilm CWD cells. Moreover, the induction of CWD cells was investigated in artificial sputum media mimicking the CF lung environment. A method for the detection of CWD cells in artificial sputum medium using fluorescence *in situ* hybridisation (FISH) was developed.

3.2 Results

3.2.1 Determination of meropenem minimum inhibitory concentration

The MIC of meropenem against *P. aeruginosa* strain PAO1 was first established under the experimental conditions used in this study and with our source of meropenem supplier (see section 2.1.1.15). Planktonic cells were exposed to different concentrations of meropenem using the microtitre broth dilution method, as detailed in section 2.2.2. After 24 h of meropenem treatment, the wells of the plates were visually analysed and the MIC was identified as the concentration in which there was no visible growth. The MIC for PAO1 under these conditions was found to be 2 μg/mL.

3.2.2 Effects of meropenem on static biofilms

As previously mentioned, planktonic *P. aeruginosa* cells survive exposure to meropenem by transitioning to a CWD spherical morphotype when treated with concentrations ≥ MIC. Static biofilms grown in 96-well microtitre plates (see section 2.2.6.1) were exposed to meropenem concentrations up to 10x MIC (2.5 μg/mL to 20 μg/mL) to investigate the effect of meropenem on biofilm viability. After 24 h of antibiotic treatment, the wells were washed with PBS and stained with crystal violet to determine biofilm biomass. The absorbance at 600 nm of the extracted crystal violet was used as indicator of relative biofilm biomass. Figure 3-1 shows that the biomass of biofilms exposed to various concentrations of meropenem did not significantly decrease compared to untreated biofilms, even at 10x MIC (20 μg/mL).

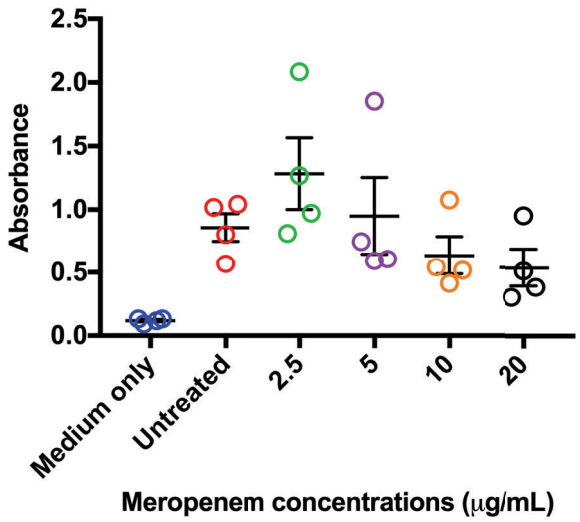

Figure 3-1: Relative biofilm biomass of 24 h static biofilms exposed to meropenem. Extracted crystal violet readings of 24 h static biofilms after treatment with meropenem at concentrations up to 10x MIC. Bars represents mean ± SEM, n = 4, including technical triplicates. Kruskal-Wallis test with multiple comparison: no significant difference.

3.2.3 Microscopy investigation of cell morphology in static biofilm

We hypothesised that biofilm eradication does not occur since biofilms are more resistant than their planktonic counterpart but also because the cells within the biofilm may undergo the transition to the CWD spherical lifestyle seen in the planktonic state and consequently be able to survive antibiotic exposure. To further investigate whether meropenem could induce the morphological transition to the CWD spherical morphotype in biofilms, biofilms were cultured in fluoro dishes for 24 h (see section 2.2.6.2) and treated with meropenem at 5x the MIC for 24 h (see section 2.2.6.4). Biofilms were then stained with the membrane dye AM1-43 (see section 2.2.7.1) and visualised with wide-field fluorescence microscopy to examine cell morphology (see section 2.2.7.3). After 24 h treatment, cells with a spherical morphology could be readily observed in meropenem-treated biofilms (Figure 3-2).

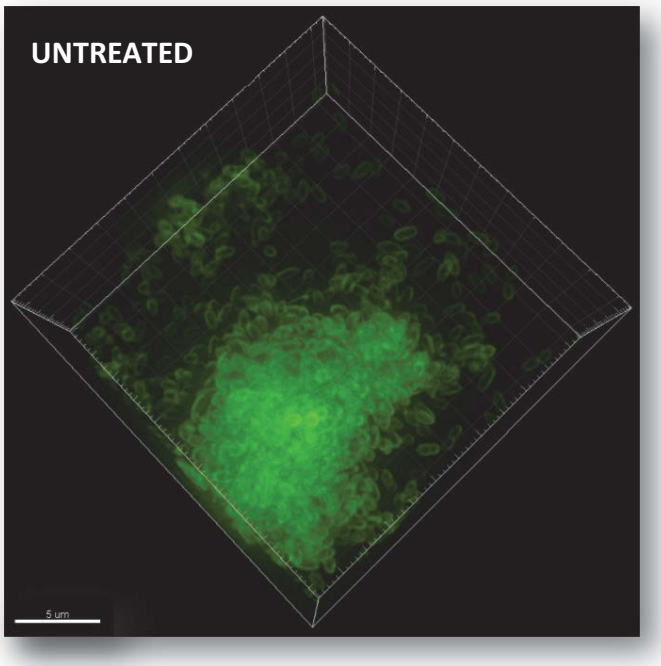

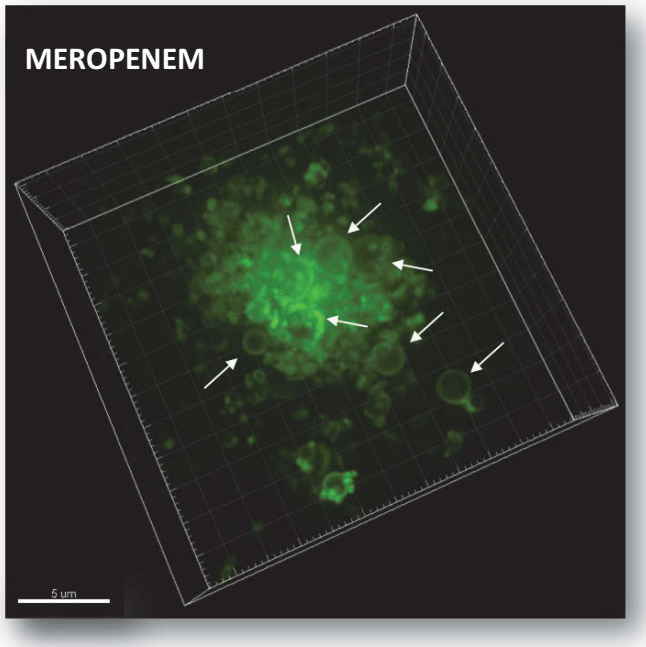

Figure 3-2: **3D projections of 24 h static biofilm.** Biofilms were stained with the membrane dye AM1-43 (green) for morphological investigation. Fluorescent images of untreated biofilm showing the bacillary shape of *P. aeruginosa* and meropenem-treated biofilms showing a mixture of bacillary and CWD spherical cells (white arrows). Images are representative of three biological repetitions. Scale bar = 5 µm.

3.2.4 Microscopy investigation of cell morphology in flow cell biofilms

We previously demonstrated that meropenem induced the formation of the CWD spherical morphotype in 24 h static biofilms. Studies have shown that the response of young biofilms to antibiotic treatments may be different to the one of more mature biofilms, therefore, we investigated whether the morphological change also occurred in more mature biofilms (*189*). For this purpose, we used the flow cell technology which enable the growth of biofilms with a continuous flow of fresh media. Moreover, this technology allows a detailed analysis of the biofilm structure in the absence of planktonic cells which are removed by flow (*76*). Thus, to investigate whether the spherical morphotype occurs in more mature biofilms and to characterise cell morphology in greater detail, biofilms were grown in flow cells for three days (see section 2.2.6.3) followed by continuous treatment with 5x the MIC meropenem for 24 h (see section 2.2.6.5). The biofilms were than stained with AM1-43 to determine cellular morphology (see section 2.2.7.2) and imaged as described in section 2.2.7.3. Spherical cells were also observed to form in three-day old biofilms, as shown in Figure 3-3, B. This was the first evidence that the CWD spherical morphotype has been identified to form in biofilms.

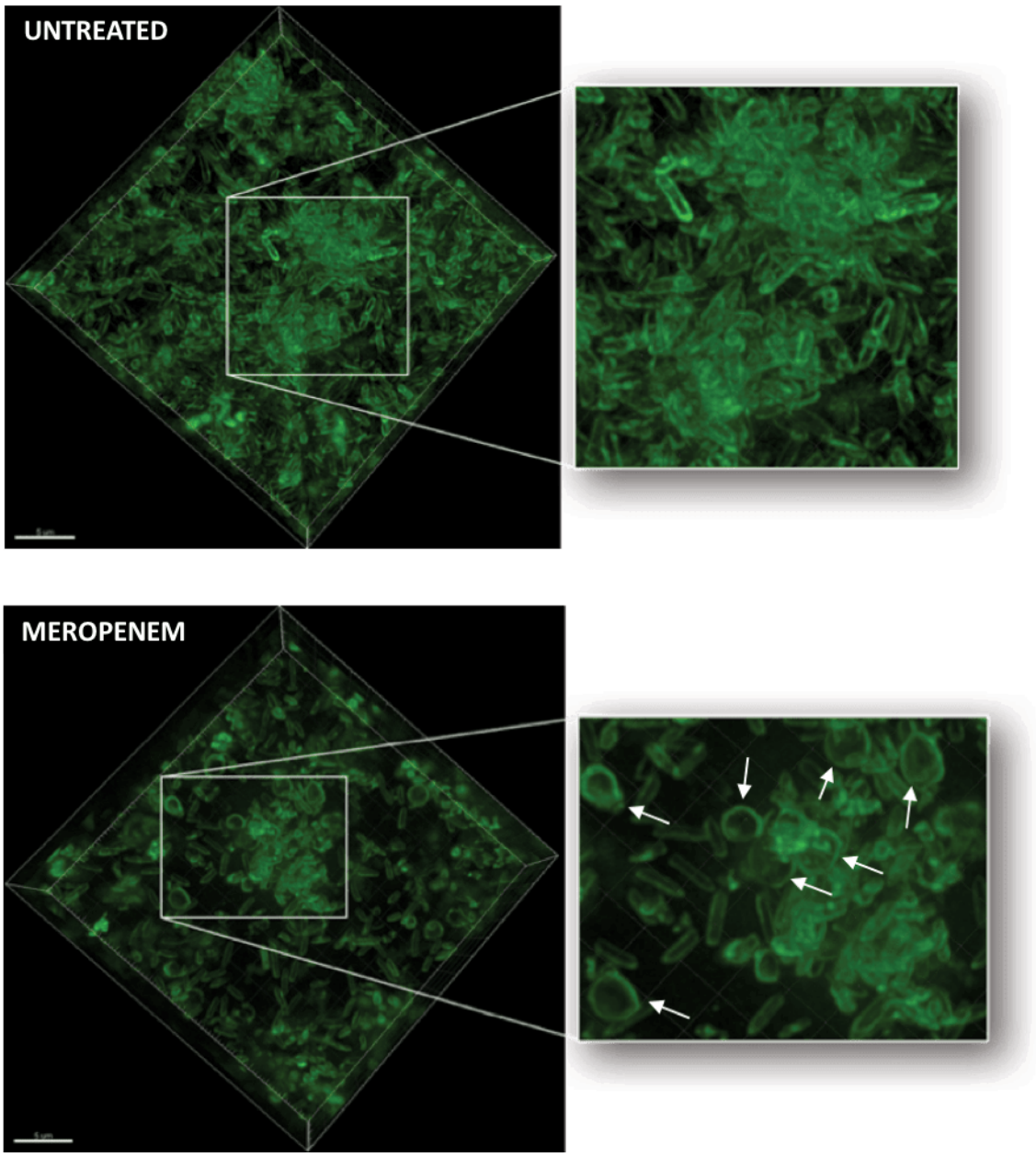

Figure 3-3: 3D projections of three-day old flow cell biofilms. Biofilms were stained with the membrane dye AM1-43 (green) for morphological investigation. Fluorescent images of flow cell untreated biofilm showing the bacillary shape of *P. aeruginosa* and meropenem-treated biofilms showing a mixture of bacillary and CWD spherical cells (white arrows). Inset images show cell morphology in more detail. Images are representative of three biological repetitions. Scale bar = 5 µm.

3.2.5 Biofilm CWD spherical cell measurements

Identifying CWD cells in biofilms may be difficult due to the orientation that cells can assume inside the microcolonies. Whilst performing microscopy, images are acquired by taking cross sections of the microcolony along the z-axis, which are then reconstructed to form a 3D structure. In the situation where a CWD cell and a bacillary cell reside on the same focal plane, the CWD cell will always appear as a sphere, while the bacilli will appear as an elongated shape or as a sphere depending on its orientation relative to the focal plane (Figure 3-4). Therefore, to be able to distinguish between bacillary and CWD cells, the cell diameter of small and large spherical cells was measured and compared. Cross sectional images from untreated (Figure 3-4) and meropenem-treated flow cell biofilms (Figure 3-4) were analysed and the diameter of round cells was measured. Round cells in untreated biofilms displayed a significantly smaller diameter ($p<0.0001$) compared to round cells in meropenem-treated biofilms (Figure 3-4, A and B). Therefore, we could confidently say that large round cells in meropenem-treated samples were the CWD spherical morphotype and they could be easily identified due to their larger size.

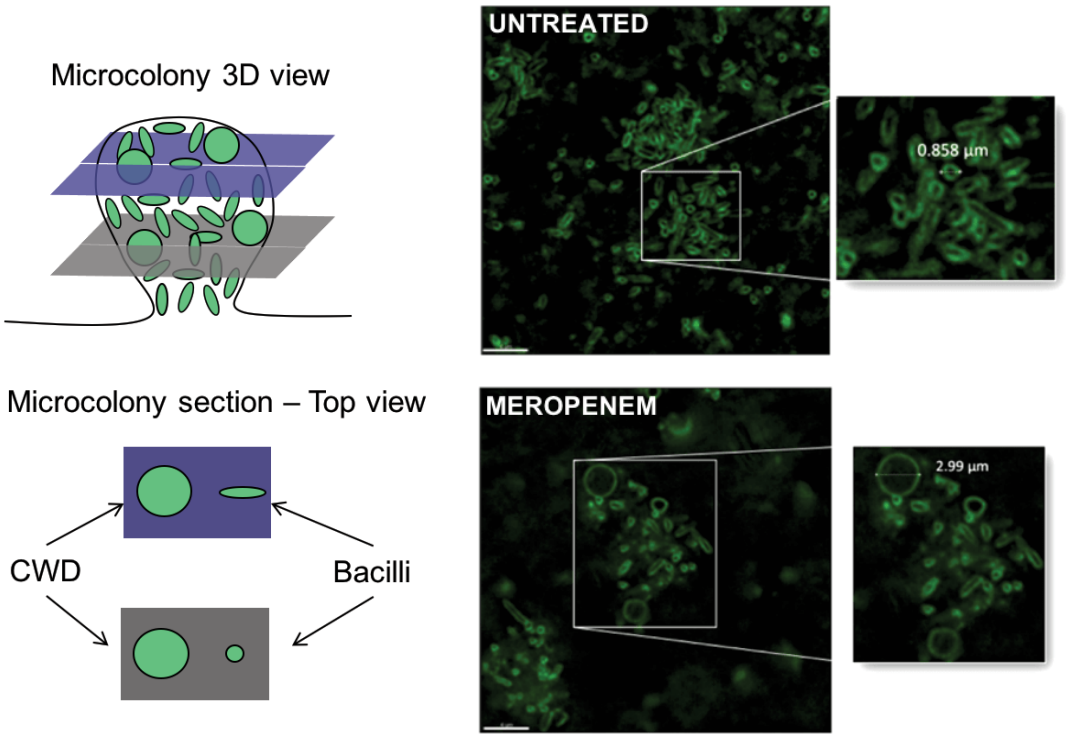

A

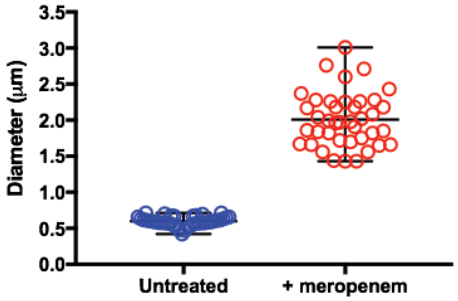

B

	Diameter (µm)		
Biofilm treatment	**Min**	**Max**	**Mean**
Untreated	0.42	0.71	0.60
Meropenem	1.43	3.01	2.00

Figure 3-4: Identification of CWD spherical cells by size in flow cell biofilms. Top left: schematic representation of cells orientation within a microcolony. Top right: cross section images of three-day old untreated and 24 h meropenem-treated flow cell biofilms. Image insets show cell diameter measurements. Images are representative of three biological repetitions. Scale bar = 4 µm. A) Round biofilm cell diameters distribution in untreated and meropenem-treated biofilms. Bars represent mean ± range for 40 measured cells. Unpaired *t*-test with Welch's correction (p****<0.0001). B) Diameter measurements for each sample.

In order to confirm that the biofilm spherical cells were similar to those in the planktonic state (see section 2.2.3), the diameter of planktonic CWD cells was measured (Figure 3-5, A) and compared it to the diameter of biofilm CWD cells (Figure 3-5, B). Planktonic as well as biofilm CWD cells were measured using the measuring tool in Imaris. Images were visualised in the "slice view" mode and measurements of the diameter was taken by drawing a line from and to the cell's extremities. After measuring 100 planktonic and biofilm spherical cells, we concluded that the CWD cells found in biofilms did not significantly differ in size compared to those found in the planktonic cultures (Figure 3-5, C and D).

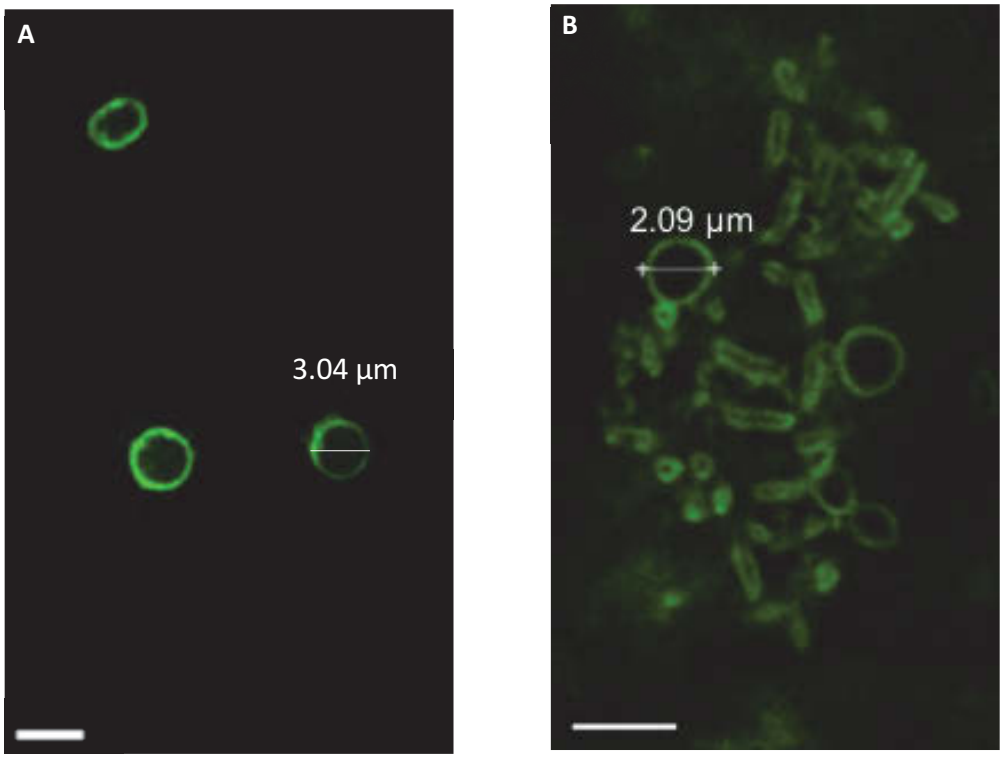

C

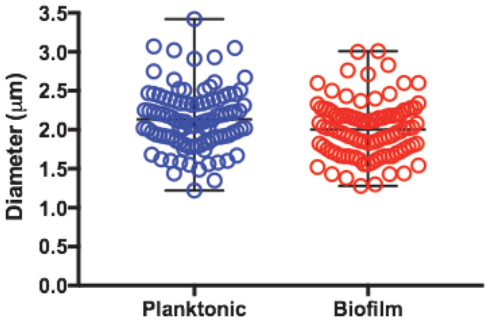

D

	Diameter (µm)		
CWD type	**Min**	**Max**	**Mean**
Planktonic	1.22	3.42	2.13
Biofilm	1.28	3.01	2.00

Figure 3-5: CWD spherical cell sizes. Images are cross sections of A) planktonic CWD spherical cells and B) biofilm CWD spherical cells. Both were treated for 24 h with meropenem at 5x the MIC. Images are representative of three biological repetitions. Scale bar = 3 µm. C) Planktonic and biofilm CWD spherical cells diameter distribution. Bars represent mean ± range. D) Diameter measurements of 100 cells from biofilm and planktonic CWD cells.

3.2.6 Microscopy investigation of cell morphology in artificial sputum medium

The morphology of *P. aeruginosa* cells was investigated in artificial sputum medium (ASM) to simulate the cystic fibrosis lung environment (*190*). Logarithmic phase cells were sub-cultured in ASM and treated with meropenem at 5x the MIC overnight (see section 2.2.3). Untreated cells were included as control. Cells were then stained with the membrane dye AM1-43 for visualisation of the cell morphology and imaged as described in section 2.2.7.4. The entire population of meropenem-treated cells converted to the CWD spherical morphotype and formed aggregates (Figure 3-6). The untreated cells formed aggregates as well but maintained their rod shape (Figure 3-6).

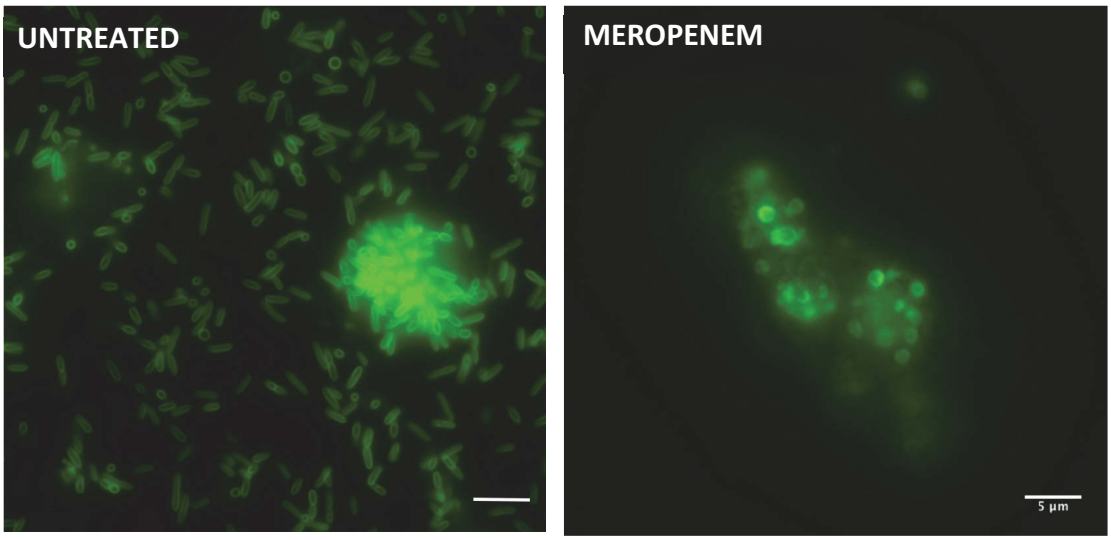

Figure 3-6: CWD cells in ASM. Fluorescent images of untreated and meropenem-treated planktonic cells stained with AM1-43 for morphology visualisation. Images are representative of three biological repetitions. Scale bar = 5 µm.

3.2.7 Development of a method to identify CWD *P. aeruginosa* in clinical samples

As previously mentioned, it has been demonstrated that planktonic *P. aeruginosa* cells respond to β-lactam antibiotics by transitioning to a viable CWD spherical morphotype as an alternative mechanism of antibiotic tolerance. Furthermore, this transition can be rapidly reversed after antibiotic removal. In this Thesis Chapter, it was demonstrated that the CWD morphotype also occurs in biofilms grown in laboratory media and also in artificial sputum medium, which mimics the sputum of CF patients. Therefore, we reasoned that this morphological transition could partially explain the recurrence and the refractory nature of *P. aeruginosa* infections. We therefore established a method to identify CWD *P. aeruginosa* in clinical samples of patients with CF and treated with β-lactam antibiotics.

CF patients are colonised not only by *P. aeruginosa* but also by other bacteria such as *Staphylococcus aureus, Haemophilus influenzae* and new emerging pathogens such as *Burkholderia cepacia* complex (*191*). The use of the membrane dye AM1-43 would therefore not be suitable for this purpose as it will not differentiate between different bacterial species. Thus, fluorescence *in situ* hybridisation (FISH) was utilised for the visualisation of meropenem-induced CWD cells in artificial sputum medium. FISH utilises fluorescent probes that bind to specific DNA or RNA sequences for the identification of single microbial cells which are then visualised using fluorescence microscopy (*192*). In this Chapter, the probe PsearA, specific for *Pseudomonas* identification and the universal bacterial probe EUB338, which are directed against the 16s rRNA genes, were used.

The methodology was developed by adjusting a technique previously described by DePas *et al.* (*193*) in which sputum samples were embedded in hydrogels and clarified in sodium dodecyl sulphate (SDS). This technique has been previously used in the preparation of tissue samples for microscopy imaging, where samples are embedded in hydrogels and successfully cleared to enable *in situ* hybridisation, immunohistochemistry and antibody labelling (*194–196*).

Here, we revisited this method as CWD cells may lyse when treated with some of the compound used for preparing and clearing the hydrogels. In order to investigate this, planktonic PAO1 cells were cultured and the morphological change was induced as detailed in section 2.2.3. CWD cells were then treated with 8 % SDS overnight as described in section 2.2.4. Cells were then placed on a microscope slide and imaged with phase contrast microscopy (Delta Vision Elite microscope, GE Healthcare). Microscopy showed that CWD cells were completely lost due to lysis after the SDS treatment (Figure 3.7). Therefore, to overcome this lysis issue, cells were embedded in acylamide: bis-acrylamide hydrogels. The hydrogels were prepared and cells were embedded in the hydrogels as detailed in section 2.2.5. After clearing the hydrogels in SDS, FISH was performed as detailed in section 2.2.7.5 and visualised with wide-field fluorescence microscopy (Delta Vision Elite microscope, GE Healthcare).

As shown in Figure 3-8, rods and CWD cells were successfully embedded in the hydrogels and CWD cells did not lyse after treatment with SDS. Therefore, the embedding of CWD cells in acrylamide-based hydrogels is essential for the conservation of the CWD cells morphology. Microscopy also showed that FISH probes successfully stained *P. aeruginosa* rod and CWD cells embedded in acrylamide-based hydrogels.

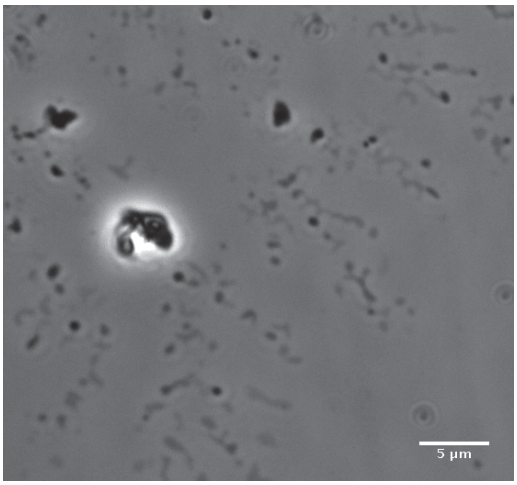

Figure 3-7: CWD cells after SDS treatment. Phase contrast image showing lysis of meropenem-treated CWD cells after overnight clearing in 8 % SDS.

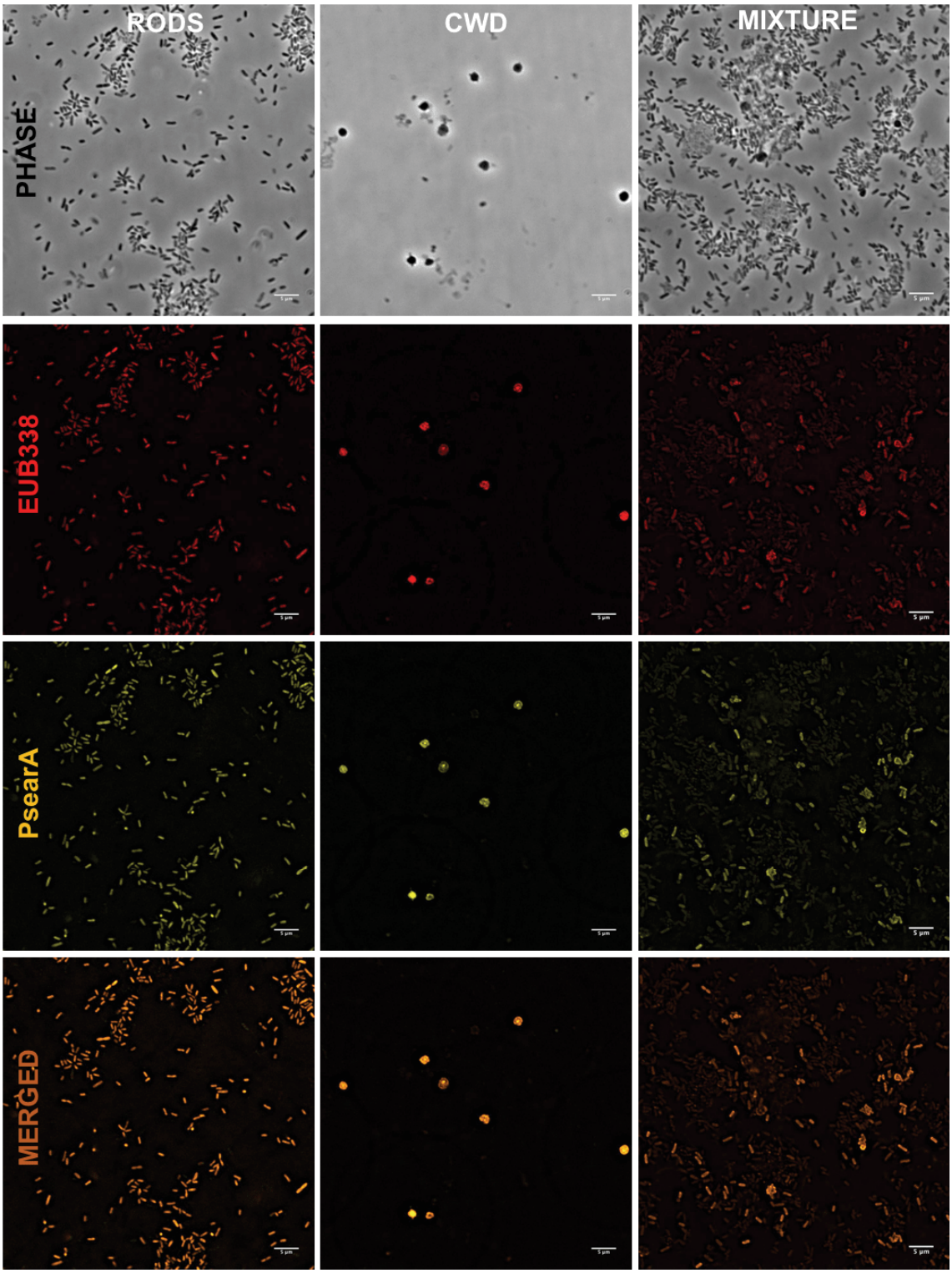

Figure 3-8: FISH of rods and CWD *P. aeruginosa* cells embedded in hydrogel blocks. Fluorescent images showing successful binding of FISH probes to both rods (untreated cells) and meropenem-treated CWD cells.

3.3 Discussion

It is well documented in the literature that *P. aeruginosa* biofilms are resistant to β - lactam antibiotics, in particular to carbapenems such as meropenem (*197*). In our study, we found that static biofilms tolerate meropenem exposure up to 10x MIC (20 µg/mL). This result was not surprising since it has been previously demonstrated that *P. aeruginosa* clinical isolates were resistant to imipenem and meropenem (*198*). Moreover, increasing rates of carbapenem-resistance have been documented in intensive care unit (ICU) and non-ICU inpatients and children with CF (*199*, *200*).

Based on previous findings in the Whitchurch laboratory where CWD planktonic *P. aeruginosa* responded to the activity of β - lactams by transitioning to a viable CWD spherical morphotype (*165*), we demonstrated here that CWD spherical cells also occur in both static and flow cell biofilms after 24 h of meropenem exposure. Moreover, we confirmed that the spherical cells seen in biofilms had similar diameter distribution as the ones found in the planktonic state. This is the first evidence that the CWD spherical morphotype forms in biofilms in response to carbapenem treatment. Many studies have been conducted to investigate the effect of β - lactams on *P. aeruginosa* and some of them have identified the occurrence of this change in the cell morphology (see section 1.9). However, these studies looked at planktonic cells and not at biofilms, which are now believed to be the cause of chronic and persistent infections (*34*, *201*). Diseases characterised by *P. aeruginosa* colonisation are very difficult to treat, and this is attributed not only to the high resistance of *P. aeruginosa* to antibiotics but also to the fact that *P. aeruginosa* can form biofilms that have a distinct resistance machinery (*187*) compared to their planktonic counterpart. The formation of CWD cells in biofilms could partially explain why *P. aeruginosa* infections re-appear after treatments. In fact, it has been seen that patients diagnosed with *P. aeruginosa* infection suffer from a recurrent cycle of infection and inflammation even after high doses of antibiotics and often such infection leads to death (*202*, *203*). Our findings suggested that therapy failures might be due to the formation of CWD cells after antibiotic exposure and the capability of those cells to revert back to the bacillary

shape upon removal of the antibiotic. Therefore, the use of β- lactam antibiotics is potentially problematic and more attention should be paid when choosing the therapy to treat such infections. In our study, it was also noticed that only a portion of the biofilm cells converted to the spherical morphotype. This could be attributed to different factors. Firstly, biofilm cells are physiologically heterogeneous, meaning that cells respond differently to antibiotic exposure based on their location within the biofilm structure. In *P. aeruginosa* biofilms, cells at the top of the microcolonies are actively dividing, while cells at the bottom have a low metabolism (*204*). This implies that in the case of meropenem which targets metabolically active cells, only those at the top or at the immediate periphery of the microcolony could respond with the morphological conversion. Secondly, antibiotics have difficulty in penetrating the dense biofilm matrix, and they could be totally or partially inactivated by β - lactamases while penetrating the biofilm. We hypothesise that the addition of a compound that causes dispersion of the biofilm cells or that increases meropenem penetration could overcome this hindrance and increase the number of cells that undergo the morphological transition.

Moreover, in this Thesis Chapter we demonstrated for the first time that the CWD spherical morphotype could be induced in media mimicking the CF lungs environment. This implies that this spherical morphotype could be relevant in clinical settings and the cause of antibiotic treatment failure. Previous studies have reported the presence of CWD cells in animal models (*205*, *206*) and postulated that CWD cells may be implicated in diseases and their persistence (*207*). Until now, there are not methods to identify *P. aeruginosa* CWD cells in clinical samples. Therefore, a method for detecting *P. aeruginosa* CWD cells in CF sputum was developed using FISH on cultures of bacterial cells embedded in acrylamide: bis-acrylamide-based hydrogels. We demonstrated that this methodology successfully detects *in vitro* induced CWD cells and may be applied to sputum samples of CF patients.

Monahan *et al.* investigated the morphology of CWD planktonic cells using scanning electron microscopy, and images showed that this morphotype is characterised by a disrupted outer membrane and a compromised cell wall. This renders CWD cells more

susceptible to the activity of membrane-permeating agents, such as AMPs. In fact, it was demonstrated that the two AMPs nisin and LL-37 were effective in killing CWD planktonic cells (*165*). As we have shown that cells within *P. aeruginosa* biofilms convert to CWD spherical morphotypes, the following Chapter of this Thesis will, therefore, investigate the effect of a combination treatment on *P. aeruginosa* biofilms.

Chapter 4

Assessing the Efficacy of a Combination of Meropenem and Nisin for the Treatment of *P. aeruginosa* Biofilms

4 Assessing the Efficacy of a Combination of Meropenem with Nisin for the Treatment of *P. aeruginosa* Biofilms

4.1 Introduction

P. aeruginosa bacterial biofilms are associated with acute and chronic infections leading to high morbidity and mortality rates (*35*, *208*, *209*). *P. aeruginosa* is a versatile opportunistic pathogen that primarily infects immunocompromised individuals and it is able to survive and persist under extremely stressful conditions, such as in the lungs of CF patients (*12*, *210*) and the nose of patients with chronic rhinosinusitis (*211*). Infections caused by *P. aeruginosa* become very difficult to treat especially due to the ability of biofilms to survive antimicrobial exposure. Until now, many strategies and alternative therapies have been proposed as single or combined treatments for chronic *P. aeruginosa* infections (*212–217*), however the current therapies often fail or provide only short-term solutions (*218*, *219*). Thus, there is an open debate regarding the efficacy of combined therapies versus monotherapies and the clinical outcomes are still controversial (*220–222*). Nevertheless, a combination treatment is generally preferred for lowering the occurrence of antimicrobial resistance, exploiting antibiotic synergism and broadening the coverage provided by antimicrobials with different modes of action (*223*). In this Chapter, we investigated the efficacy of a combination of meropenem, a carbapenem antibiotic, with nisin, a cationic antimicrobial peptide for the treatment of *P. aeruginosa* biofilms. In Chapter 3 of this Thesis, we reported that concentrations of meropenem up to 10x MIC did not eradicate established biofilms but induced a morphological change into a viable CWD spherical morphotype. It has been discussed in the literature that this morphotype presents a different cell wall structure compared to that of bacillary *P. aeruginosa*. In fact, the CWD cells lose the outer membrane and have a defective cell wall, leaving the inner membrane exposed to the external environment. For this reason, CWD cells are more susceptible to the activity of membrane-permeating agents, such as antimicrobial peptides (AMPs) and non-ionic surfactants (*173*, *224*, *225*). In fact, it was found that planktonic CWD cells of *P.*

aeruginosa were efficiently and rapidly killed by the AMPs LL-37 and nisin, whereas these AMPs alone had no effect on cell viability when planktonic cells were in the bacillary state (*165*). Thus, we conjectured that a combination of meropenem and nisin could be effective in treating *P. aeruginosa* biofilms. We first tested different combinations of concentrations of meropenem and nisin on biofilms grown statically in 96-well microtitre plates using the crystal violet assay. This methodology easily allowed us to examine the effect of a high number of antibiotic combination concentrations for identifying the one that showed the greatest efficacy in eradicating biofilms. However, the crystal violet assay is not ideal for assessing biofilm viability as it does not distinguish between live and dead bacteria (*226*, *227*). Therefore, submerged biofilms were grown statically on coverslip-bottomed fluoro dishes or under flow conditions and stained with a membrane/dead cell stain mixture to evaluate the total and dead biofilm biomass after the antibiotic treatments. This methodology allows for the quantification of bacterial cell viability whilst simultaneously visualising individual bacterial cell morphology (*228*, *229*). The combination treatment was first investigated on static biofilms and then on flow cell biofilms. The flow cell technology allows the growth of biofilms in the absence of planktonic cells which are removed by flow and a detailed investigation of an array of biofilm parameters such as biofilm biomass, roughness, substratum coverage and biofilm thickness (*77*). Thus, this Chapter aims to investigate different concentration combinations of meropenem and nisin on 24 h microtitre biofilms for the identification of a combination that would eradicate or reduce the relative biofilm biomass. Then the effect of the combination on static biofilms was assessed using wide-field fluorescence microscopy and COMSTAT. Finally, the flow cell technology was utilised for assessing the efficacy of the combination in greater details and for examining biofilm structural changes after single and combined treatments.

4.2 Results

4.2.1 Susceptibility of static biofilms to meropenem and nisin

The susceptibility of *P. aeruginosa* PAO1 biofilms to combination treatments with meropenem and nisin was investigated. Static biofilms were grown in 96-well microtitre plates for 24 h and exposed to different concentration combinations of meropenem and nisin for 24 h. After treatments, the wells were washed with PBS and stained with crystal violet to determine biofilm biomass. The absorbance at 600 nm of the extracted crystal violet was used as a measure of relative biofilm biomass (see section 2.2.6.1). Not surprisingly, different concentrations of nisin combined with meropenem below the MIC and at the MIC (2 μg/mL), did not show a decrease in biofilm biomass. Instead, either a variable response or an increase in biofilm biomass was observed (Figure 4-1, A and B). The latter, was significant for meropenem below the MIC combined with nisin at 128 μg/mL and 256 μg/mL (Figure 4-1, A). More interestingly, a significant decrease in biofilm biomass occurred when nisin was combined with meropenem at 2.5x MIC (5 μg/mL) and 5x MIC (10 μg/mL). Specifically, the biofilm biomass significantly decreased with meropenem at 5 μg/mL combined with nisin at 32 and 64 μg/mL (Figure 4-1, C) and with meropenem at 10 μg/mL combined with nisin at 8, 32, 64 and 128 μg/mL (Figure 4-1, D). No difference in relative biofilm biomass was found for either meropenem or nisin single treatments (Figure 4-1, E and F). The combination concentration that provided the greatest decrease in biomass was meropenem at 5x MIC with nisin at 64 μg/mL. This was determined by comparison of meropenem 5 μg/mL with nisin at 64 μg/mL (**p = 0.0064) and meropenem 10 μg/mL with nisin at 64 μg/mL (**p = 0.0020) to untreated biofilm. In addition, 5x MIC is the clinical concentration used for β-lactam antibiotics to ensure efficacy of the antibiotic in the human body (*230*, *231*).

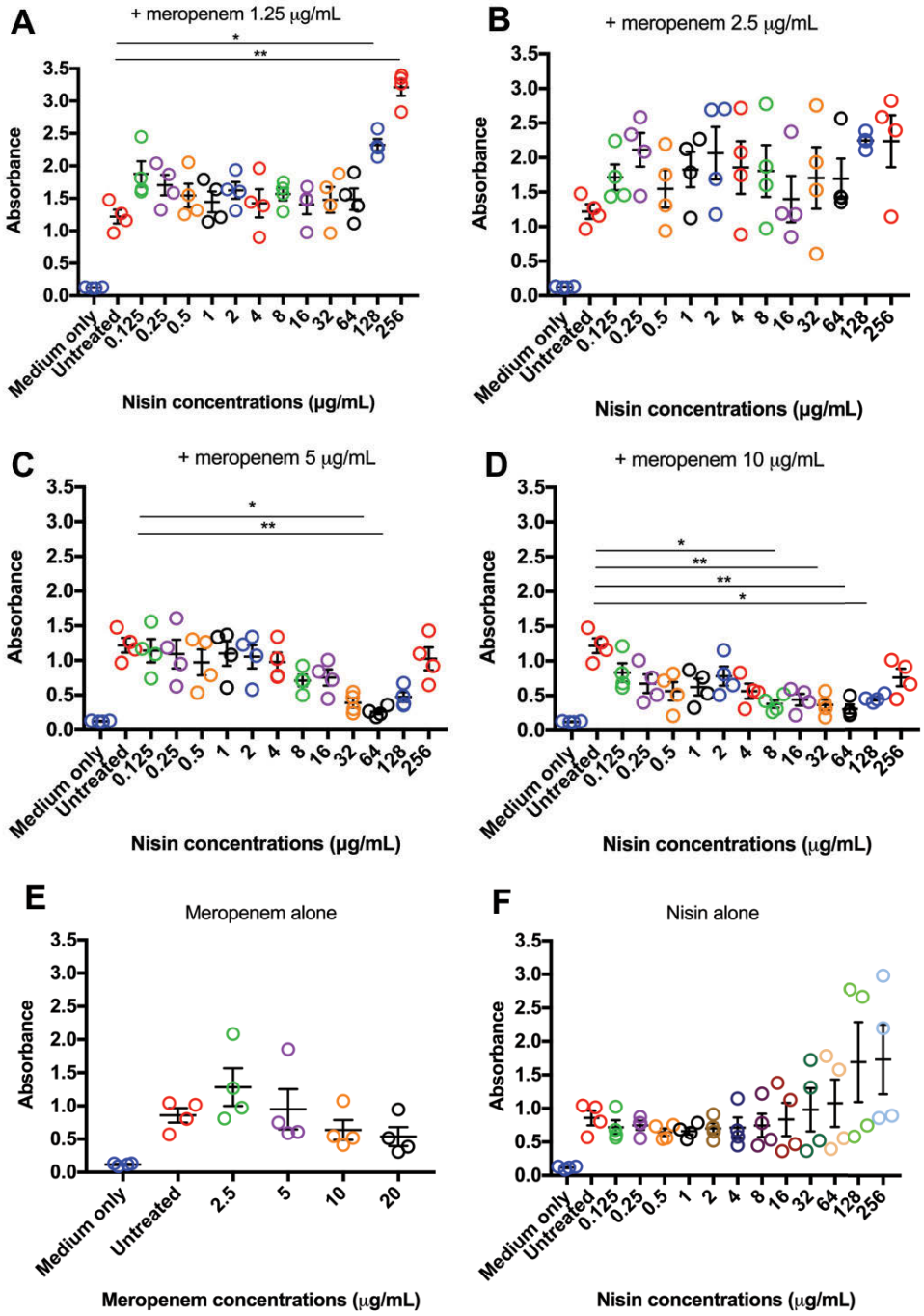

Figure 4-1: Extracted crystal violet readings for PAO1 static biofilms after 24 h treatment. Biofilms were treated with different nisin concentration in combination with A) meropenem sub-MIC (1.25 μg/mL) B) meropenem at about the MIC (2 μg/mL), C) meropenem 2.5x MIC (5 μg/mL), D) meropenem 5x MIC (10 μg/mL), E) meropenem control and F) nisin control. Figure 4-1 E is a repeat of figure 3-1 Bars represent mean ± SEM, n=4, including technical triplicates. Kruskal-Wallis test with comparison to untreated biofilms (*p≤0.05, **p≤0.01).

4.2.2 Microscopy visualisation of combination-treated static biofilms

In order to visualise and further quantify the meropenem-nisin combination effect, biofilms were grown statically for 24 h in a coverslip-bottomed fluoro dish (see section 2.2.6.2) and treated with meropenem at 10 μg/mL and/or nisin at 64 μg/mL for 24 h (see section 2.2.6.4). Biofilms were stained with the membrane dye AM1-43 that fluoresces green upon binding with the lipids of the membrane of both live and dead bacteria; whereas the dead biomass was visualised and quantified by staining the treated biofilms with the orange nucleic acid dye ethidium homodimer III (EthD-III) that binds to the DNA of cells with a compromised membrane (see section 2.2.7.1). Biofilms were analysed with wide-field fluorescence microscopy (see section 2.2.7.3) and quantified with COMSTAT (see section 2.2.4.1). The results demonstrated that the total biofilm biomass significantly decreased after treatments with all the compounds, individually or in combination. Specifically, the combination of meropenem with nisin gave the greatest decrease in total biomass (Figure 4-2, A) and a significant increase in dead biomass (Figure 4-2, B) compared to untreated biofilms, as also demonstrated in the fluorescent images (Figure 4-3). Moreover, the combination treatment significantly reduced biofilm thickness in comparison with untreated and single antibiotic treatments (Figure 4-2, C).

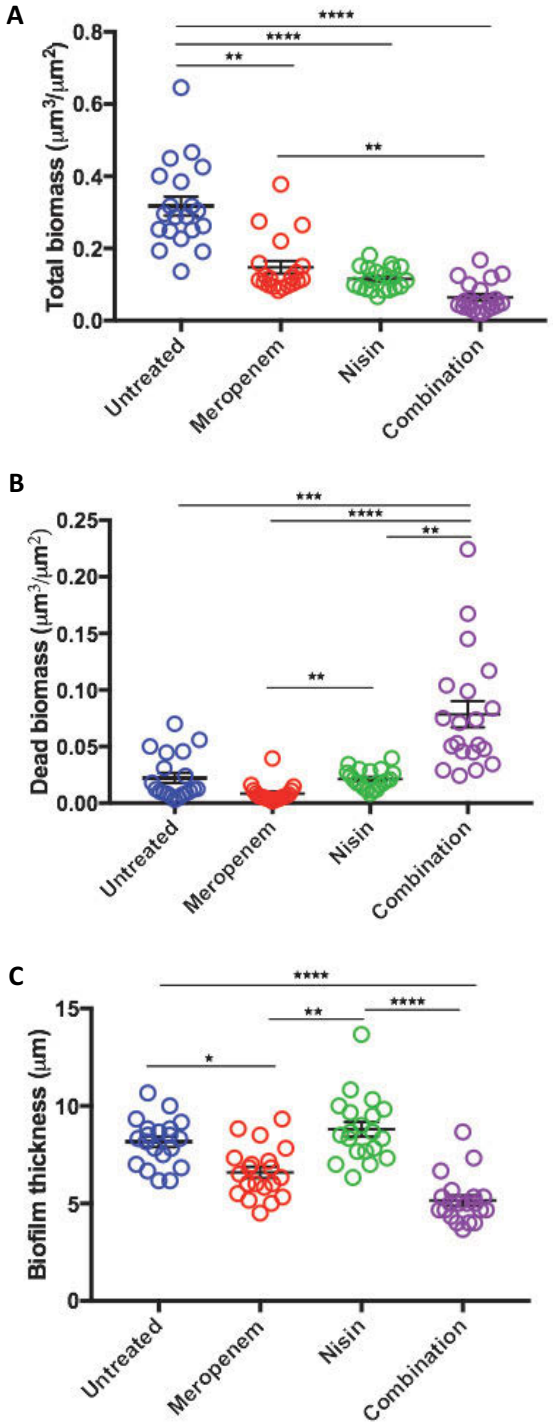

Figure 4-2: COMSTAT quantification of static biofilms after 24 h treatment. A) total, B) dead biofilm biomass and C) biofilm thickness after 24 h treatment with 10 µg/mL meropenem and 64 µg/mL nisin. Bars represent mean ± SEM, n=3. Kruskal-Wallis test with multiple comparison (*p≤0.05, ** p≤0.01, *** p≤0.001, **** p≤0.0001).

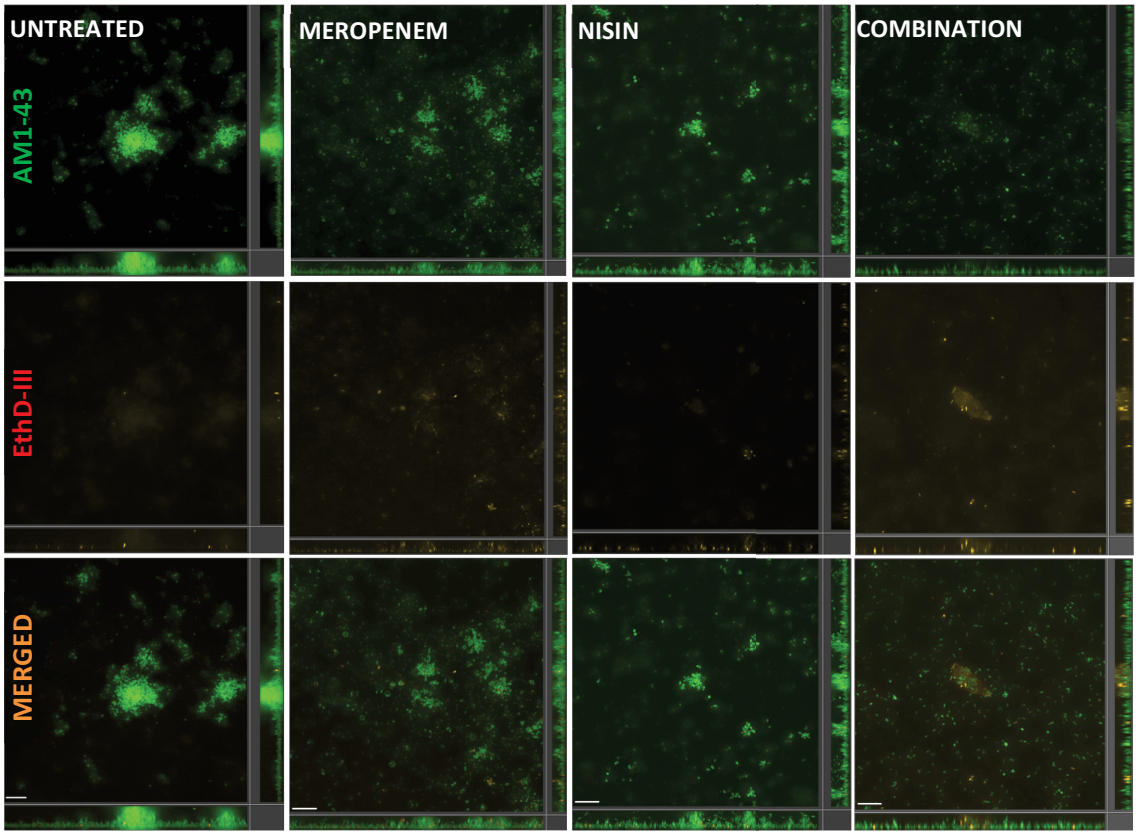

Figure 4-3: Section view of static fluoro dish biofilms after 24 h treatment. Biofilms were stained with AM1-43 (green, total biomass) and EthD-III (orange, dead biomass) for investigation of biofilm viability after 24 h treatment with 10 µg/mL meropenem and 64 µg/mL nisin. Images are representative of three independent experiments performed in duplicate. Scale bar 10 µm.

4.2.3 Microscopy visualisation of combination-treated flow cell biofilms

The flow cell technology was used in order to better assess biofilm structure and antibiotic efficacy under continuous flow of fresh medium and antibiotic. Biofilms were cultured in flow cells for three days (see section 2.2.6.3) and treated with meropenem at 10 µg/mL and nisin at 64 µg/mL for 24 h, individually and in combination (see section 2.2.6.5). Biofilms were stained as described in section 2.2.7.2, visualised with wide-field fluorescence microscopy (see section 2.2.7.3) and quantified with COMSTAT (see section 2.2.8.1). The quantification of the green fluorescence (indicating total biomass) demonstrated that nisin and combination treatments significantly reduced the total biofilm biomass compared to untreated and meropenem treated biofilms, which did not show a significant difference in total biofilm biomass (Figure 4-4, A). The reduction of total biomass, displayed in green, was also demonstrated with fluorescence images (Figure 4-5). In contrast, the quantification of the orange fluorescence (indicating dead biomass) revealed that the combination treatment caused a significant increase in dead biomass (Figure 4-4, B) compared to untreated and single treatments. The increase in dead biomass, displayed in orange, was also demonstrated with fluorescence images (Figure 4-5).

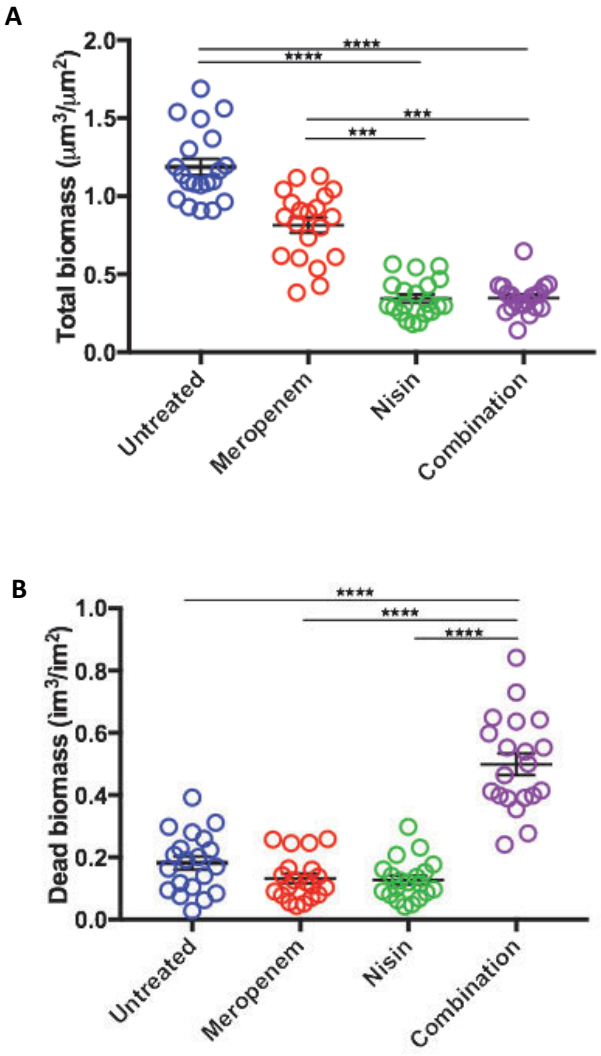

Figure 4-4: COMSTAT quantification of flow cell biofilms after 24 h treatment. A) Total biofilm biomass and B) dead biofilm biomass quantification after 24 h treatment with 10 µg/mL meropenem and 64 µg/mL nisin using COMSTAT. Bars represent mean ± SEM, n=3. Kruskal-Wallis test with multiple comparison (*** p≤0.001 **** p≤0.0001).

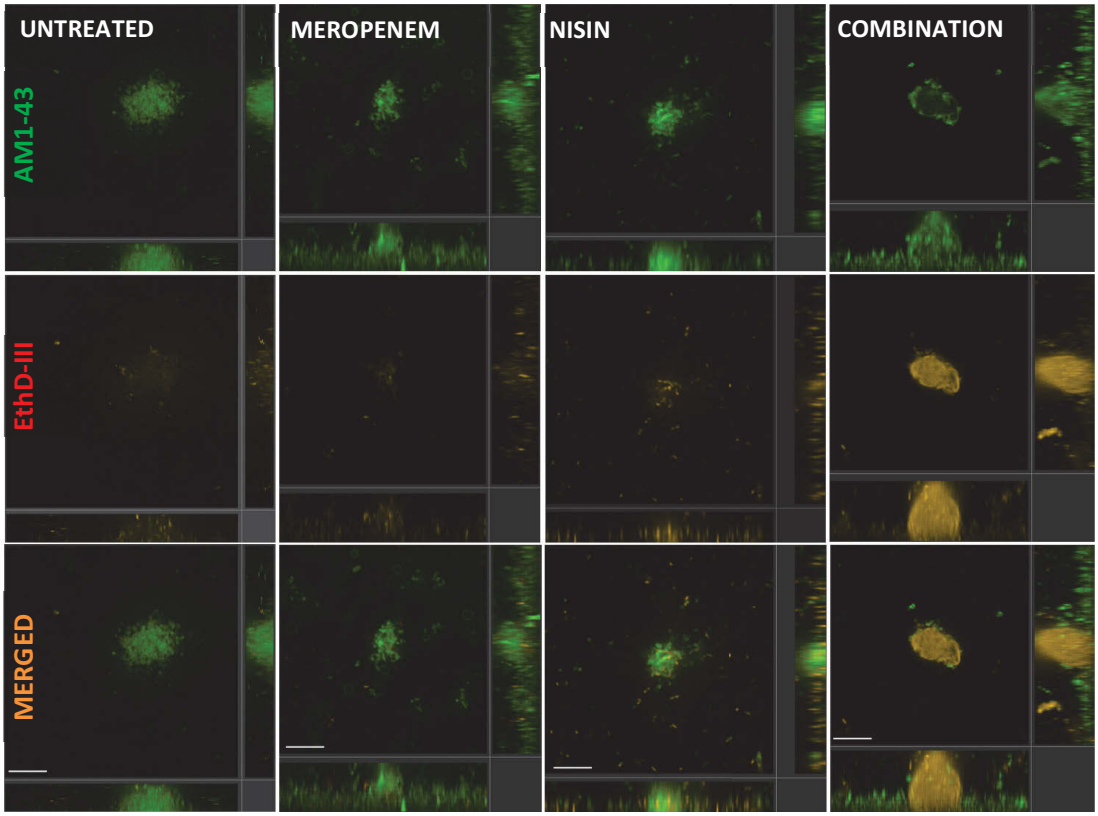

Figure 4-5: Cross sections images of flow cell biofilms after 24 h treatments. Biofilms were stained with AM1-43 (green, total biomass) and EthD-III (orange, dead biomass) for investigation of biofilm viability after 24 h treatment with 10 µg/mL meropenem and 64 µg/mL nisin. Images are representative of three biological replicates. Scale bar 10 µm.

4.2.4 Colony forming unit assay of combination-treated flow cell biofilms

To further confirm the effectiveness of the combination, the colony forming unit (CFU) assay was performed. Flow cell biofilms were grown as detailed in section 2.2.6.3 and antibiotic-treated as described in section 2.2.6.5. Biofilms were then detached from the flow cell and harvested and the CFU/mL was determined as detailed in section 2.2.6.6. The results showed that the combination treatment significantly reduced the viability of flow cell biofilms after 24 h of treatment compared to untreated biofilms (Figure 4-6). This result further confirmed the efficacy of the combination that was previously determined with microscopy. Also, meropenem-treated biofilms did not show a significant reduction in biofilm viability compared to untreated biofilms confirming that *P. aeruginosa* biofilms tolerate meropenem exposure.

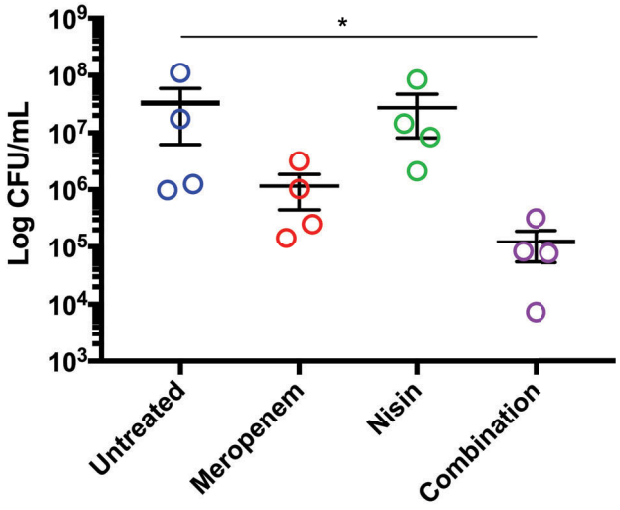

Figure 4-6: Biofilm viability after 24 h treatments determined with the CFU count assay. Biofilm viability determined with the CFU count after 24 h treatment with 10 µg/mL meropenem and 64 µg/mL nisin. Bars represent mean ± SEM, n=3. Kruskal-Wallis test with multiple comparison (* p≤0.05).

4.2.5 Nisin efficiently killed meropenem-induced CWD spherical cells

The number of CWD spherical cells was counted in meropenem and combination-treated flow cell biofilms to evaluate nisin efficiency in killing the meropenem-induced CWD cells. The percentage of CWD cells decreased from 7.84 % to 0.65 % after the combination treatment (Figure 4-7). This indicates therefore that nisin was efficient in lysing almost the entire population of CWD cells present in the biofilms. This result is consistent with the outcomes of the CFU assay which showed that there is 1-log difference between the meropenem-treated and combination-treated biofilms (Figure 4-6).

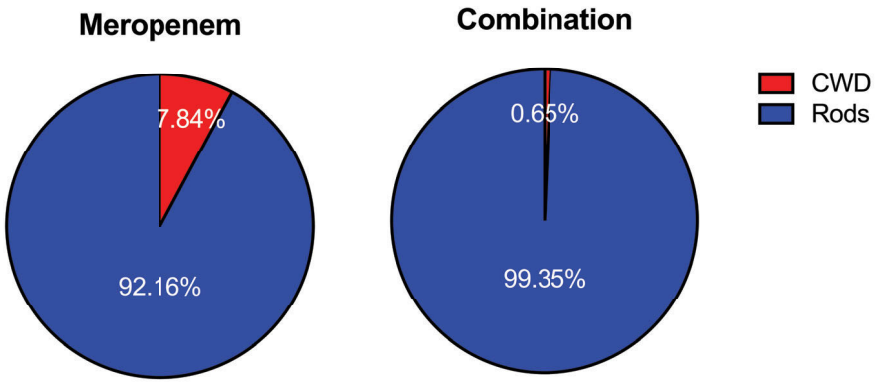

Figure 4-7: Ratio of CWD and rod cells in meropenem and combination-treated flow cell biofilms. All cells were counted from 20 images randomly selected from three independent experiments and results are expressed as average percentage.

4.2.6 Investigation of biofilm structure after antibiotic treatment

The structure of the antibiotic-treated biofilms was investigated to further assess the effect of the treatments. Therefore, the green channel was quantified using COMSTAT for determining the substratum coverage, roughness coefficient and the maximum thickness. Biofilms treated with nisin showed similar characteristic to the untreated biofilms, where cells were mainly aggregated into microcolonies (Figure 4-8, A). On the other hand, biofilms treated with meropenem and the combination showed more

coverage of the substratum (Figure 4-8, A). These observations were confirmed by determining the substratum coverage percentage. Meropenem and combination-treated biofilms had a substratum coverage of 19.13 ± 0.79 % and 19.67 ± 0.47 %, respectively. This was significantly higher than the coverage of untreated and nisin-treated biofilms, which was 4.76 ± 0.22 % and 4.92 ± 0.27 %, respectively (Figure 4-8, B). All biofilms, untreated and treated, had a roughness coefficient greater than one, meaning that they all revealed a patchy structure (Figure 4-8, C). The maximum thickness of nisin-treated biofilms presented a significant reduction when compared to the other treatments and untreated biofilms. Interestingly, the combination treatment did not show a difference in biofilm thickness when compared to the untreated and meropenem-treated biofilms (Figure 4-9, A and B). A summary of the biofilm structure characteristics is presented in table 4-1.

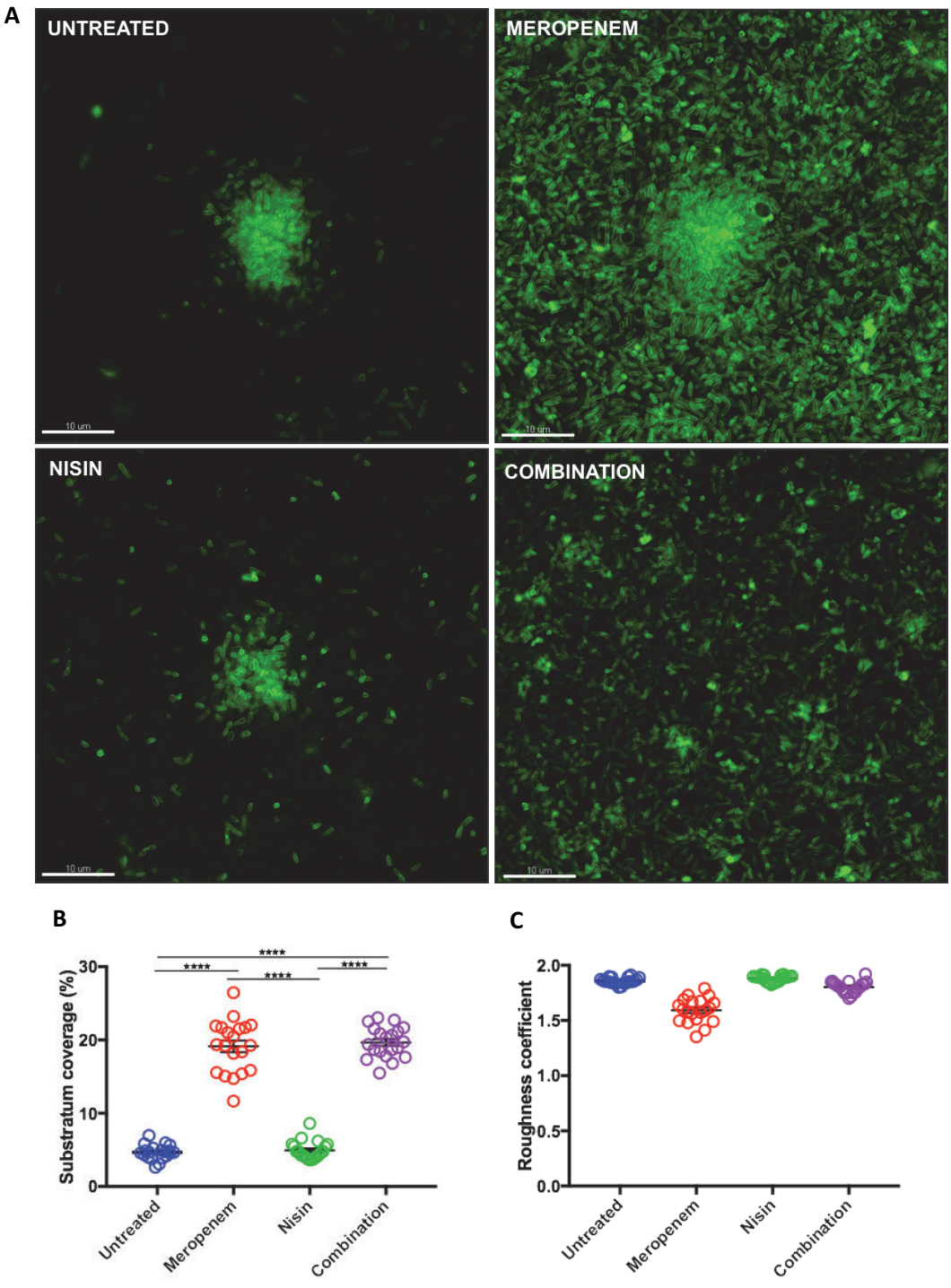

Figure 4-8: Biofilm substratum coverage and roughness after 24 h treatment. A) Fluorescent images of the substratum of untreated, meropenem, nisin and combination-treated biofilms. B) Substratum coverage percentage and C) roughness coefficient quantified from green fluorescence. Images are representative of three independent experiments. Bars represent mean ± SEM, n=3. Kruskal-Wallis test with multiple comparison (** p≤0.01, **** p≤0.0001).

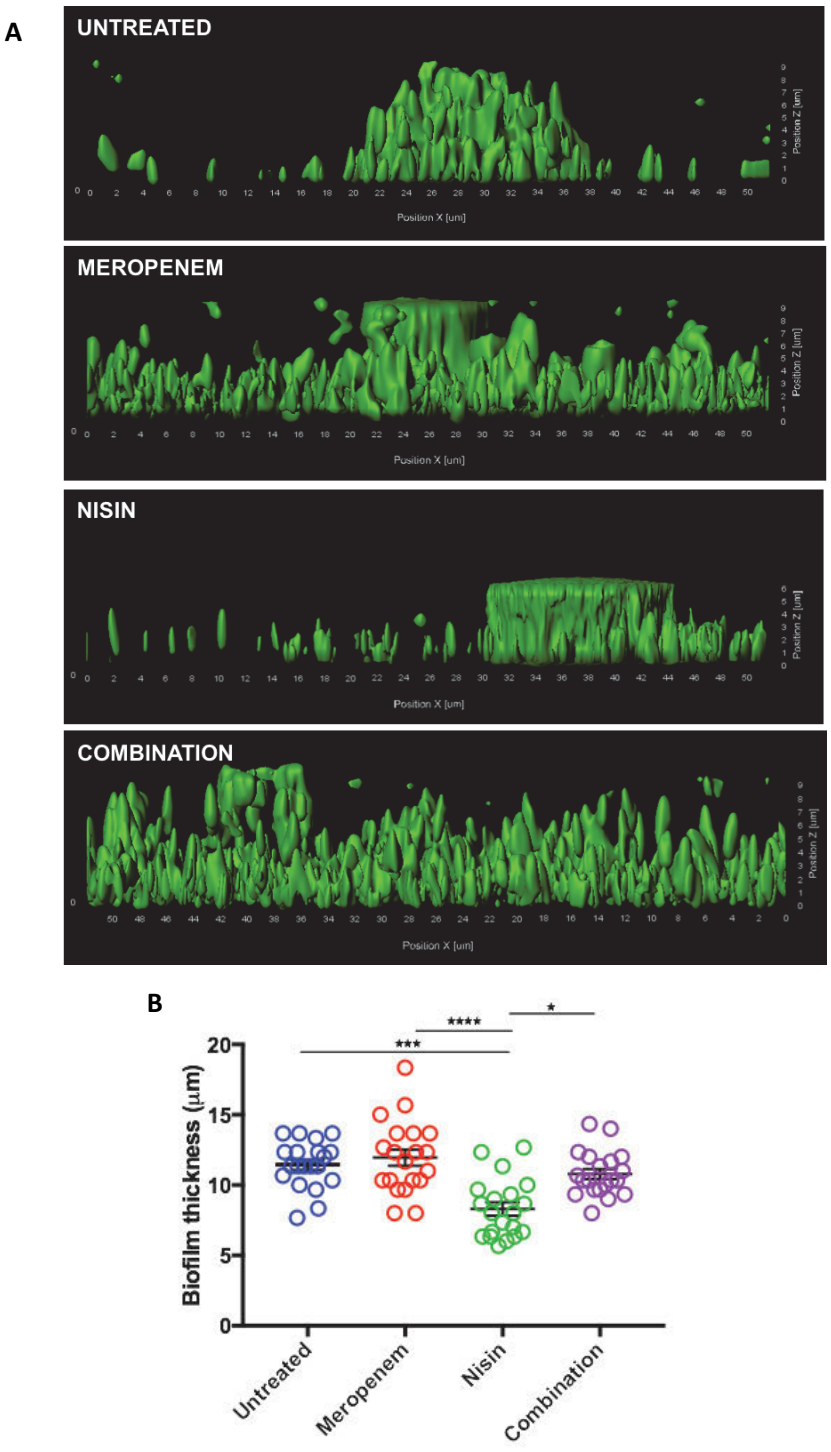

Figure 4-9: Biofilm thickness after 24 h treatment. A) 3D orthogonal view of antibiotic-treated biofilms. A surface was created on the green fluorescence to better visualise biofilm thickness using Imaris. B) COMSTAT quantification of biofilm thickness. Images are representative of three independent experiments. Bars represent mean ± SEM, n=3. Kruskal-Wallis test with multiple comparison (*p≤0.05, *** p≤0.001, **** p≤0.0001).

Moreover, images of the combination-treated biofilms were further analysed to investigate whether the dead biomass dispersed from the biofilm. A visual analysis of the combination-treated biofilms revealed that the dead biomass remained encased into the biofilm matrix (Figure 4-10, A and B) and interestingly, it was noticed that live bacterial cells surrounded the dead biomass (Figure 4-10, A and B).

A

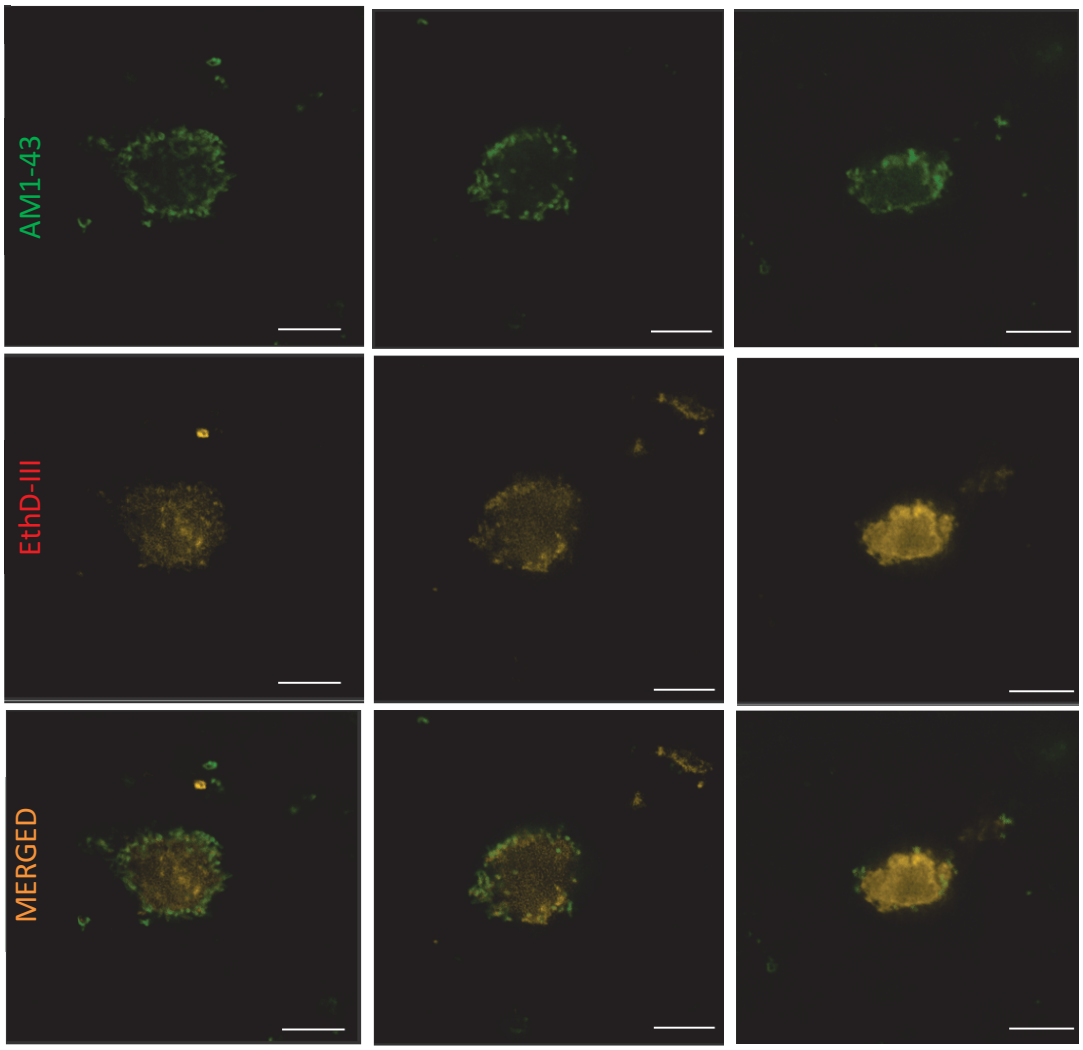

B

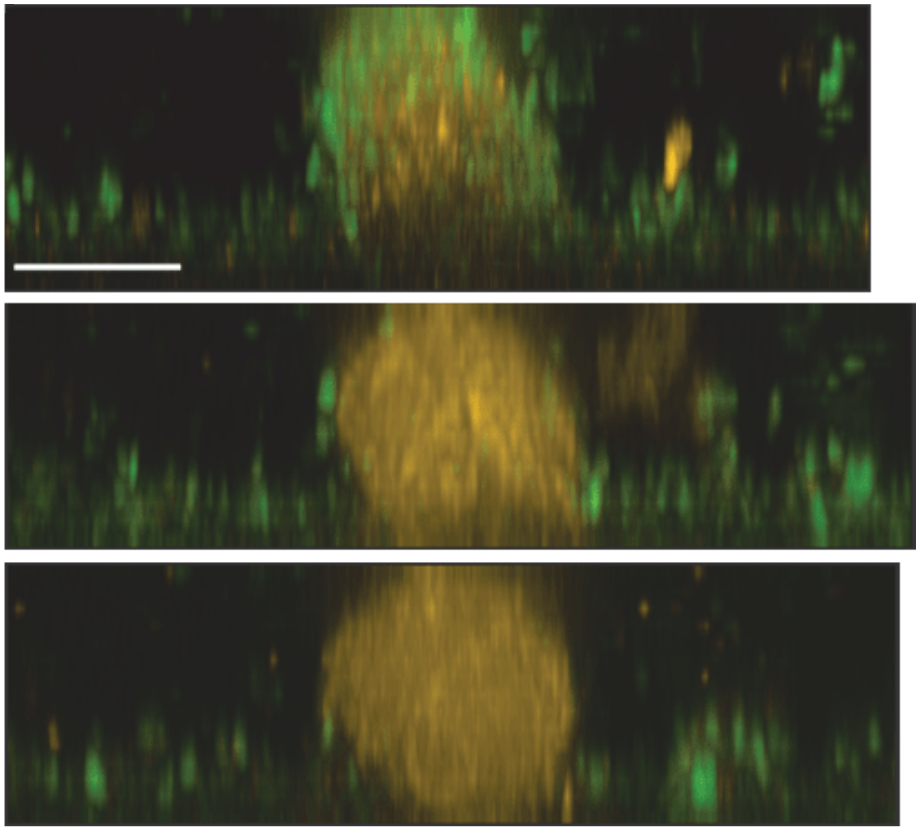

Figure 4-10: Visual analysis of dead biomass in combination-treated biofilms. Cross sections of combination-treated biofilms along A) XY axis and B) YZ axis. Total biomass is visualised in green and dead biomass in orange. Images are representative of three biological replicates.

Treatments	Substratum coverage (%)	Roughness coefficient	Maximum thickness (μm)	Total biomass ($\mu m^3/\mu m^2$)	Dead biomass ($\mu m^3/\mu m^2$)
Untreated	4.67 ± 0.22	1.85 ± 0.01	11.45 ± 0.37	1.18 ± 0.05	0.18 ± 0.02
Meropenem	19.13 ± 0.79	1.59 ± 0.02	11.95 ± 0.57	0.81 ± 0.04	0.13 ± 0.02
Nisin	4.92 ± 0.27	1.88 ± 0.01	8.3 ± 0.46	0.34 ± 0.02	0.13 ± 0.01
Combination	19.67 ± 0.47	1.80 ± 0.01	10.78 ± 0.35	0.34 ± 0.02	0.49 ± 0.03

Table 4-1: Summary table of biofilm structural characteristics and viability quantified with COMSTAT. Data represent mean ± SEM of three biological replicates.

4.3 Discussion

In Chapter 3, we demonstrated that a subset of the population of biofilm cells responded to 5x MIC meropenem treatment by converting their morphology from a rod-shaped bacterium to a CWD spherical morphotype similar in morphology to those observed in planktonic culture. We also showed that the CWD cells found in biofilms were similar in size to the ones found in the planktonic state. It was previously demonstrated that planktonic *P. aeruginosa* CWD cells could be rapidly killed by the AMPs nisin and LL-37, causing the CWD cells to lyse and release the cellular content into the external environment (*165*). Therefore, we investigated whether a combination of meropenem and nisin could eradicate or decrease biofilm biomass. In our study, we utilised the cationic peptide nisin as it is one of the most characterised AMPs (*232*), its mode of action is well known (*233*) and resistance to nisin has not yet been documented outside the laboratory setting (*234*). Nisin binds to the Lipid II receptor creating pores in the cell membrane and consequently causing cell lysis (*235*, *236*). Lipid II is found in the membrane of both Gram-positive and Gram-negative bacteria and it is the precursor of peptidoglycan synthesis, responsible for the cell wall rigidity (*237*).

In this Chapter, we demonstrated the efficacy of the combination treatment on *P. aeruginosa* PAO1 biofilms, under different conditions. The results from the microtitre plate assays showed that *P. aeruginosa* static biofilms were not susceptible to the activity of nisin alone, even at the highest concentrations tested (Figure 4-1, E). This result was expected for the following reasons: *P. aeruginosa* is a Gram-negative bacterium with a low membrane permeability and nisin is a large size peptide (1.8-4.6 kDa), therefore nisin might not be able to cross the outer membrane and reach Lipid II (*108*); biofilms are intrinsically more tolerant to antimicrobials than planktonic cells therefore nisin might not be able to diffuse through the biofilm matrix (*238*). The fact that nisin was not effective on *P. aeruginosa* biofilms is also in agreement with the study conducted by Monahan *et al.* showing that nisin was not effective against planktonic *P. aeruginosa.* On the other hand, the combination of nisin with meropenem at concentrations above the MIC demonstrated a reduction in the relative biofilm biomass (Figure 4-1, C and D). In particular, meropenem at 10 μg/mL (5x MIC)

with nisin at 64 μg/mL showed the highest reduction of relative biofilm biomass. It has been previously demonstrated that nisin in combination with other antibiotics efficiently eradicated pre-established biofilms, whereas when used alone did not affect biofilm growth (*239*). In Chapter 3, we showed that meropenem at 5x MIC induced the morphological conversion to the CWD spherical morphotype. As these cells lack an intact outer membrane consequently, Lipid II might be exposed to the external environment. It could perhaps be for this reason that nisin was effective in causing cell lysis in meropenem-induced CWD spherical cells, as they lack the double membrane characteristic of Gram-negative bacteria.

Interestingly, it was also noticed that combinations of nisin with meropenem at concentrations below and at the MIC stimulated biofilm growth (Figure 4-1, A and B). Other studies observed similar results when exposing *P. aeruginosa* biofilms to antibiotic concentrations below the MIC and demonstrated that biofilm growth stimulation was caused by an increased alginate production (*240–242*). Further studies are needed to investigate whether meropenem might stimulate alginate production at concentrations below the MIC or cause the activation of other signals since the mechanisms of biofilm stimulation are complex and may differ between different classes of antibiotics (*243*). It is possible that meropenem in this circumstance is able to increase alginate production and consequently reduce the effect of nisin, yet the interaction between meropenem and nisin needs to be explored in more detail. However, we could not confirm whether the combination of these two antibiotics had any interaction, either a synergistic or antagonistic effect as no MIC was found for nisin and therefore we could not determine the FIC index (*244*). The crystal violet assay allowed the identification of the best concentration combination for biofilm eradication, however, crystal violet also binds extracellular DNA, polysaccharides and proteins; therefore it cannot be used as an indicator of cell viability (*245*).

We then assessed biofilm viability by visualising antibiotic-treated biofilms with wide-field fluorescence microscopy and quantifying biofilm biomass using COMSTAT (*74*). The total biomass was visualised and quantified by staining the treated biofilms with the membrane dye AM1-43 (green), whereas the nucleic acid dye EthD-III was used to visualise the dead biomass (orange).

Microscopy investigation of static biofilms grown on the coverslip-bottomed fluoro dish and treated with a combination meropenem at 10 µg/mL (5x MIC) with nisin at 64 µg/mL did not present microcolonies but only a thin layer of cells attached to the substratum (Figure 4-3) in comparison with the untreated and single treatment biofilms, which were characterised by the presence of microcolonies (Figure 4-3). Furthermore, the quantification of the biofilm biomass confirmed that the combination was effective in significantly reducing the total biomass (Figure 4-2, A) and significantly increasing the dead biomass of static biofilms (Figure 4-2, B). In addition, biofilms treated with the antibiotic combination showed a significant decrease in thickness compared to the untreated and single treatment biofilms (Figure 4-2, C), confirming that only a thin layer of cells remained viable after the treatment.

The effect of the combination was further investigated in flow cell biofilms, as we wanted to explore whether the combination was effective in eradicating stronger biofilms grown under a continuous flow of fresh nutrients. Fluorescent images showed that the antibiotic combination of meropenem and nisin was effective in reducing biofilm viability also in flow cell biofilms (Figure 4-5), as confirmed by the results of COMSTAT quantification in which combination-treated biofilms presented significantly less total biomass (Figure 4-4, A) and significantly higher dead biomass (Figure 4-4, B) than the untreated and single treatment biofilms. The efficacy of the combined formulation was furthermore confirmed by the colony forming unit assay, which revealed a significant decrease in biofilm viability compared in relation to untreated and single treatment biofilms (Figure 4-6).

We hypothesise that the increase in dead biomass is caused by the efficiency of nisin in lysing the spherical morphotype cells induced by meropenem as these are more susceptible to the activity of membrane-permeating agents. To confirm this, spherical cells were counted in meropenem-treated and combination-treated biofilms. The results showed that the percentage of CWD cells in the combination-treated biofilms was 0.65 % compared to the 7.65 % found in the meropenem-treated biofilms (Figure 4-7), indicating the effectiveness of nisin in lysing the spherical morphotype cells. This result was also consistent with the outcome of the CFU assay, which showed 1-log difference in viability between meropenem and combination-treated biofilms. Despite the low conversion to the CWD morphotype in meropenem-treated samples, the

reduction in total biofilm biomass was found significant when biofilms were treated with the antibiotic combination (Figure 4-4, A). The cells present in the outer part of biofilms are more exposed to the activity of antibiotics and more metabolically active than those in the inner part and therefore, the target of β - lactam antibiotics, such as meropenem. We therefore speculate that these cells may have undergone the morphological transition to CWD cells, and were then lysed by nisin and washed away by the flow of the media. This could then possibly explain the observed significant reduction in biomass upon the combination treatment.

Interestingly, we also determined that the thickness of the combination-treated biofilms did not decrease compared to the other treatments (Figure 4-9, A and B). To further investigate this, fluorescent images were carefully visualised and it was noticed that the dead biomass remained trapped within the biofilm matrix and live bacterial cells were surrounding the dead biomass (Figure 4-10, A and B). While time constraints did not allow us to investigate this phenomenon and analyse the phenotype of those live bacterial cells, a similar behaviour was noticed in a study by Lin Chua *et al.* in which they demonstrated that colistin-tolerant *P. aeruginosa* subpopulations migrated to the top of dead biofilms activating quorum sensing factors for promoting the formation of new antibiotic-tolerant microcolonies (*246*), or simply these cells migrated to the top of the dead biomass seeking iron (*247*). Iron is an important source for normal biofilm development (*248*) and it was shown that iron limitation induces twitching motility (*249*). Therefore, we postulated that these cells might be a subpopulation of antibiotic-tolerant cells (*250*) that started to migrate to the top of the dead biomass looking for fresh nutrients, such as iron. We, consequently, assumed that biofilm thickness did not decrease in the combination-treated biofilms due to the presence of these subpopulation surrounding the matrix-encased dead biomass.

It was also noticed that the structure of the biofilms changed after single and combined antibiotic treatments. The results from the substratum coverage and roughness coefficient suggested that the combination treatment caused a biofilm structural change in comparison to untreated and nisin-treated biofilms. In the meropenem and combination-treated biofilms, cells mainly covered the substratum (Figure 4-8, A), while the untreated and nisin-treated biofilms presented cells aggregated into separated microcolonies (Figure 4-8, A). Nisin-treated biofilms showed

similar structure to the untreated biofilms, growing in microcolonies (Figure 4-8, A) which was confirmed by the substratum coverage percentage (Figure 4-8, B) and roughness coefficient (Figure 4-8, C). The treatment with nisin also caused a significant decrease in the total biomass (Figure 4-4, A) and thickness (Figure 4-9, A and B) but no increase in dead biomass was determined (Figure 4-4, B). We, therefore, reasoned that nisin might cause dispersion of biofilm cells as some antimicrobial peptides have been shown to induce biofilm dispersal. Alternatively, nisin could induce initial killing followed by a resumed biofilm development (*251*, *252*). Further analysis looking at the effluent of biofilms treated with nisin alone is required for determining whether nisin could induce biofilm dispersal.

Overall, our results suggested that the combination treatment of meropenem at 5x MIC with nisin at 64 μg/mL efficiently reduced biofilm viability in biofilms due to the ability of meropenem to induce the morphological transition to the CWD spherical morphotype and the efficiency of nisin in lysing the spherical cells. Thus, this antibiotic combination may represent a promising strategy for treating *P. aeruginosa* biofilms like the ones found in respiratory infections, such as in chronic rhinosinusitis. Chapter 5 of this Thesis will then explore the suitability and the effectiveness of this antibiotic combination for nasal administration.

Chapter 5

Development of a Novel Nasal Formulation for the Treatment of *P. aeruginosa* Biofilms

5 Development of a Novel Nasal Formulation for the treatment of *P. aeruginosa* Biofilms

5.1 Introduction

Biofilm-associated infections caused by *P. aeruginosa* are found in various disease settings such as pathologies that affect the respiratory tract (*253*, *254*). In 2004, the presence of biofilms in chronic rhinosinusitis was discovered and, in the following years, other studies confirmed biofilm formation on the nasal mucosa of patients suffering from chronic rhinosinusitis (*23*, *255*, *256*). Until now, the available treatments have not shown a long-term solution, especially with the rise of antibiotic-resistant bacteria *P. aeruginosa* (*22*). In chronic rhinosinusitis, biofilms form in the sinonasal mucosa, where they cause a reduction in the ciliary beat frequency or the complete disruption of the cilia. Biofilms growing in the nasal mucosa are very difficult to treat due to the high resistance to antimicrobials (*257*).

In Chapter 4, it was demonstrated that a combination of meropenem at 5x MIC with nisin at 64 μg/mL was effective in reducing biofilm viability due to the ability of meropenem to induce the morphological transition to the CWD spherical morphotype and nisin to lyse the CWD cells. Therefore, in this Chapter, the development of a nasal formulation comprised of meropenem and nisin was investigated as a possible therapy for the treatment of *P. aeruginosa* biofilms in the nose. The nasal administration was chosen to directly target biofilms on the mucosa and to ensure a rapid onset of action.

Different parameters regulate the deposition of nasal drug formulations, often associated with the design of the nasal device and the valve used to generate the spray, the atomised formulation, patient handling of the device during administration and inhalation of the spray, and the anatomical complexity of the nose (*258*). Droplets size and plume characterisations are generally accepted as predictive of aerosol deposition performances in the nose since these parameters directly affect the delivery of the drug to the intended biological target (*130*). The Food and Drug Administration (FDA) requirement for the droplets size suitable for nasal delivery is between 20 and 200 μm since particles below 10 μm can be inhaled and reach the lungs or deposited in the throat (*259*). The deposition of nasal products is generally

investigated using *in vitro* models such as the silicone nasal cast which originated from a Japanese male cadaver Koken (Koken LM-005, Bunkyo-ku Tokyo, Japan) and the Pharmacopeia impactors (*260*). Moreover, a modified chamber for the study of the deposition and permeation of nasal products was previously designed by Pozzoli *et al.* (*261*) based on the design of the Pharmacopeia impactors. These apparatuses, however do not allow the study of nasal formulations on biofilms. Therefore, for the purpose of this study, a novel nasal apparatus was designed to assess the effect of nasal formulations on biofilms grown on Snapwell™ cell culture inserts.

The target area for optimal drug absorption in the nasal cavity is the nasal mucosa (*110*). Thus, the apparatus was developed referring to literature studies on the nasal anatomy, which showed that the distance between the nostril and the end of the nasal mucosa is about 10 cm (*262*). Generally, the tip of the nasal pump enters the nostril for about 1.5 cm (*125*) therefore, the distance of 5 cm between the device inlet and the deposition area was chosen for delivering the formulation approximately at the centre of the mucosa. Moreover, this distance was used with the Spraytec (Malvern Instruments, Oxfordshire, UK) to ensure that the droplet size was similar to the *in vivo* situation, as it has been demonstrated that different actuation distances significantly decreased the aerodynamic diameter of the emitted spray droplets (*263*). In order to validate the novel apparatus as an *in vitro* tool for the assessment of transport and deposition of nasal sprays, fluorescein-sodium (Flu-Na) was used. Flu-Na is a manufactured organic compound and dye (MW 367 Da) widely used as a fluorescent tracer for many applications. For the purpose of this study, Flu-Na at a concentration of 0.25 mg/mL was used as a marker to visualise the deposition of the plume on Snapwell™ cell culture inserts and to assess the layer integrity of the RPMI 2650 cells after the delivery of the formulations. Moreover, this formulation was also assessed for its plume characteristics in order to confirm that this concentration does not modify the device atomisation. The novel apparatus was designed for assessing delivery performances of a local nasal administration without the use of inhalation flow. The absence of the flow reduces the dispersion of the plume droplets that may occur due to the geometry of the device but it has been reported that changes in the inspiratory flow rate (0 to 60 L/min) do not affect the deposition efficiency of nasal sprays (*264*) and does effect deposition location (*265*, *266*). Moreover, patients

suffering from chronic rhinosinusitis present sinus blockage and in some cases nasal polyps which could lead to airflow limitation (*267–269*). Therefore, to overcome possible deposition issues due to the use of an inspiratory flow rate, the novel apparatus was designed without flow".

In this Chapter, the development and evaluation of a nasal formulation containing meropenem (carbapenem antibiotic) and nisin (cationic antimicrobial peptide) were assessed for the treatment of *P. aeruginosa* biofilm infections. A simple and accurate UV method was validated to quantify meropenem in unknown samples after deposition and transport studies on RPMI 2650 nasal cells. No analytical method could be developed for the quantification of nisin due to the complex matrix of the product (*232*). To overcome this limitation, an accurate characterisation of the spray plume was performed by investigating the droplet size, droplet size distribution, obscuration profile and plume angle. These parameters may be then utilised for the prediction of nisin deposition performance. Finally, the nasal spray formulation was assessed for its efficacy on biofilm viability grown on Snapwell™ cell culture inserts. Formulations containing meropenem alone, nisin alone and 0.9% NaCl were evaluated for their characteristics and biological effect also as single compounds.

5.2 Results

5.2.1 UV method validation for meropenem quantification

A simple but accurate method for the detection and quantification of meropenem (Figure 5-1, A) in unknown samples was developed following the ICH Q2 (R1) guidelines (see section 2.2.9) (*270*). The maximum UV absorbance for meropenem was determined between 200 and 400 nm and found to be 298 nm (Figure 5-1, B) in accordance with the literature (*181*, *182*).

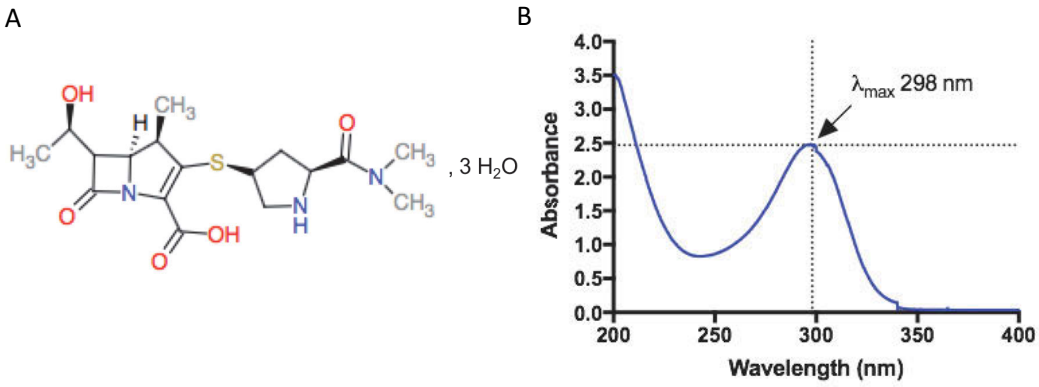

Figure 5-1: Meropenem trihydrate. A) Meropenem trihydrate chemical structure. B) UV spectrum for meropenem trihydrate in 0.9 % NaCl. Arrow indicates the wavelength (λ) with the maximum absorbance.

The range of concentration chosen for the validation of the method was 1.5 to 75 μg/mL, including the 80 and 120 % of the target concentration, which was 9 μg/mL, as required by the ICH guidelines. The linearity study showed a linear regression with a correlation coefficient R^2 = 0.9999 (Figure 5-2, A). The accuracy of the method was evaluated by analysing in triplicate the 80 – 100 – 120 % of the target concentration and it showed a RSD % < 1 % (Figure 5-2, C). The precision of the analytical procedure was considered at two levels: repeatability and intermediate precision (different days). The repeatability was tested by analysing six times the target concentration and the results showed a RSD % < 2 %. The intermediate precision was evaluated by measuring the concentration range of 1.5 to 75 μg/mL on three different days, obtaining a RSD % < 1 % (Figure 5-2, B). The limit of quantification (LOQ) for meropenem was found to be 0.24 μg\mL and the limit of detection was 0.079 μg\mL.

A

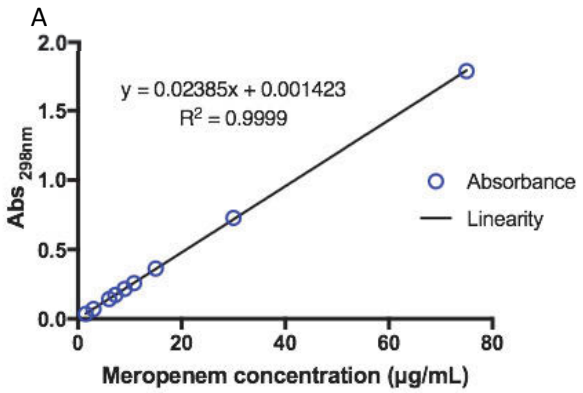

B

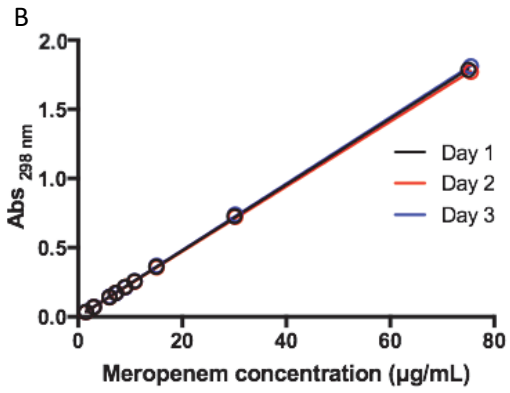

C

Concentration (mg/mL)	Mean abs (nm)	Mean RSD (%)
10.8	0.256	0.8
9	0.215	
7.2	0.172	

Figure 5-2: Meropenem UV method validation. A) Linearity of meropenem within the concentration range of 1.5 to 75 µg/mL. B) Intra-day precision with RSD = 1.5 %. C) Accuracy of the method for the 80, 100 and 120 % of the target concentration.

5.2.2 Formulation characterisation

The nasal spray formulations were prepared as detailed in section 2.2.10.1. and analysed with laser diffraction for the characterisation of droplet size, droplet population and obscuration profile. Moreover, the plume angle was measured by recording the emission of the plume using a high-speed camera (Phantom Phantom Miro C-210, Vision Research, USA). These analyses were performed to determine whether the nasal formulations were suitable for nasal delivery. A spray solution of 0.25 mg/mL Flu-Na was also characterised to allow comparison with the other formulations since it was used for the validation of the novel nasal apparatus.

5.2.2.1 Droplet size measurements

In order to determine whether the formulations were suitable for nasal delivery, the droplet size was determined (see section 2.2.10.2). The results for the droplet size measurements of all formulations are summarised in Table 5-1 whereas the droplet size distribution is represented in Figure 5-3. The spray formulations revealed no significant difference in the droplet size measurements ($p>0.999$) (Figure 5-3) for all the formulations tested. The median volume diameter (Dv_{50}) calculated as average of all the formulations was 31.57 ± 1.14 μm. Therefore, all the spray solutions proved to be suitable for nasal delivery in terms of the droplet size exiting the device as they were found to have the required range for nasal deposition (20 – 200 μm). The percentage of the droplet population below 10 μm for meropenem, nisin and the combination was 8.06 ± 3.27, 8.07 ± 2.88 and 6.56 ± 3 %, respectively. To better investigate whether this population represented a respirable fraction, the aerosol deposition performance of meropenem nasal formulation was evaluated using the Andersen Cascade Impactor with a flow rate of 28.3 L/min, in accordance with the FDA guidelines (see section 5.2.2.4) (*271*).

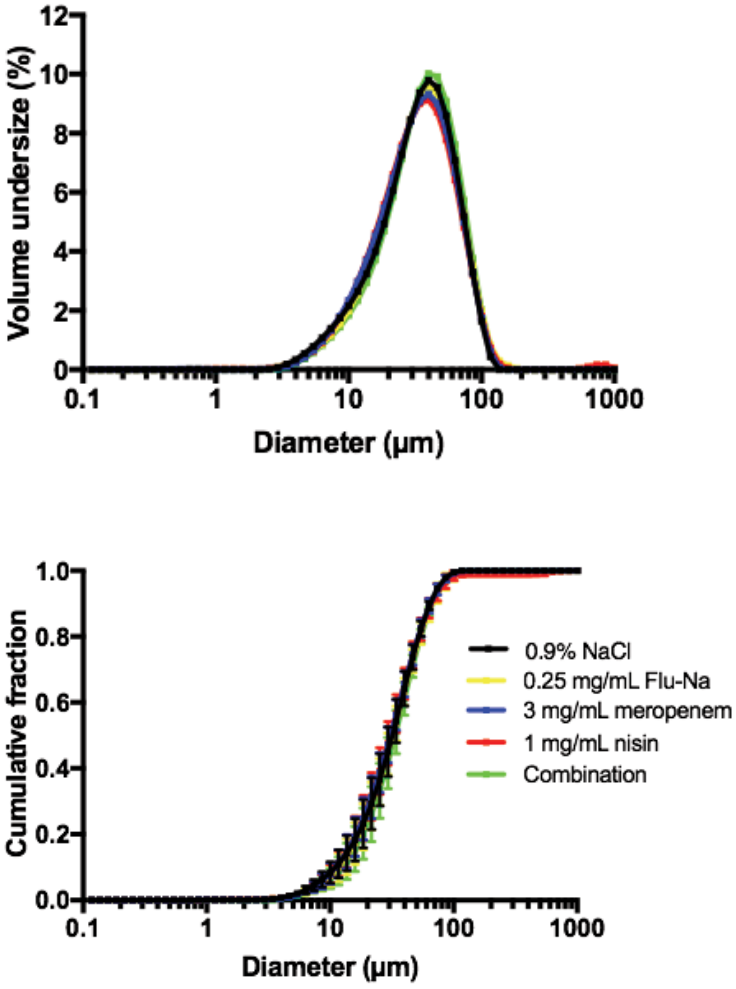

Figure 5-3: Droplet size analysis by laser diffraction of nasal spray solutions. Data represent mean ± StDev of five measurements. No significant difference was observed (ordinary one-way ANOVA with multiple comparison).

	Mean ± StDev				
	0.9 % NaCl	**0.25 mg/mL Flu-Na**	**3 mg/mL meropenem**	**1 mg/mL nisin**	**Meropenem + nisin combination**
Transmittance (%)	85.39 ± 1.22	86.70 ± 0.82	85.86 ± 1.92	86.91 ± 1.27	85.40 ± 1.13
Dv_{10} (µm)	11.64 ± 2.27	12.39 ± 2.82	11.56 ± 2.23	11.57 ± 2.21	13.26 ± 2.90
Dv_{50} (µm)	31.61 ± 31.61	31.93 ± 2.98	30.65 ± 2.68	30.41 ± 3.26	33.27 ± 3.72
Dv_{90} (µm)	63.90 ± 1.91	67.24 ± 7.06	64.26 ± 3.88	65.64 ± 5.79	66.65 ± 1.84
% V>10 µm	91.59 ± 3.25	92.67 ± 3.31	91.94 ± 3.27	91.93 ± 2.88	93.44 ± 3.00
Span (%)	1.67 ± 0.22	1.74 ± 0.40	1.73 ± 0.24	1.80 ± 0.30	1.63 ± 0.27
Obscuration (%)	14.61 ± 1.22	13.30 ± 0.82	14.14 ± 1.92	13.09 ± 1.27	14.60 ± 1.13
% V<10 µm	8.41 ± 3.25	7.33 ± 3.31	8.06 ± 3.27	8.07 ± 2.88	6.56 ± 3.00

Table 5-1: Plume and droplet size characteristics determined by laser diffraction. Data are mean ± StDev of five measurements. No significant difference was observed between Dv_{50} and Dv_{90} of the formulations (p= 0.6659 and p= 0.7332, respectively. Ordinary one-way ANOVA with multiple comparison).

5.2.2.2 Plume obscuration profiles

In order to characterise the development of the nasal plume, the laser obscuration profiles were analysed (see section 2.2.10.2). Obscuration profiles are shown in Figure 5-4 and are expressed as an average of five measures for each formulation. The results demonstrated that all the formulations presented a similar plume profile in the formation (F), stable (S) and dissipation (D) phases. This result further confirmed the similarity in the plume emission of all the formulations.

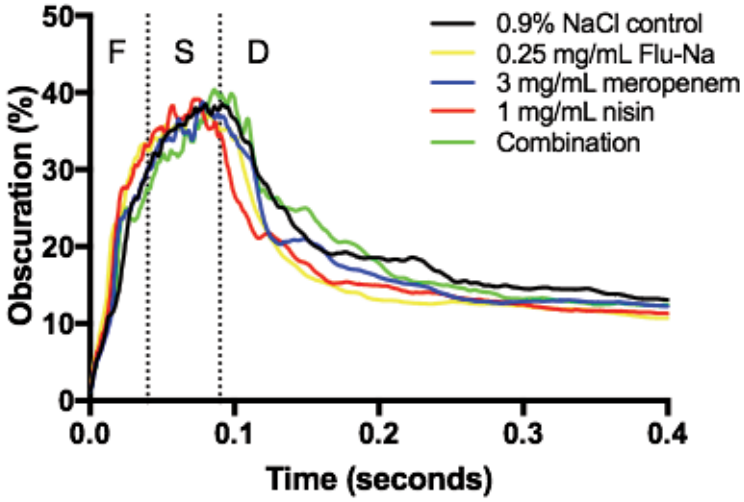

Figure 5-4: Obscuration profile for the nasal spray formulations during the formation (F), stable (S) and dissipation (D) phases. Data represent the mean of five measurements.

5.2.2.3 Plume angle characterisation

According to the literature, the plume angle is a key measurement to understand the deposition profile of nasal sprays (*264*, *272*). Therefore, an accurate evaluation of the emitted plume angle was obtained for all the formulations by recording the plume emission with the high-speed camera (Phantom Miro C-210, Vision Research, USA) at 1800 fps (see section 2.2.10.3). The emitted plumes were captured as movie clips at a rate of 1800 frames/sec. The video was then processed with the Vision Research Phantom software and the plume angle of each formulation was measured. The

measurements of the angles showed that all the formulations had a similar width at the nostril outlet (Table 5-2). Images of the nasal spray plume showed that the formulations maintained a similar profile after the emission (Figure 5-5). Therefore, the results demonstrated that the formulations are expected to have similar deposition performance.

0.9 % NaCl	0.25 mg/mL Flu-Na	3 mg/mL meropenem	1 mg/mL nisin	Combination
58.68 ± 1.01°	61.69 ± 1.61°	59.27 ± 0.76°	63.38 ± 2.29°	59.81 ± 2.93°

Table 5-2: Plume angle measurements. Data are mean ± StDev of three measurements. No significant difference was observed (Ordinary one-way ANOVA, Turkey's multiple comparison).

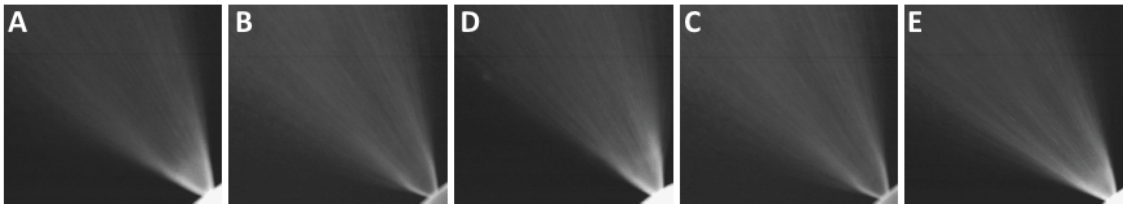

Figure 5-5: Plume emission snapshots of A) 0.9 % NaCl, B) 0.25 mg/mL Flu-Na, C) 3 mg/mL meropenem, D) 1 mg/mL nisin and E) meropenem-nisin combination.

5.2.2.4 Aerosol performances of meropenem nasal spray solution

The droplet size analysis (see section 5.2.2.1) revealed that the combined formulation may exhibit a respirable fraction (% V <10 µm was 6.56 ± 3.00 %, Table 5-1). Meropenem spray solution was used as a standard to quantify the deposition performance (see section 2.2.10.4) since all the formulations showed similar characteristics in droplet size, droplet size distribution, obscuration profile and plume emission. Data are presented as the percentage of the total drug recovered after deposition on the chamber, connection tube, stages and filter. The results

demonstrated that 100 ± 4.63 % of the delivered dose deposited in the glass chamber and no drug was recovered from the lower stages (Table 5-3). This result confirmed that there was no respirable fraction and confirmed the suitability of the formulation for nasal delivery, satisfying the pharmacopeia standards.

Part / Stage	Cut off diameter (μm)	Deposition % (mean ± StDev)
Expansion chamber	-	100.52±4.63
Connection tube	-	< LOQ
Stage 0-7	9 - 0.4	< LOQ
Filter	<0.4	< LOQ

Table 5-3: Meropenem aerosol performance. Drug percentage recovered in each impactor component after three shots. Data represent mean ± StDev of three independent experiments. LOQ = 0.24 μg\mL.

5.2.3 Validation of the novel nasal apparatus

A novel nasal apparatus was developed for better assessing the deposition and transport of the nasal formulations, which was described in section 2.2.12.1. The apparatus was validated by assessing deposition performance and cell layer integrity.

5.2.3.1 Deposition study

The performance of the novel apparatus was characterised using 0.25 mg/mL of Flu-Na to determine the deposition on Snapwell™ inserts and to evaluate the possible accumulation and run-off of the formulation after administration (see section 2.2.12.2.1). The deposition was evaluated for ensuring that a similar amount of drug deposited on the cell inserts for then assessing transport and delivery studies. For this purpose, three shots of Flu-Na were delivered to empty Snapwell™ cell inserts using

the Aptar nasal spray pump. The amount of Flu-Na deposited on the different parts of the chamber was quantified. The cell insert membrane, ring edge and the body of the apparatus were separately washed and the Flu-Na absorbance was quantified (see section 2.2.12.2.3). Results showing the deposition on the different components of the novel nasal apparatus are summarised in the Table 5-4. Images of the deposition of Flu-Na was obtained using a Nikon Coolpix-B500 and a 25 w blue spectra LED lamp (Figure 5-6). The total recovery of Flu-Na from the Snapwell™ inserts was 90.67 ± 1.02 %, which is in the range required from the pharmacopoeia for *in vitro* aerosol test (*130*), confirming the reliability and suitability of the novel nasal apparatus for drug deposition.

Apparatus component		**Flu-Na amount (mean ± StDev µg)**	**Flu-Na recovery (mean ± StDev %)**
Top Snapwell	**Edge**	2.77 ± 0.64	3.69 ± 0.86
	Membrane	1.17 ± 0.52	1.56 ±0.69
Left Snapwell	**Edge**	2.05 ± 0.69	2.73 ± 0.92
	Membrane	3.09 ± 0.36	4.12 ± 0.48
Right Snapwell	**Edge**	2.27 ± 0.68	3.03 ± 0.91
	Membrane	0.97 ± 0.55	1.29 ± 0.74
Chamber		55.68 ± 1.08	74.24 ± 1.45

Table 5-4: Summary of Flu-Na deposition assessed using the novel nasal apparatus. Data are mean ± StDev of three independent experiments.

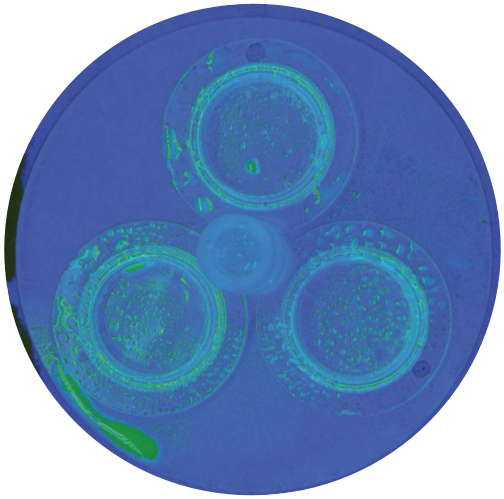

Figure 5-6: Flu-Na deposition on Snapwell™ cell inserts after delivery of three shots.

5.2.3.2 Barrier integrity of nasal cell model

The novel nasal apparatus was also characterised for performing transport studies. The permeation of a Flu-Na solution was investigated to ensure that the integrity of the RPMI 2650 nasal epithelial cells was maintained after spray deposition (see section 2.2.12.2.2). The transport of Flu-Na across the cell layer was evaluated over a period of 4 h after one and three shots of PBS. The amount of Flu-Na was quantified as described in section 2.2.12.2.3 and the permeation coefficient was calculated using the equation in section 2.2.12.2.2. The P_{app} values showed no statistical difference in the permeability after the delivery of one or three shots of PBS (Figure 5-7) in comparison with the untreated cell layer. Therefore, the integrity of the cell layer was maintained when delivering a nasal spray solution using the novel nasal apparatus.

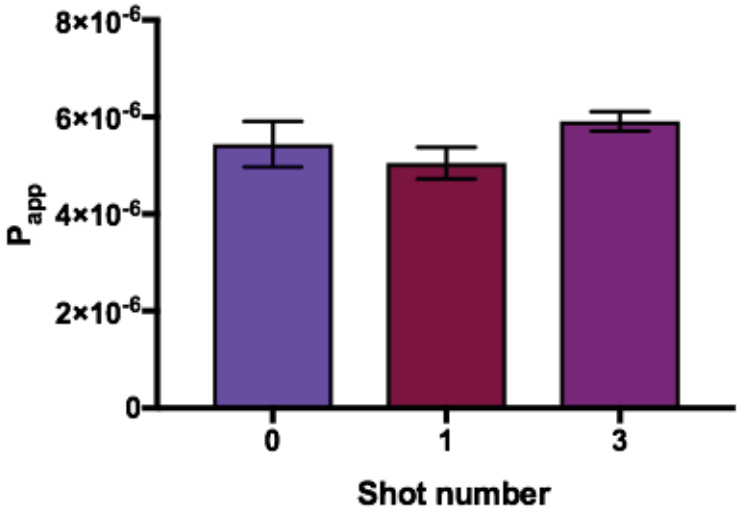

Figure 5-7: Barrier integrity of the RPMI 2650 cells. P_{app} values of Flu-Na permeation across the RPMI 2650 cell layer after 0, 1 and 3 shots of PBS over a period of 4 h delivered with the Aptar nasal spray. Data are mean ± SEM of three replicates.

5.2.4 Meropenem transport study

The transport of meropenem across the RPMI 2650 cell layer was assessed to investigate the biological interaction of this drug with the nasal epithelium. In order to determine this, the RPMI 2650 cells were cultured and then grown on Snapwell™ inserts in ALI conditions for 14 days (see sections 2.2.11.1 and 2.2.11.2). The transport of meropenem across the RPMI 2650 cell layer was evaluated over a period of 4 h after three shots using the novel nasal apparatus (see section 2.2.13.1). Figure 5-8 shows the percentage of meropenem transported across the nasal cell layer over 4 h. The permeation after the first hour was 36.9 ± 2.20 % of the total drug delivered. After 4 h, the total amount of meropenem that reached the basal compartment was 81.7 ± 1.867 %, while 11.55 ± 1.47 % and 6.8 ± 0.4 % remained on the apical surface and inside the cell layer, respectively.

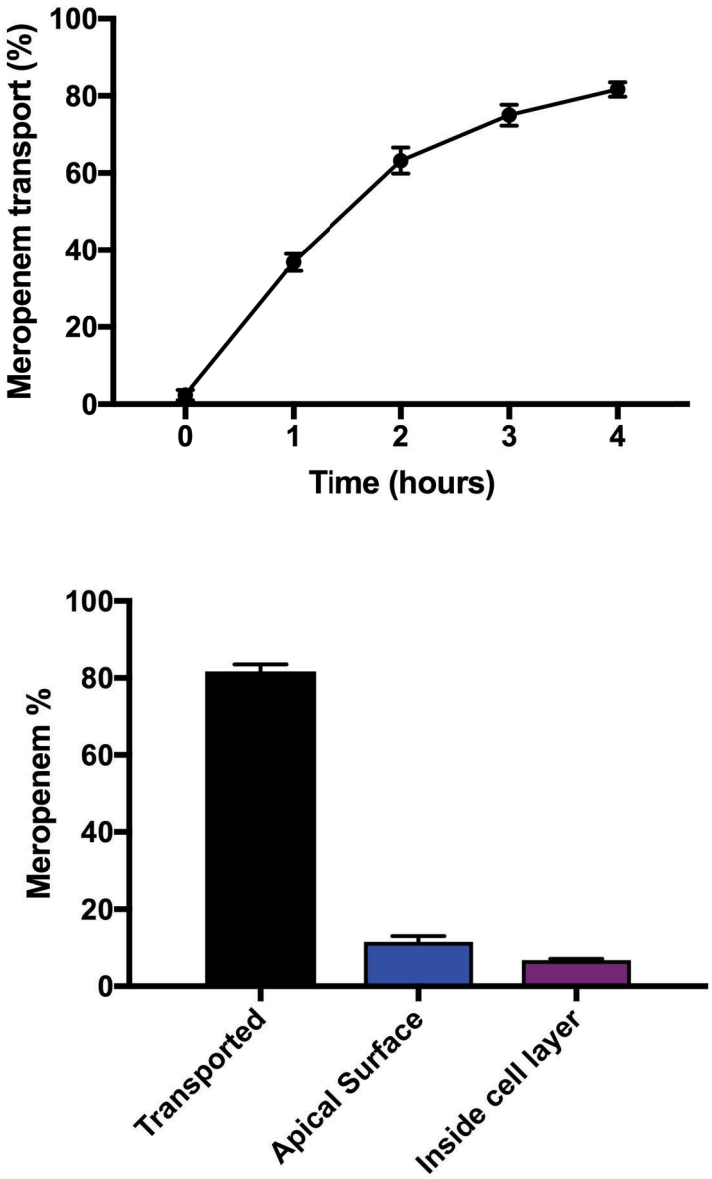

Figure 5-8: Meropenem transport across RPMI 2650 cells. A) Meropenem transport over time. B) Percentage of meropenem recovered after 4 h. Data are mean ± SEM of three replicates.

5.2.5 Cytotoxicity assays on nasal epithelial cells

The toxicity of meropenem and nisin on the RPMI 2650 nasal cell line was assessed using the lactate dehydrogenase and the Propidium Iodide dye assays.

5.2.5.1 Lactate dehydrogenase (LDH) assay

RPMI 2650 cells were seeded in 96-well microtitre plates and treated with different concentrations of meropenem and nisin, separately. After 24 h, the LDH release was quantified using the LDH-Cytotoxicity Assay Kit II (see section 2.2.14.1). Results showed that meropenem did not cause LDH leakage, even at the highest concentration tested (Figure 5-9, A). On the contrary, 0.5 mg/mL and 1 mg/mL nisin caused a higher release of LDH, compared to the positive control and the lower concentrations tested (Figure 5-9, B).

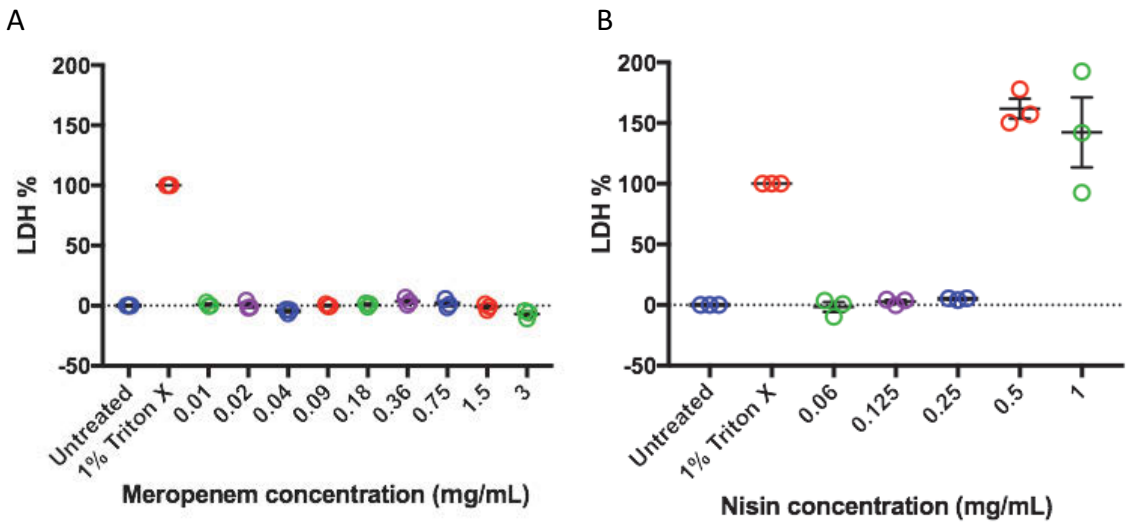

Figure 5-9: LDH leakage after 24 h. Percentage of LDH released by the RPMI 2650 cells after 24 h of A) meropenem and B) nisin treatment. Data are mean ± SEM of three replicates.

5.2.5.2 Propidium iodide assay

The cytotoxicity of meropenem and nisin was also evaluated by propidium iodide (PI) staining and analysed with the flow cytometer BD Accuri (see section 2.2.14.2). RPMI 2650 cells were seeded in 24 well plates and treated with different concentrations of meropenem and nisin, separately. After 24 h treatment, cells were lysed, suspended in

PBS and analysed for determining the viability. Results showed that meropenem did not have a toxic effect on the RPMI 2650 cells at all the concentrations tested (Figure 5-10, A). Whereas, nisin at 0.5 μg/mL and 1 μg/mL was found to be toxic to the cells, showing cell viability of 48.98 ± 5.10 % and 24.54 ± 11.52 %, respectively (Figure 5-10, B). These outcomes also confirmed the results determined with the LDH assay.

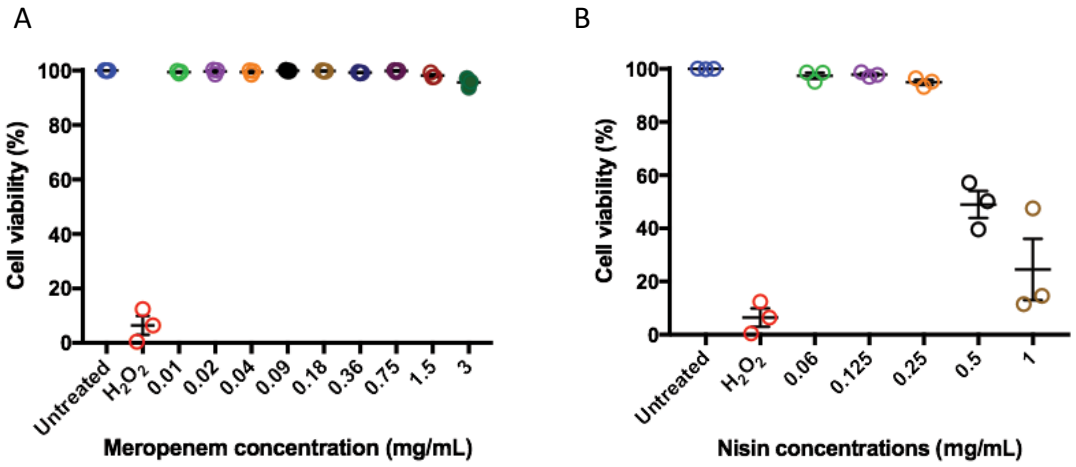

Figure 5-10: Propidium iodide assay. RPMI 2650 cell viability after 24 h for A) meropenem and B) nisin determined with PI staining. Data are mean ± SEM of three replicates.

5.2.6 Nasal spray formulation delivery on *P. aeruginosa* biofilms

The novel nasal apparatus was also utilised for developing an *in vitro* model for the study of biofilm viability after delivery of nasal sprays. A combined formulation of meropenem at 3 mg/mL with nisin at 1 mg/mL was developed for the treatment of *P. aeruginosa* biofilm infections in the nose, such as chronic rhinosinusitis. For this purpose, the combination treatment was assessed for its efficacy as a nasal spray formulation on *P. aeruginosa* biofilms. PAO1 biofilms were grown on Snapwell™ cell inserts for 24 h in static conditions and then treated with 3 mg/mL meropenem and/or 1 mg/mL nisin nasal spray formulations for 24 h (see section 2.2.15). Biofilm viability

after treatment was determined by performing CFU count (see section 2.2.15). These results showed that biofilms treated with the combined nasal formulation resulted in a significant lower viability compared to the untreated and single treated biofilms (Figure 5-11).

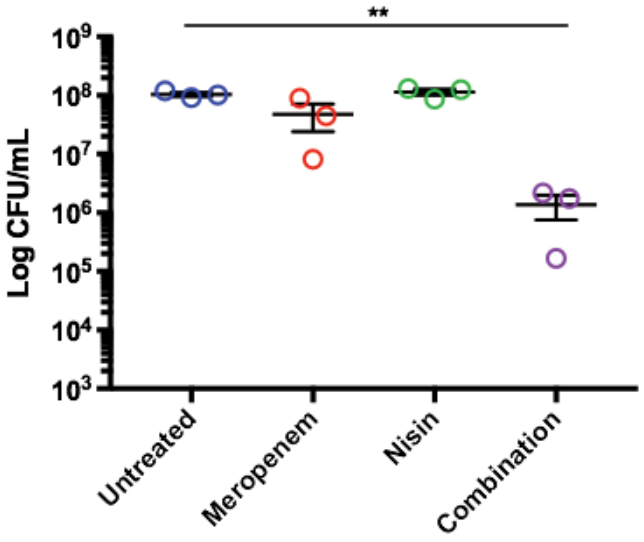

Figure 5-11: Biofilm viability after nasal spray delivery. Colony forming units per mL (CFU/mL) was used to determine cell viability of PAO1 biofilms after nasal spray treatment with the combination of 3 mg/mL meropenem with 1 mg/mL nisin. Data are mean ± SEM of three replicates.

The harvested biofilm cells were also visualised with wide-field fluorescence microscopy to confirm the morphological conversion to the CWD spherical morphotype in the meropenem-treated biofilms and the efficacy of the combination treatment (see section 2.2.15.1). Images showed that CWD spherical cells occurred in biofilms when treated with a spray solution of meropenem (Figure 5-12). In comparison with untreated biofilms, no cell death was detected in biofilms treated with meropenem and nisin alone (Figure 5-13). Whereas in the combination-treated

biofilms, dead cells and debris were detected (Figure 5-13), confirming the decrease of biofilm viability assessed with the CFU count.

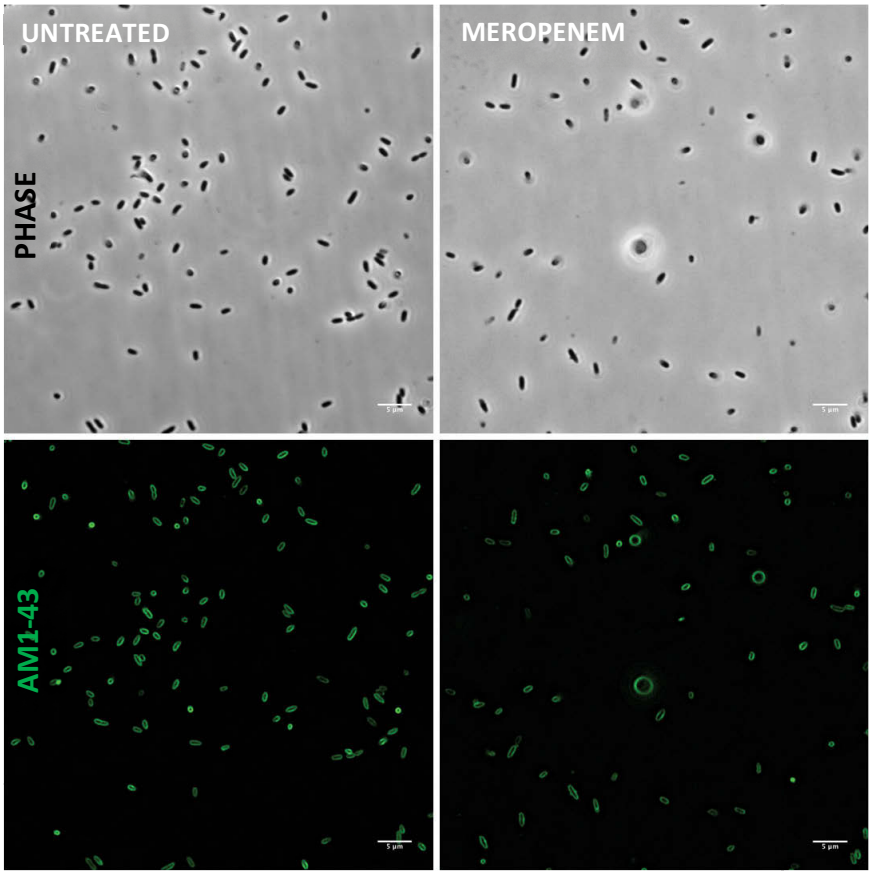

Figure 5-12: Harvested biofilm cell morphology. Phase contrast and fluorescent images of harvested biofilms cells stained with the membrane dye AM1-43 (green) to investigate cell morphology. Images show untreated biofilm cells with a rod morphology and meropenem-treated biofilm cells as a mixture of rod and CWD cells. Images are representative of three replicates. Scale bar 5 µm.

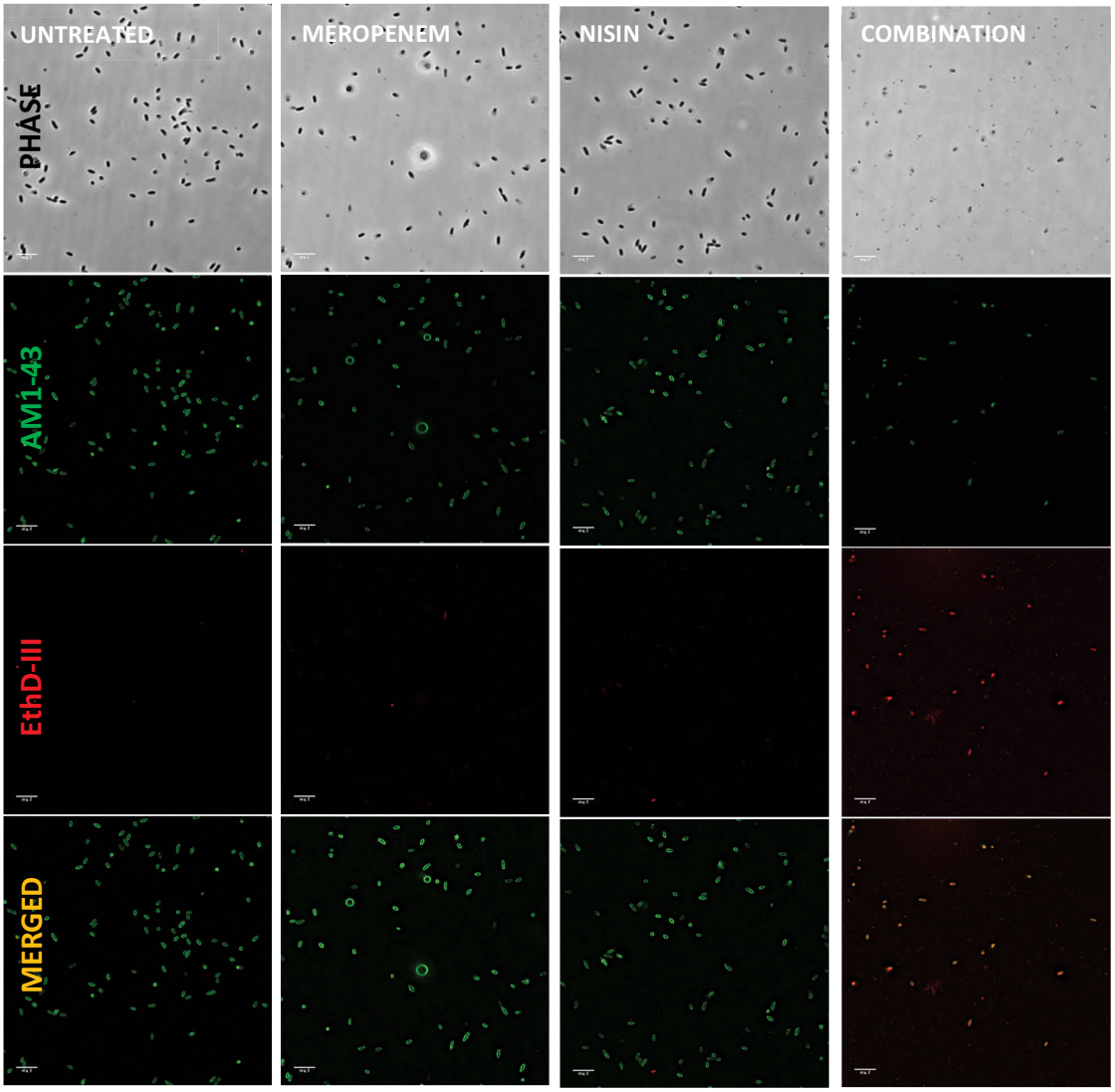

Figure 5-13: Harvested biofilm cells viability. Phase contrast and fluorescent images of harvested biofilms cells stained with a mixture of the membrane dye AM1-43 (total biomass, green) with EthD-III (dead biomass, red) to visualise cell viability. Images are representative of three replicates. Scale bar = 5 µm.

5.3 Discussion

The most common antibiotics used for the treatment of acute and chronic bacterial infections in the nose are macroides, quinolones, penicillins (*273*) and saline irrigations with topical corticosteroids (*274*). However, as mentioned earlier, these therapies often fail due to the presence of bacterial biofilms and their high resistance to antibiotics.

In Chapter 4, we demonstrated that a combination of meropenem with nisin was effective in significantly reducing the viability of *P. aeruginosa* biofilms. Thus, this antibiotic combination was investigated as a nasal formulation for the treatment of *P. aeruginosa* biofilms in the nose.

In this Chapter, a simple but accurate UV method was validated for the quantification of meropenem in unknown samples. Data showed that all the parameters (linearity, precision, accuracy and limit of quantification and detection) were in line with the ICH guideline requirements and the concentration range of 1.5 - 75 µg/mL was suitable for the analytic measurements in this study. Single and combined nasal spray solutions of meropenem and nisin were prepared in 0.9 % NaCl since it has been reported that β-lactam antibiotics showed higher stability in saline solution than in water (*179*). A solution of meropenem at 3 mg/mL was chosen based on other commercial nasal antibiotic formulations for the treatment of chronic rhinosinusitis (*183*). The nisin solution was prepared at 1 mg/mL based on its solubility and stability at acidic pH. The pH of nisin was then measured to confirm solubility at 1 mg/mL and found to be 3.21 which was within the range of solubility (*103*). Moreover, the pH of 0.9 % NaCl, 3 mg/mL meropenem and the combination of meropenem with nisin was also measured and found to be 6.17, 4.95, 3.21 and 3.42, respectively. As nisin was purchased as a mixture of denatured milk solids and NaCl (see section 2.1.1.16) and due to time constraints and the complex matrix of the peptide (*232*), it was not possible to validate a quantification method.

The laser diffraction analyses showed that the droplets size of the combined formulation was within the required range of 20 - 200 µm as the Dv_{50} was 33.27 ± 3.72 µm and Dv_{90} was 66.65 ± 1.84 µm. Moreover, the deposition study performed using the Andersen Cascade Impactor equipped with the 2 L glass chamber, confirmed the absence of a respirable fraction since no drug was recovered from the lower stages of the impactor. Therefore, we concluded that the droplet population with a diameter below 10 µm determined with the laser diffraction analysis may simply reflect the measurements of the droplets during the dissipation phase since the measurements were performed at 45° to the laser beam of the Spraytec. The droplet size measurements, plume obscuration profile and plume angle measurements demonstrated that the single and combined formulations of meropenem and nisin were suitable for nasal delivery and had similar characteristics in terms of plume emission and therefore may have similar *in vivo* deposition performances. Therefore, given the similarity of all the formulations in terms of the emitted plume, we used meropenem as a reference for predicting nisin and the combination deposition performances.

A novel nasal apparatus was designed for assessing drug transport through the nasal epithelium and for delivering the nasal spray formulation on biofilms reproducing the anatomic distance from the nostril to the mucosa (5 cm). The deposition and permeation studies performed using a solution of 0.25 mg/mL Flu-Na demonstrated that the novel apparatus is a reproducible and valid tool to study nasal formulation deposition and transport through a nasal epithelium model. The apparatus was then applied to investigate the transport of meropenem through the RPMI 2650 cell layer. The estimation of drug transport across the nasal epithelium is an important aspect for the characterisation of new formulations (*275*). Therefore, the transport of meropenem across the RPMI 2650 cell layer was investigated. The results of this experiment revealed that meropenem was mainly transported through the cell layer, probably due to the chemical-physical characteristics of the drug, which is a small polar molecule able to cross the cell layer via the paracellular mechanism (*276*).

The novel nasal apparatus also allowed the delivery and analysis of the effect of the nasal spray formulations on biofilms. The use of this novel *in vitro* model demonstrated that *P. aeruginosa* biofilm cells responded to meropenem with a subset undergoing the morphological transition from a rod-shaped cell to the CWD spherical morphotype when the antibiotic is delivered as a nasal spray formulation. Moreover, the delivery of the combined nasal formulation of meropenem with nisin was effective in reducing biofilm viability presumably due to the ability of nisin to lyse the CWD cells. These results further confirmed the effectiveness of the combined formulation demonstrated in Chapter 4.

The cytotoxicity assays revealed that meropenem was not toxic to the RPMI 2650 nasal cells; therefore safe for nasal delivery. However, nisin was found to be toxic to nasal cells at 0.5 mg/mL and 1 mg/mL, probably due to the ability of nisin to form pores in the cell membrane. In fact, nisin at these concentrations showed a high LDH release percentage and nisin is known to be a pore-forming cationic peptide (*101*). The toxicity of nisin could be overcome by reducing its concentration to 0.25 mg/mL and re-assessing the effectiveness of the combination on biofilms. Also, since nisin was used in this study as a proof of concept, other antimicrobial peptides that are not toxic to nasal cells could be used.

Overall in this Thesis Chapter, we demonstrated that it is possible to formulate a combination of meropenem and nisin for nasal delivery and its efficacy in reducing *P. aeruginosa* biofilm viability.

Chapter 6

General Discussion

6 General discussion

6.1 Background

Antimicrobial resistance (AMR) is now a concerning global health problem. Bacteria and other pathogens have evolved to evade the effects of new drugs that are commonly used to treat infections. Resistance to antibiotics has spread significantly in the last decade due to increased use and misuse of antibiotics. In a review on AMR published in 2013, Jim O'Neill stated that *Klebsiella pneumoniae, Escherichia coli* and *Staphylococcus aureus* were already showing concerning levels of resistance and in 2017 many other bacteria were considered priority pathogens for research and development (R&D) of new antibiotics (*52*, *277*, *278*). Among these pathogens, *P. aeruginosa* was classified second as a critical pathogen for the development of new antimicrobials due to its resistance against a wide range of antibiotics and in particular to carbapenems.

P. aeruginosa is an opportunistic Gram-negative bacterium that causes nosocomial infections and has become a serious public health threat and a major cause of nosocomial infections worldwide (*279*). In 2004, the presence of *P. aeruginosa* biofilms in the sinuses from patients with chronic rhinosinusitis (CRS) was identified for the first time (*255*). Chronic rhinosinusitis is an inflammation of the nasal mucosa where symptoms persist for longer than 12 weeks and it occurs in up to 5 % of the population (*280*). Since the discovery of biofilms in CRS, many studies have been conducted to confirm the presence and elucidate the role of biofilms in this infection (*25*). It has been shown that the majority of patients suffering from chronic sinusitis were biofilm-positive (*23*, *256*, *281*, *282*) and associated with infection caused by pathogens such as *P. aeruginosa* (3-14%), *Staphylococcus aureus* (14-24%), *Streptococcus pneumoniae* (10%) and *Haemophilus influenzae* (*20*, *283*). The direct role of biofilms in CRS remains unclear. However, it has been proposed that biofilms are associated with a disruption of the epithelial barrier and increased presence of macrophages and T cells, which leads to an enhanced inflammatory response (*284*). Another hypothesis is that the

formation of biofilms is promoted by an overproduction of mucins, which are synthesised by goblet cells and submucosal cells in healthy conditions (*285*).

Generally, patients suffering from CRS *P. aeruginosa* infections are treated with courses of systemic antibiotics and topical corticosteroids. However, such treatment remains insufficient to eradicate the infection (*286*). A comparative review discussing the medical therapies for biofilms in the sinuses supported the use of high-volume saline irrigation with topical corticosteroid as first-line therapy for the treatment of chronic rhinosinusitis (*274*). However, this therapy may only reduce the inflammation associated with the infection as corticosteroids are anti-inflammatory drugs and saline irrigation would only reduce the symptoms (*287*). Nebulised antibiotics, such as tobramycin, did not show benefit in the treatment of chronic rhinosinusitis or only limited effects (*83*, *288*).

Studies have demonstrated that infections of the nasal cavity caused by *P. aeruginosa* are refractory to antibiotics not only due to the variety of resistance mechanisms that this bacterium possesses but also due to the spread of the infection between the upper and lower respiratory tract. Ciofu *et al.* demonstrated that there is an exchange of *P. aeruginosa* isolates between the paranasal sinuses and the lungs in CF patients with chronic infections (*289*). Other studies have also demonstrated that the paranasal sinuses may act as a reservoir for bacteria (*290*). *P. aeruginosa* can hide there during antibiotic therapy and is then able to re-colonise the airways when the therapy is concluded. (*291–295*). The re-colonisation of the airways by *P. aeruginosa* is attributed to its adaptation in the CF lung environment and this is due to a variety of factors (*296*). *P. aeruginosa* is able to evade the immune defence by losing or reducing immunogenic factors such as the secretion of virulence factors (*297*) or motility (*298*); it can also change its metabolism by expressing genes required for growth under the conditions of the CF lungs, such as increasing the transcription of genes or proteins involved in the metabolism of fatty acids and amino acids (*299*); it can survive antibiotic treatment by forming biofilms and by acquiring mutations that confer antibiotic resistance though genetic changes (*300*).

The nasal cavity is constantly exposed to inhaled microbes and despite the host defences within the nasal cavity and the upper airways, pathogens colonise the epithelium and cause disease. It has also been demonstrated that bacteria that infect the sinuses not only cause a local infection but are capable of accessing the central nervous system by penetrating the blood-brain barrier or the blood-cerebrospinal fluid barrier and via the olfactory epithelium (*301*). The ability of bacteria to migrate through these biological barriers is life-threatening and can lead to meningitis and brain abscesses. *P. aeruginosa* has been associated with the central nervous system causing both meningitis and brain abscesses, which leads to mortality rates between 5 % and 32 % (*302*–*305*).

It then becomes clear that *P. aeruginosa* is a ubiquitous pathogen and can lead to diseases with high morbidity and mortality. The ability of this bacterium to adapt to extreme environments and escape antibiotic treatment highlights the challenge of finding effective antibiotic therapies. Despite the difficulties and challenges in treating infections caused by *P. aeruginosa*, recent studies have revealed possible alternative approaches for treating *P. aeruginosa* biofilm infections.

6.1.1 *P. aeruginosa* alternative lifestyle to survive antibiotic exposure

A study conducted in the Whitchurch laboratory revealed a novel mechanism for *P. aeruginosa* to evade the effect of β-lactam antibiotics. It was demonstrated that planktonic *P. aeruginosa* cells survived exposure to β-lactam antibiotics by converting their morphology from rod-shaped cells to a viable cell wall deficient (CWD) spherical morphotype. It was also determined for the first time that *P. aeruginosa* CWD cells transitioned back to its original rod shape after antibiotic removal and continue to grow and divide normally. Therefore, it is plausible that the transition to this alternative lifestyle may represent another strategy for *P. aeruginosa* to evade antibiotics and re-cause infection after the termination of the antibiotic therapy.

As the CWD cells lack a functional cell wall and outer membrane, it was proposed that these cells may be susceptible to antimicrobials that interact directly with membrane lipids inducing cell death via the formation of pores in the cytoplasmic membrane. In fact, the addition of antimicrobial peptides (AMPs) to meropenem-induced CWD cells were found to efficiently and rapidly kill planktonic *P. aeruginosa* (*165*). Thus, it was proposed that the lack of the outer membrane could be exploited to treat *P. aeruginosa* infections using a combination treatment comprised of a cell wall-inhibiting compound with a membrane-permeating agent (*165*).

The focus of this Thesis was to determine whether it is possible to exploit this strategy to treat *P. aeruginosa* biofilms. The principal aims of this Thesis were to firstly, investigate the occurrence of the CWD morphotype in biofilms. Next, the combination of meropenem with the cationic antimicrobial peptide nisin was explored for assessing its efficacy in eradicating *P. aeruginosa* biofilms. It was then evaluated whether the combination treatment was suitable for nasal delivery since current treatments do not specifically target biofilms in the sinuses. Subsequently, the combined nasal formulation was assessed for investigating a potential reduction in biofilm viability.

6.2 *P. aeruginosa* cell wall deficient morphotype also occurs in biofilms

In Chapter 3 of this Thesis, the effect of meropenem was investigated on static and flow cell biofilms. The results demonstrated that static biofilms survived meropenem exposure up to 10x MIC. Analyses performed with fluorescence microscopy allowed the investigation of the morphology of biofilm cells down to the single cell level. The results revealed that the CWD spherical morphotype also occurred in both static and flow cell biofilms upon 5x MIC meropenem treatment. It was also shown that upon meropenem treatment, the spherical cells found in biofilms were the same size as those found in planktonic cultures.

Studies have shown that other bacteria are also capable of changing their morphology to a cell wall deficient form in response to antibiotics. Billings *et al.* have shown that *E. coli* transitioned to a CWD form after exposure to the cephalosporin cefsulodin and it was also able to revert back to its rod shape after antibiotic removal (*306*). Other researchers have shown that *Listeria monocytogenes*, *Enterococcus spp*., *Staphylococcus aureus*, *Bacillus subtilis* and *Vibrio cholerae* are also capable of transitioning to a CWD morphotype in response to fosfomycin, D-cycloserine, penicillins, and carbapenems (*162*, *173*, *307–309*). The fact that a variety of bacterial species are able to modify their shape to survive antibiotic exposure when they are in the planktonic state suggests that they may exhibit a similar response to antibiotics also when they form biofilms. However, the morphological transition of these bacteria in the biofilms state has not been explored yet. In this Thesis, we showed for the first time that the CWD spherical morphotype transition in response to β-lactam antibiotics also occurs in *P. aeruginosa* biofilms.

6.2.1 *P. aeruginosa* cell wall deficient morphotype may be relevant in recurrent infections

Since it was hypothesised that the transition to CWD cells and their ability to revert to the rod shape in the absence of antibiotic treatment might be implicated in the recurrence of infections, we investigated the induction of this morphotype in artificial sputum medium (ASM). We demonstrated that the CWD cells could also be induced in *P. aeruginosa* cultured in media mimicking the CF lungs environment.

The fact that CWD cells also exist in biofilms and ASM-cultured cells after antibiotic treatment suggests that this spherical morphotype may be relevant in disease. Even though this was beyond the scope of this project, we successfully developed a microscopy method in order to visualise *in vitro P. aeruginosa* CWD cells cultured in ASM. The fluorescence *in situ* hybridisation (FISH) was utilised to specifically identify *P. aeruginosa* and general bacteria. Our results showed that CWD cells were successfully

detected. This technique could be applied to determine the presence of CWD *P. aeruginosa* cells in CF patients that have been treated with β-lactam antibiotics. This would allow us to understand the clinical relevance of CWD cells and determine their association with recurrent diseases. This technique could also be extended for the identification of other bacterial species that transition to the CWD morphotype by modifying or combining different probes to explore whether this morphological change is clinically relevant in other bacterial species.

6.3 The combination of meropenem with nisin is effective in reducing biofilm viability

In Chapter 4 the effect of the combination of meropenem with nisin was investigated on static and flow cell biofilms. We identified that the combination of meropenem at 5x MIC (10 μg/mL) with nisin at 64 μg/mL significantly reduced the relative biomass of static biofilms. This antibiotic combination was further assessed for its efficacy on static biofilms with wide-field fluorescence microscopy using AM1-43 and EthD-III as indicators of total and dead biomass, respectively. Our results demonstrated that this antibiotic combination was effective in eradicating static biofilms, showing a significant increase in dead biomass. The combination was also evaluated on flow cell biofilms using wide-field microscopy and the colony forming unit assay. The fluorescence quantification showed that the combination significantly increased the dead biomass and the CFU assay demonstrated a significant reduction in biofilm viability, confirming the efficacy of the combined treatment. The use of antibiotic combinations is not novel, in fact other studies have already showed that a combination of a β-lactam antibiotic with AMPs is successful in treating *P. aeruginosa* biofilm (*310–314*). However, the morphology of the cells within the biofilm after antibiotic treatment has not previously been investigated.

As Monahan *et al.* showed that the killing of planktonic *P. aeruginosa* CWD cells depends on the ability of nisin to lyse CWD cells, we wanted to confirm that this also

occurred in biofilms. Thus, CWD cells in meropenem and combination-treated flow biofilms were counted and our results showed that nisin efficiently killed CWD cells, furthermore confirming the effectiveness of this strategy.

The use of wide-field fluorescence microscopy showed that the cell population in biofilms did not entirely convert to the CWD spherical morphotype. This was probably due to differences in growth rates and metabolism of cells within a biofilm. As antibiotics normally target metabolically active cells, cells with a slow metabolism and slow growth rate might not be affected by the activity of antibiotics (*70*) and therefore do not convert to the CWD morphotype. In fact, we showed that only about 8 % of the cells in the biofilm transitioned to CWD cells. Nonetheless, the combination was efficacious at reducing biofilm viability. The portion of biofilm cells undergoing this morphological transition may be enhanced by stimulating the metabolism of the cells. In order to achieve this, dispersing agents may be used to induce dispersal reactivating the metabolism of biofilm cells (*315*). Examples of compounds that cause *P. aeruginosa* biofilm dispersal are nitric oxide (*316*), mannitol (*317*) and EDTA (*318*). Therefore, the addition of dispersing compounds to meropenem may increase the number of cells that undergo the morphological transition to CWD cells.

6.3.1 Antibiotic-tolerant cells surround the dead biomass of flow cell biofilms

In Chapter 4, a detailed analysis of biofilms treated with the antibiotic combination revealed that rod-shaped live bacteria were present around the dead biomass that remained encased in the matrix. A study conducted by S.L. Chua *et al.* determined that *P. aeruginosa* biofilm cells surviving colistin treatment migrated to the top of biofilm dead cells overexpressing type IV pili for a targeted migration, proposing a model explaining the development of colistin-tolerant subpopulations (*246*). They also argued that these tolerant cells migrate to acquire iron as demonstrated in a study by Yang *et*

al. (*247*). More studies are needed to determine whether the live cells surrounding the dead biomass of meropenem-nisin treated biofilms were a subpopulation of tolerant cells and whether it is possible to target them effectively.

In Chapter 4 it was also shown that when biofilms were treated with the antibiotic combination, rod-shaped live cells were still present at the substratum of the biofilm. We reasoned that these cells might represent a subpopulation of dormant cells, known as persisters. These cells are dormant and therefore are not recognised by antibiotics and survive their exposure. Therefore, the phenotype of the cells surrounding the dead biomass of the flow cell biofilms should be investigated. This would determine whether these cells are a subpopulation of antibiotic-tolerant cells.

Studies have shown that some compounds are able to re-activate the metabolism of persister cells, such as sugars or glycolysis intermediates and then use traditional antibiotics to target them successfully (*319*, *320*). Another approach could be the use of drugs that do not require cell metabolic activity or any cell machinery for uptake antibiotics and therefore may be effective in targeting dormant cells (*321*). Mitomycin C and cisplatin are two example of drugs which have been shown to be effective in targeting *E. coli*, *S. aureus* and *P. aeruginosa* persister cells (*322*, *323*). Barraud *et al.* demonstrated that also mannitol enhanced antibiotic sensitivity of persisters in *P. aeruginosa* biofilms and increased the efficacy of tobramycin (*324*). Therefore, the addition of one of those compounds may significantly improve the killing rate of the meropenem-nisin combination used in this Thesis.

Considering the properties of mannitol as a dispersing agent and enhancer of antibiotic sensitivity of persister cells, it could represent a promising compound to increase the efficacy of the antibiotic combination proposed in this Thesis for the following reasons. The use of mannitol in addition to the meropenem-nisin combination could both disperse and re-activate the metabolism of the persister cells. Subsequently, these re-activated cells could be targeted by meropenem to induce the morphological switch. The activity of nisin would then lyse meropenem-induced CWD cells and lead to biofilm eradication. In a possible antibiotic synergism, this three-drug combination

may eradicate the entire biofilm avoiding the colonisation of new niches by antibiotic-tolerant cells.

In addition, mannitol is an osmotic agent that increases the water content into the airways. Studies have shown that inhaled mannitol improves mucociliary clearance by increasing the osmotic pressure of the mucosal surfaces. This induces trans-cellular water migration into the airway surfaces reducing the viscosity of mucus and hence increases clearance by cilia transport mechanism, ultimately enhancing lung function (*325–328*).

The presence of viable cells at the substratum of the biofilm could be due to either the presence of antibiotic-tolerant cells or the inability of the combination therapy to penetrate the biofilm. Studies investigating the ability of meropenem and nisin to penetrate *P. aeruginosa* biofilms could be assessed to elucidate this aspect.

Overall in Chapter 4, we showed that the combination of meropenem at 5x MIC with nisin at 64 μg/mL significantly reduced biofilm viability. It was demonstrated for the first time that *P. aeruginosa* cells undergo the transition to the CWD spherical cells in biofilms and it is possible to exploit this antibiotic-susceptible morphotype to reduce biofilm viability due to the ability of nisin to efficiently lyse CWD cells. These findings suggest that a cell wall-inhibiting compound in combination with a membrane-active agent may represent a promising strategy for the treatment of *P. aeruginosa* biofilm infections.

6.4 The combination of meropenem with nisin is suitable for nasal delivery and reduced biofilm viability

The choice of route of administration in the treatment of infections is important to ensure that the correct dose of the drug (above the MIC) reaches the target site and avoid the rise of resistance. In the case of upper and lower respiratory tract infections, the inhalation delivery should be the preferred route of administration as it targets infections directly in the airways. The advantages of inhalation delivery are many.

Drugs delivered orally or by injections are administered in high doses to ensure that an adequate dose reaches the target site of infection. The high dose may have higher cost and also cause side effects. Whereas, the dose of inhaled drugs can be significantly lower and still achieve equivalent potency of the same drug administered via the mouth or by injection. Also, it is possible to deliver high doses to achieve superior therapeutic efficacy without causing side effects as the delivery is localised and specific (*259*, *329*).

We previously discussed that current treatments for biofilms in CRS often fail. When the pharmacologic therapy fails, sinus surgery may be used to improve symptoms, however the majority of CRS patients experienced no benefit or improved quality of life (*330*, *331*). Until now, there is no evidence of nebulised antibiotics that successfully treat or target biofilms in the nasal cavity (*332*, *333*).

For this reason, in Chapter 5 of this Thesis, we examined whether the antibiotic combination of meropenem with nisin could be developed as a nasal formulation for directly targeting *P. aeruginosa* biofilms in the nose. A nasal spray pump system was utilised to assess the formulation for nasal delivery at clinically relevant concentrations. A simple and accurate UV spectroscopy method for the quantification of meropenem in samples was developed and validated. This method allowed us to evaluate the aerosol performance of the formulation. The results from the laser diffraction analyses demonstrated that the single and combined nasal formulations had similar deposition performances. Furthermore, the combined formulation presented the required droplet size for nasal delivery. This was also confirmed by the deposition study, where the nasal spray entirely deposited on the glass chamber, which represents the nasal cavity and no respirable fraction was recovered. Altogether, these results demonstrated that the combination of meropenem with nisin was suitable for nasal delivery.

A novel apparatus for assessing drug deposition and permeation studies and that also allowed the delivery of the formulation on biofilms was developed. The apparatus was designed to reproduce the anatomic distance from the point of administration (nostril)

to the delivery area (nasal sinuses). The combined nasal formulation was then delivered on static biofilms cultured on Snapwell™ cell culture inserts using the novel nasal apparatus. The results demonstrated that the combination significantly reduced biofilm viability also in the form of a nasal spray solution. We confirmed that CWD cells also occurred in static biofilms cultured under the conditions reported in Chapter 5 and that nisin was effective in lysing CWD cells.

Toxicity studies were also performed to ensure that the concentrations of meropenem and nisin were not toxic to nasal epithelial cells. In order to achieve this, we used the nasal cell line RPMI 2650, originated from a carcinoma of the nasal septum, which is a relatively new model for assessing various drug studies. The results showed that meropenem was not toxic at any of the concentrations tested. However, nisin was toxic at 1 mg/mL, which is the concentration used in this study. The toxicity of nisin has been evaluated on different eukaryotic cell types and studies have shown contrasting results (*334–338*). This may depend on the type of cell line used and on the fact that we used the crude form of the peptide, whereas studies that demonstrated the safety of nisin utilised the pure form of nisin. Nevertheless, the concentration of nisin at 0.25 mg/mL tested in our study did not show toxicity on the RPMI 2650 cells, therefore the drug combination of meropenem with nisin could be re-formulated with this concentration of nisin and re-assessed for its effectiveness on biofilms viability. Also, other AMPs or membrane-permeating compounds could be used in combination with meropenem and investigated for their efficiency in killing *P. aeruginosa* CWD cells.

Overall the results presented in Chapter 5 demonstrated that the antibiotic combination of meropenem with nisin presented the aerosol characteristics required from the Food and Drug Administration (FDA) and the European Medicines Agency guidelines for the development of nasal formulations. Thus, the combined formulation was suitable for nasal delivery. Moreover, we demonstrated that the biofilm viability was significantly reduced after delivery of the nasal formulation using a novel *in vitro* model to assess the effectiveness of nasal sprays on biofilms.

6.5 Overall conclusion

The work presented in this Thesis was undertaken utilising some novel research approaches. The use of wide-field fluorescence microscopy allowed the visualisation of biofilm cells down to the single cell level and the possibility to acquire a high number of images without the use of fixing agents that could create artifacts. The use of the fluorescent membrane/cell death dye mixture allowed the simultaneous quantification of total biofilm biomass, dead biomass and visualisation of single biofilm cell morphology. Pozzoli *et al.* recently demonstrated for the first time the suitability of RPMI 2650 as a model to closely reproduce the human nasal mucosa since this cell line was able to produce mucus and express xenobiotic transporters under air-liquid interface (ALI) conditions (*141*). In this Thesis, the RPMI 2650 nasal cell line was used as a model for studying the transport of drugs in combination with our novel nasal apparatus showing that the RPMI 2650 cell line represents a powerful *in vitro* tool to assess drug permeation studies of nasal products. Also, the development of the novel nasal apparatus allowed the analysis of biofilm viability after delivery of the nasal formulation and it could be further used as an *in vitro* system to study the effect of inhaled antibiotics on biofilms.

Overall, the work presented in this Thesis demonstrates for the first time that the CWD spherical morphotype also occurs in *P. aeruginosa* biofilms exposed to the carbapenem meropenem. We also showed that the CWD cells could be efficiently killed by the cationic AMP nisin. Until now, there are no nasal sprays that directly target biofilms in the nasal cavity or formulated as a drug combination. In this Thesis, we demonstrated that the combined nasal spray formulation was suitable for nasal delivery and most importantly significantly reduced *P. aeruginosa* biofilm viability.

As previously discussed in this Thesis, studies determined that also other bacterial species respond to the activity of some antibiotics modifying their morphology into a CWD morphotype, therefore the antibiotic strategy proposed in this Thesis could be effective in treating biofilms developed by other bacteria. Moreover, the antibiotic

combination of meropenem with nisin could potentially be used to treat biofilm infection in the lungs. This could be achieved by decreasing the particle size of the aerosol to ensure delivery to the lungs.

This Thesis demonstrated that the use of a β-lactam antibiotic able to induce the transition to the CWD spherical morphotype in combination with a membrane-permeating agent may represent a novel strategy to defeat *P. aeruginosa* biofilm infections. This Thesis also showed that CWD cells form in conditions that mimic the environment of CF lungs, implying that this morphotype may explain the reason of recurrent infections. Furthermore, this Thesis revealed that the antibiotic combination is suitable for nasal delivery and significantly decreased biofilm viability.

In conclusion, this Thesis demonstrated that the combination of a β-lactam antibiotic with a cation antimicrobial peptide may represent a promising therapy to specifically target and treat *P. aeruginosa* biofilms in the nose.

7 References

1. D. Elad, M. Wolf, T. Keck, Air-conditioning in the human nasal cavity. *Respir Physiol Neurobiol*. **163**, 121–127 (2008).
2. R. Dahl, N. Mygind, Anatomy, physiology and function of the nasal cavities in health and disease. *Adv Drug Deliv Rev*. **29**, 3–12 (1998).
3. J. R. Rock, S. H. Randell, B. L. M. Hogan, Airway basal stem cells: a perspective on their roles in epithelial homeostasis and remodeling. *Dis Model Mech*. **3**, 545–556 (2010).
4. E. R. Lillehoj, K. C. Kim, Airway mucus: its components and function. *Arch Pharm Res*. **25**, 770–780 (2002).
5. 2009 John Wiley & Sons, Ed., *Lung Function: Physiology, Measurement and Application in Medicine - John E. Cotes, David J. Chinn, Martin R. Miller - Google Books*.
6. H. Ellis, The respiratory system. *Anaesthesia & Intensive Care Medicine*. **12**, 533–538 (2011).
7. A. Iwasaki, E. F. Foxman, R. D. Molony, Early local immune defences in the respiratory tract. *Nat Rev Immunol*. **17**, 7–20 (2017).
8. D. F. Rogers, P. J. Barnes, Treatment of airway mucus hypersecretion. *Ann Med*. **38**, 116–125 (2006).
9. M. R. Knowles, R. C. Boucher, Mucus clearance as a primary innate defense mechanism for mammalian airways. *J Clin Invest*. **109**, 571–577 (2002).
10. J. V. Fahy, B. F. Dickey, Airway mucus function and dysfunction. *N Engl J Med*. **363**, 2233–2247 (2010).
11. J. B. Lyczak, C. L. Cannon, G. B. Pier, Lung infections associated with cystic fibrosis. *Clin Microbiol Rev*. **15**, 194–222 (2002).
12. N. Høiby, O. Ciofu, T. Bjarnsholt, Pseudomonas aeruginosa biofilms in cystic fibrosis. *Future Microbiol*. **5**, 1663–1674 (2010).
13. S. S. Yoon *et al.*, Pseudomonas aeruginosa anaerobic respiration in biofilms:

relationships to cystic fibrosis pathogenesis. *Dev Cell*. **3**, 593–603 (2002).

14. M. D. Bethesda, “Cystic Fibrosis Foundation Patient Registry. 2001 ” (Annual Data Report to the Center Directors., Cystic Fibrosis Foundation., 2002).
15. R. L. Gibson, J. L. Burns, B. W. Ramsey, Pathophysiology and management of pulmonary infections in cystic fibrosis. *Am J Respir Crit Care Med*. **168**, 918–951 (2003).
16. D. E. O’Donnell, P. Laveneziana, K. Webb, J. A. Neder, Chronic obstructive pulmonary disease: clinical integrative physiology. *Clin Chest Med*. **35**, 51–69 (2014).
17. T. F. Murphy *et al.*, Pseudomonas aeruginosa in chronic obstructive pulmonary disease. *Am J Respir Crit Care Med*. **177**, 853–860 (2008).
18. A. F. Barker, Bronchiectasis. *N Engl J Med*. **346**, 1383–1393 (2002).
19. C. S. Haworth, J. E. Foweraker, P. Wilkinson, R. F. Kenyon, D. Bilton, Inhaled colistin in patients with bronchiectasis and chronic Pseudomonas aeruginosa infection. *Am J Respir Crit Care Med*. **189**, 975–982 (2014).
20. M. S. Benninger *et al.*, Adult chronic rhinosinusitis: definitions, diagnosis, epidemiology, and pathophysiology. *Otolaryngol Head Neck Surg*. **129**, S1-32 (2003).
21. H. H. Ramadan, J. A. Sanclement, J. G. Thomas, Chronic rhinosinusitis and biofilms. *Otolaryngol Head Neck Surg*. **132**, 414–417 (2005).
22. B. A. Tajudeen, J. S. Schwartz, J. N. Palmer, Understanding biofilms in chronic sinusitis. *Curr Allergy Asthma Rep*. **16**, 10 (2016).
23. A. R. Sanderson, J. G. Leid, D. Hunsaker, Bacterial biofilms on the sinus mucosa of human subjects with chronic rhinosinusitis. *Laryngoscope*. **116**, 1121–1126 (2006).
24. B. J. Ferguson, D. B. Stolz, Demonstration of biofilm in human bacterial chronic rhinosinusitis. *Am J Rhinol*. **19**, 452–457 (2005).
25. R. J. Harvey, V. J. Lund, Biofilms and chronic rhinosinusitis: systematic review of evidence, current concepts and directions for research. *Rhinology*. **45**, 3–13

(2007).

26. M. Mahdavinia, A. Keshavarzian, M. C. Tobin, A. L. Landay, R. P. Schleimer, A comprehensive review of the nasal microbiome in chronic rhinosinusitis (CRS). *Clin Exp Allergy*. **46**, 21–41 (2016).

27. A. Schick, R. Kassen, Rapid diversification of Pseudomonas aeruginosa in cystic fibrosis lung-like conditions. *BioRxiv* (2017), doi:10.1101/231050.

28. M. Bassetti, M. Merelli, C. Temperoni, A. Astilean, New antibiotics for bad bugs: where are we? *Ann Clin Microbiol Antimicrob*. **12**, 22 (2013).

29. Infectious Diseases Society of America, The 10 x ’20 Initiative: pursuing a global commitment to develop 10 new antibacterial drugs by 2020. *Clin Infect Dis*. **50**, 1081–1083 (2010).

30. H. S. Sader, P. R. Rhomberg, D. J. Farrell, R. N. Jones, Antimicrobial activity of CXA-101, a novel cephalosporin tested in combination with tazobactam against Enterobacteriaceae, Pseudomonas aeruginosa, and Bacteroides fragilis strains having various resistance phenotypes. *Antimicrob Agents Chemother*. **55**, 2390–2394 (2011).

31. B. Moya *et al.*, Activity of a new cephalosporin, CXA-101 (FR264205), against beta-lactam-resistant Pseudomonas aeruginosa mutants selected in vitro and after antipseudomonal treatment of intensive care unit patients. *Antimicrob Agents Chemother*. **54**, 1213–1217 (2010).

32. V. Aloush, S. Navon-Venezia, Y. Seigman-Igra, S. Cabili, Y. Carmeli, Multidrug-resistant Pseudomonas aeruginosa: risk factors and clinical impact. *Antimicrob Agents Chemother*. **50**, 43–48 (2006).

33. L. G. Rahme *et al.*, Plants and animals share functionally common bacterial virulence factors. *Proc Natl Acad Sci U S A*. **97**, 8815–8821 (2000).

34. J. W. Costerton, P. S. Stewart, E. P. Greenberg, Bacterial biofilms: a common cause of persistent infections. *Science*. **284**, 1318–1322 (1999).

35. J. B. Lyczak, C. L. Cannon, G. B. Pier, Establishment of Pseudomonas aeruginosa infection: lessons from a versatile opportunist. *Microbes Infect*. **2**, 1051–1060

(2000).

36. I. Chatzinikolaou *et al.*, Recent Experience With Pseudomonas aeruginosa Bacteremia in Patients With Cancer. *Arch Intern Med*. **160**, 501 (2000).

37. L. Hall-Stoodley, J. W. Costerton, P. Stoodley, Bacterial biofilms: from the natural environment to infectious diseases. *Nat Rev Microbiol*. **2**, 95–108 (2004).

38. H. J. Busscher, H. C. van der Mei, How do bacteria know they are on a surface and regulate their response to an adhering state? *PLoS Pathog*. **8**, e1002440 (2012).

39. R. M. Donlan, Biofilms: microbial life on surfaces. *Emerging Infect Dis*. **8**, 881–890 (2002).

40. P. Watnick, R. Kolter, Biofilm, city of microbes. *J Bacteriol*. **182**, 2675–2679 (2000).

41. K. Hori, S. Matsumoto, Bacterial adhesion: From mechanism to control. *Biochem Eng J*. **48**, 424–434 (2010).

42. T. R. Garrett, M. Bhakoo, Z. Zhang, Bacterial adhesion and biofilms on surfaces. *Progress in Natural Science*. **18**, 1049–1056 (2008).

43. W. M. Dunne, Bacterial adhesion: seen any good biofilms lately? *Clin Microbiol Rev*. **15**, 155–166 (2002).

44. D. Dufour, V. Leung, C. M. Lévesque, Bacterial biofilm: structure, function, and antimicrobial resistance. *Endod. Topics*. **22**, 2–16 (2010).

45. G. O'Toole, H. B. Kaplan, R. Kolter, Biofilm formation as microbial development. *Annu Rev Microbiol*. **54**, 49–79 (2000).

46. M. Valentini, D. Gonzalez, D. A. Mavridou, A. Filloux, Lifestyle transitions and adaptive pathogenesis of Pseudomonas aeruginosa. *Curr Opin Microbiol*. **41**, 15–20 (2017).

47. O. E. Petrova, K. Gupta, J. Liao, J. S. Goodwine, K. Sauer, Divide and conquer: the Pseudomonas aeruginosa two-component hybrid SagS enables biofilm formation and recalcitrance of biofilm cells to antimicrobial agents via distinct

regulatory circuits. *Environ Microbiol*. **19**, 2005–2024 (2017).

48. H.-C. Flemming, J. Wingender, The biofilm matrix. *Nat Rev Microbiol*. **8**, 623–633 (2010).
49. E. Karatan, P. Watnick, Signals, regulatory networks, and materials that build and break bacterial biofilms. *Microbiol Mol Biol Rev*. **73**, 310–347 (2009).
50. E. Drenkard, Antimicrobial resistance of Pseudomonas aeruginosa biofilms. *Microbes Infect*. **5**, 1213–1219 (2003).
51. I. Olsen, Biofilm-specific antibiotic tolerance and resistance. *Eur J Clin Microbiol Infect Dis*. **34**, 877–886 (2015).
52. O. Lawe-Davies, WHO publishes list of bacteria for which new antibiotics are urgently needed. *World Health Organisation, Media Centre* (2017).
53. L. S. Moore, J. Cunningham, H. Donaldson, A clinical approach to managing Pseudomonas aeruginosa infections. *Br J Hosp Med (Lond)*. **77**, C50-4 (2016).
54. J. Jeukens *et al.*, Comparative genomics of isolates of a Pseudomonas aeruginosa epidemic strain associated with chronic lung infections of cystic fibrosis patients. *PLoS ONE*. **9**, e87611 (2014).
55. D. I. Andersson, D. Hughes, Antibiotic resistance and its cost: is it possible to reverse resistance? *Nat Rev Microbiol*. **8**, 260–271 (2010).
56. K. Lewis, Platforms for antibiotic discovery. *Nat Rev Drug Discov*. **12**, 371–387 (2013).
57. J. M. A. Blair, M. A. Webber, A. J. Baylay, D. O. Ogbolu, L. J. V. Piddock, Molecular mechanisms of antibiotic resistance. *Nat Rev Microbiol*. **13**, 42–51 (2015).
58. J. M. A. Blair, G. E. Richmond, L. J. V. Piddock, Multidrug efflux pumps in Gram-negative bacteria and their role in antibiotic resistance. *Future Microbiol*. **9**, 1165–1177 (2014).
59. Inactivation of Antibiotics and the Dissemination of Resistance Genes on JSTOR, (http://www.jstor.org.ezproxy.lib.uts.edu.au/stable/pdf/2883605.pdf?seq=1#page_scan_tab_contents).

60. C. Alvarez-Ortega, I. Wiegand, J. Olivares, R. E. W. Hancock, J. L. Martínez, Genetic determinants involved in the susceptibility of Pseudomonas aeruginosa to beta-lactam antibiotics. *Antimicrob Agents Chemother*. **54**, 4159–4167 (2010).

61. K. N. Schurek *et al.*, Involvement of pmrAB and phoPQ in polymyxin B adaptation and inducible resistance in non-cystic fibrosis clinical isolates of Pseudomonas aeruginosa. *Antimicrob Agents Chemother*. **53**, 4345–4351 (2009).

62. E. B. M. Breidenstein, C. de la Fuente-Núñez, R. E. W. Hancock, Pseudomonas aeruginosa: all roads lead to resistance. *Trends Microbiol*. **19**, 419–426 (2011).

63. L. Fernández, E. B. M. Breidenstein, R. E. W. Hancock, Creeping baselines and adaptive resistance to antibiotics. *Drug Resist Updat*. **14**, 1–21 (2011).

64. H. Van Acker, P. Van Dijck, T. Coenye, Molecular mechanisms of antimicrobial tolerance and resistance in bacterial and fungal biofilms. *Trends Microbiol*. **22**, 326–333 (2014).

65. M. S. Aparna, S. Yadav, Biofilms: microbes and disease. *Braz J Infect Dis*. **12**, 526–530 (2008).

66. M. Chen, Q. Yu, H. Sun, Novel strategies for the prevention and treatment of biofilm related infections. *Int J Mol Sci*. **14**, 18488–18501 (2013).

67. M. C. Walters, F. Roe, A. Bugnicourt, M. J. Franklin, P. S. Stewart, Contributions of antibiotic penetration, oxygen limitation, and low metabolic activity to tolerance of Pseudomonas aeruginosa biofilms to ciprofloxacin and tobramycin. *Antimicrob Agents Chemother*. **47**, 317–323 (2003).

68. E. Werner *et al.*, Stratified growth in Pseudomonas aeruginosa biofilms. *Appl Environ Microbiol*. **70**, 6188–6196 (2004).

69. S. J. Pamp, M. Gjermansen, H. K. Johansen, T. Tolker-Nielsen, Tolerance to the antimicrobial peptide colistin in Pseudomonas aeruginosa biofilms is linked to metabolically active cells, and depends on the pmr and mexAB-oprM genes. *Mol Microbiol*. **68**, 223–240 (2008).

70. O. Gefen, N. Q. Balaban, The importance of being persistent: heterogeneity of bacterial populations under antibiotic stress. *FEMS Microbiol Rev*. **33**, 704–717 (2009).

71. K. Lewis, Persister cells, dormancy and infectious disease. *Nat Rev Microbiol*. **5**, 48–56 (2007).

72. H. Lappin-Scott, S. Burton, P. Stoodley, Revealing a world of biofilms--the pioneering research of Bill Costerton. *Nat Rev Microbiol*. **12**, 781–787 (2014).

73. T. Coenye, H. J. Nelis, In vitro and in vivo model systems to study microbial biofilm formation. *J Microbiol Methods*. **83**, 89–105 (2010).

74. A. Heydorn *et al.*, Quantification of biofilm structures by the novel computer program COMSTAT. *Microbiology (Reading, Engl)*. **146 (Pt 10)**, 2395–2407 (2000).

75. A. Heydorn *et al.*, Experimental reproducibility in flow-chamber biofilms. *Microbiology (Reading, Engl)*. **146 (Pt 10)**, 2409–2415 (2000).

76. S. J. Pamp, C. Sternberg, T. Tolker-Nielsen, Insight into the microbial multicellular lifestyle via flow-cell technology and confocal microscopy. *Cytometry A*. **75**, 90–103 (2009).

77. S. A. Crusz *et al.*, Bursting the bubble on bacterial biofilms: a flow cell methodology. *Biofouling*. **28**, 835–842 (2012).

78. Pseudomonas aeruginosa Infections Treatment & Management: Approach Considerations, Medical Care, Surgical Care, (available at https://emedicine.medscape.com/article/226748-treatment).

79. N. Høiby *et al.*, Diagnosis of biofilm infections in cystic fibrosis patients. *APMIS*. **125**, 339–343 (2017).

80. J. Nelson, P. Karempelis, J. Dunitz, R. Hunter, H. Boyer, Pulmonary aspiration of sinus secretions in patients with cystic fibrosis. *Int Forum Allergy Rhinol*. **8**, 385–388 (2017).

81. T. Ganz, Antimicrobial polypeptides in host defense of the respiratory tract. *J. Clin. Invest.* **109**, 693–697 (2002).

82. J. E. Payne *et al.*, Activity of innate antimicrobial peptides and ivacaftor against clinical cystic fibrosis respiratory pathogens. *Int J Antimicrob Agents*. **50**, 427–435 (2017).

83. S. Esposito, C. Rosazza, C. S. Sciarrabba, N. Principi, Inhaled antibiotic therapy for the treatment of upper respiratory tract infections. *J Aerosol Med Pulm Drug Deliv*. **30**, 14–19 (2017).

84. M. I. Page, The mechanisms of reactions of .beta.-lactam antibiotics. *Acc Chem Res*. **17**, 144–151 (1984).

85. K. M. Papp-Wallace, A. Endimiani, M. A. Taracila, R. A. Bonomo, Carbapenems: past, present, and future. *Antimicrob Agents Chemother*. **55**, 4943–4960 (2011).

86. C. T. Ong, P. R. Tessier, C. Li, C. H. Nightingale, D. P. Nicolau, Comparative in vivo efficacy of meropenem, imipenem, and cefepime against Pseudomonas aeruginosa expressing MexA-MexB-OprM efflux pumps. *Diagn Microbiol Infect Dis*. **57**, 153–161 (2007).

87. J.-Y. Lee *et al.*, Clinical Features and Risk Factors for Development of Breakthrough Gram-Negative Bacteremia during Carbapenem Therapy. *Antimicrob Agents Chemother*. **60**, 6673–6678 (2016).

88. C.-H. Lee *et al.*, Risk factors and clinical significance of bacteremia caused by Pseudomonas aeruginosa resistant only to carbapenems. *J Microbiol Immunol Infect*. **50**, 677–683 (2017).

89. V. Estepa *et al.*, Characterisation of carbapenem-resistance mechanisms in clinical Pseudomonas aeruginosa isolates recovered in a Spanish hospital. *Enfermedades infecciosas y microbiologia clinica (English ed.)*. **35**, 141–147 (2017).

90. Y. Dickstein *et al.*, Multicentre open-label randomised controlled trial to compare colistin alone with colistin plus meropenem for the treatment of severe infections caused by carbapenem-resistant Gram-negative infections (AIDA): a study protocol. *BMJ Open*. **6**, e009956 (2016).

91. R. Rich, J. Montero, 641. *Crit Care Med*. **46**, 307 (2018).

92. R. Yadav, J. B. Bulitta, R. L. Nation, C. B. Landersdorfer, Optimization of Synergistic Combination Regimens against Carbapenem- and Aminoglycoside-Resistant Clinical Pseudomonas aeruginosa Isolates via Mechanism-Based Pharmacokinetic/Pharmacodynamic Modeling. *Antimicrob Agents Chemother*. **61** (2017), doi:10.1128/AAC.01011-16.

93. A. Louie, W. Liu, S. Fikes, D. Brown, G. L. Drusano, Impact of meropenem in combination with tobramycin in a murine model of Pseudomonas aeruginosa pneumonia. *Antimicrob Agents Chemother*. **57**, 2788–2792 (2013).

94. N. Anan, S. Toba, A. Ito, R. Nakamura, M. Tsuji, [In vitro combination effects of doripenem with aminoglycoside or ciprofloxacin against Pseudomonas aeruginosa]. *Jpn J Antibiot*. **64**, 203–216 (2011).

95. T.-P. Lim *et al.*, Effective antibiotics in combination against extreme drug-resistant Pseudomonas aeruginosa with decreased susceptibility to polymyxin B. *PLoS ONE*. **6**, e28177 (2011).

96. A. P. Zavascki, J. B. Bulitta, C. B. Landersdorfer, Combination therapy for carbapenem-resistant Gram-negative bacteria. *Expert Rev Anti Infect Ther*. **11**, 1333–1353 (2013).

97. O. McAuliffe, R. P. Ross, C. Hill, Lantibiotics: structure, biosynthesis and mode of action. *FEMS Microbiol Rev*. **25**, 285–308 (2001).

98. M. Hassan, M. Kjos, I. F. Nes, D. B. Diep, F. Lotfipour, Natural antimicrobial peptides from bacteria: characteristics and potential applications to fight against antibiotic resistance. *J Appl Microbiol*. **113**, 723–736 (2012).

99. S. H. White, W. C. Wimley, M. E. Selsted, Structure, function, and membrane integration of defensins. *Curr Opin Struct Biol*. **5**, 521–527 (1995).

100. R. E. Hancock, Peptide antibiotics. *The Lancet*. **349**, 418–422 (1997).

101. K. M. Scherer, J.-H. Spille, H.-G. Sahl, F. Grein, U. Kubitscheck, The lantibiotic nisin induces lipid II aggregation, causing membrane instability and vesicle budding. *Biophys J*. **108**, 1114–1124 (2015).

102. J. Delves-Broughton, P. Blackburn, R. J. Evans, J. Hugenholtz, Applications of the

bacteriocin, nisin. *Antonie Van Leeuwenhoek*. **69**, 193–202 (1996).

103. W. Liu, J. N. Hansen, Some chemical and physical properties of nisin, a small-protein antibiotic produced by Lactococcus lactis. *Appl Environ Microbiol*. **56**, 2551–2558 (1990).

104. A. Giacometti, O. Cirioni, F. Barchiesi, M. Fortuna, G. Scalise, In-vitro activity of cationic peptides alone and in combination with clinically used antimicrobial agents against Pseudomonas aeruginosa. *J Antimicrob Chemother*. **44**, 641–645 (1999).

105. M. R. Yeaman, N. Y. Yount, Mechanisms of antimicrobial peptide action and resistance. *Pharmacol Rev*. **55**, 27–55 (2003).

106. R. E. Hancock, R. Lehrer, Cationic peptides: a new source of antibiotics. *Trends Biotechnol*. **16**, 82–88 (1998).

107. B. Mishra, S. Reiling, D. Zarena, G. Wang, Host defense antimicrobial peptides as antibiotics: design and application strategies. *Curr Opin Chem Biol*. **38**, 87–96 (2017).

108. I. M. Helander, T. Mattila-Sandholm, Permeability barrier of the gram-negative bacterial outer membrane with special reference to nisin. *Int J Food Microbiol*. **60**, 153–161 (2000).

109. C. T. Lohans, J. C. Vederas, Development of class iia bacteriocins as therapeutic agents. *Int J Microbiol*. **2012**, 386410 (2012).

110. L. Illum, Nasal drug delivery: new developments and strategies. *Drug Discov Today*. **7**, 1184–1189 (2002).

111. S. Türker, E. Onur, Y. Ozer, Nasal route and drug delivery systems. *Pharm World Sci*. **26**, 137–142 (2004).

112. Opportunities and Challenges for the Nasal Administration of Nano...: Ingenta Connect, (available at http://www.ingentaconnect.com.ezproxy.lib.uts.edu.au/content/ben/ctmc/2015/00000015/00000004/art00010).

113. P. Arora, S. Sharma, S. Garg, Permeability issues in nasal drug delivery. *Drug*

Discov Today. **7**, 967–975 (2002).

114. L. Illum, Nasal drug delivery--possibilities, problems and solutions. *J Control Release*. **87**, 187–198 (2003).

115. K. H. Moore *et al.*, Safety, tolerability, and pharmacokinetics of sumatriptan in healthy subjects following ascending single intranasal doses and multiple intranasal doses. *Cephalalgia*. **17**, 541–550 (1997).

116. F. W. H. M. Merkus, N. G. M. Schipper, W. A. J. J. Hermens, S. G. Romeijn, J. C. Verhoef, Absorption enhancers in nasal drug delivery: efficacy and safety. *J Control Release*. **24**, 201–208 (1993).

117. (17) Nasal drug delivery system - an overview, (available at https://www.researchgate.net/publication/49601002_Nasal_drug_delivery_system_-_an_overview).

118. L. Illum, Nasal drug delivery - recent developments and future prospects. *J Control Release*. **161**, 254–263 (2012).

119. L. Casettari, L. Illum, Chitosan in nasal delivery systems for therapeutic drugs. *J Control Release*. **190**, 189–200 (2014).

120. H. Kublik, M. T. Vidgren, Nasal delivery systems and their effect on deposition and absorption. *Adv Drug Deliv Rev*. **29**, 157–177 (1998).

121. N. Klöcker *et al.*, Antimicrobial safety of a preservative-free nasal multiple-dose drug administration system. *Eur J Pharm Biopharm*. **57**, 489–493 (2004).

122. W. R. Ryan, P. H. Hwang, Safety of a preservative-free acidified saline nasal spray: a randomized, double-blind, placebo-controlled, crossover clinical trial. *Arch Otolaryngol Head Neck Surg*. **136**, 1099–1103 (2010).

123. E. O. Meltzer, P. E. Korenblat, B. Q. Lanier, L. Kelley, S. K. Tantry, Beclomethasone dipropionate nasal aerosol with an integrated dose counter: functionality and performance. *Allergy Asthma Proc*. **34**, 534–541 (2013).

124. N. K. Ostrom, The history and progression of treatments for allergic rhinitis. *Allergy Asthma Proc*. **35 Suppl 1**, S3-10 (2014).

125. P. G. Djupesland, Nasal drug delivery devices: characteristics and performance

in a clinical perspective-a review. *Drug Deliv Transl Res*. **3**, 42–62 (2013).

126. M. Pozzoli *et al.*, Dry powder nasal drug delivery: challenges, opportunities and a study of the commercial Teijin Puvlizer Rhinocort device and formulation. *Drug Dev. Ind. Pharm.* (2016).

127. H. R. Costantino, L. Illum, G. Brandt, P. H. Johnson, S. C. Quay, Intranasal delivery: physicochemical and therapeutic aspects. *Int J Pharm*. **337**, 1–24 (2007).

128. L. Tiozzo Fasiolo *et al.*, Opportunity and challenges of nasal powders: Drug formulation and delivery. *Eur J Pharm Sci* (2017), doi:10.1016/j.ejps.2017.09.027.

129. *Guideline on the pharmaceutical quality of inhalation and nasal products.* (2006).

130. U.S. Department of Health and Human Services, Food and Drug Administration, Center for Drug Evaluation and Research. Bioavailability and Bioequivalence Studies for Nasal Aerosol and Nasal Sprays for Local Action, 1–37 (2003).

131. J. D. Suman, B. L. Laube, T. Lin, G. Brouet, R. Dalby, Validity of in Vitro Tests on Aqueous Spray Pumps as Surrogates for Nasal Deposition. *Pharm Res* (2002).

132. J. D. Suman, Current understanding of nasal morphology and physiology as a drug delivery target. *Drug Deliv Transl Res*. **3**, 4–15 (2013).

133. J. D. Suman, B. L. Laube, R. Dalby, Comparison of nasal deposition and clearance of aerosol generated by nebulizer and an aqueous spray pump. *Pharm Res*. **16**, 1648–1652 (1999).

134. J. E. Polli, In vitro studies are sometimes better than conventional human pharmacokinetic in vivo studies in assessing bioequivalence of immediate-release solid oral dosage forms. *AAPS J*. **10**, 289–299 (2008).

135. M. Azimi, P. W. Longest, M. Hindle, Towards clinically relevant in vitro testing of locally acting nasal spray suspension products. 12(1), 121-130. *Respiratory Drug Delivery Europe* (2015).

136. P. F. DeCarlo, J. G. Slowik, D. R. Worsnop, P. Davidovits, J. L. Jimenez, Particle

morphology and density characterization by combined mobility and aerodynamic diameter measurements. part 1: theory. *Aerosol Science and Technology*. **38**, 1185–1205 (2004).

137. J. Heyder, Deposition of inhaled particles in the human respiratory tract and consequences for regional targeting in respiratory drug delivery. *Proc Am Thorac Soc*. **1**, 315–320 (2004).

138. P. Kolhe, M. Shah, N. Rathore, Eds., *Sterile Product Development: Formulation, Process, Quality and Regulatory Considerations* (Springer Science & Business Media, illustrated., 2013).

139. N. Diffraction, T. Spraytec, Nasal Spray Device Measurement Using Laser Diffraction and the Malvern Spraytec, (available at https://www.azom.com/article.aspx?ArticleID=2837).

140. J. Mitchell, S. Newman, H.-K. Chan, In vitro and in vivo aspects of cascade impactor tests and inhaler performance: a review. *AAPS PharmSciTech*. **8**, E110 (2007).

141. M. Pozzoli *et al.*, Application of RPMI 2650 nasal cell model to a 3D printed apparatus for the testing of drug deposition and permeation of nasal products. *Eur J Pharm Biopharm*. **107**, 223–233 (2016).

142. S. A. Shah *et al.*, Design of experiments to optimize an in vitro cast to predict human nasal drug deposition. *J Aerosol Med Pulm Drug Deliv*. **27**, 21–29 (2014).

143. V. Kundoor, R. N. Dalby, Assessment of nasal spray deposition pattern in a silicone human nose model using a color-based method. *Pharm Res*. **27**, 30–36 (2010).

144. J. T. Kelly, B. Asgharian, J. S. Kimbell, B. A. Wong, Particle deposition in human nasal airway replicas manufactured by different methods. part I: inertial regime particles. *Aerosol Science and Technology*. **38**, 1063–1071 (2004).

145. R. Hughes, J. Watterson, C. Dickens, D. Ward, A. Banaszek, Development of a nasal cast model to test medicinal nasal devices. *Proc Inst Mech Eng H*. **222**, 1013–1022 (2008).

146. J. Xi, P. W. Longest, Numerical predictions of submicrometer aerosol deposition in the nasal cavity using a novel drift flux approach. *Int J Heat Mass Transf*. **51**, 5562–5577 (2008).

147. M.-K. Lee *et al.*, Air-liquid interface culture of serially passaged human nasal epithelial cell monolayer for in vitro drug transport studies. *Drug Deliv*. **12**, 305–311 (2005).

148. H. X. Ong *et al.*, Primary Air-Liquid Interface Culture of Nasal Epithelium for Nasal Drug Delivery. *Mol Pharm*. **13**, 2242–2252 (2016).

149. J.-W. Yoo *et al.*, Serially Passaged Human Nasal Epithelial Cell Monolayer for in Vitro Drug Transport Studies. *Pharm Res*.

150. S. Dimova, M. E. Brewster, M. Noppe, M. Jorissen, P. Augustijns, The use of human nasal in vitro cell systems during drug discovery and development. *Toxicol In Vitro*. **19**, 107–122 (2005).

151. C. Ehrhardt, K.-J. Kim, *Biotechnology: Pharmaceutical Aspects* (2008).

152. M. C. Schmidt, H. Peter, S. R. Lang, G. Ditzinger, H. P. Merkle, In vitro cell models to study nasal mucosal permeability and metabolism. *Adv Drug Deliv Rev*. **29**, 51–79 (1998).

153. RPMI 2650 ATCC ® CCL-30™ Homo sapiens nasal septum; derived, (available at https://www.atcc.org/Products/All/CCL-30.aspx).

154. B. Srinivasan *et al.*, TEER measurement techniques for in vitro barrier model systems. *J Lab Autom*. **20**, 107–126 (2015).

155. S. Reichl, K. Becker, Cultivation of RPMI 2650 cells as an in-vitro model for human transmucosal nasal drug absorption studies: optimization of selected culture conditions. *J Pharm Pharmacol*. **64**, 1621–1630 (2012).

156. A. Wengst, S. Reichl, RPMI 2650 epithelial model and three-dimensional reconstructed human nasal mucosa as in vitro models for nasal permeation studies. *Eur J Pharm Biopharm*. **74**, 290–297 (2010).

157. L. Kürti *et al.*, Retinoic acid and hydrocortisone strengthen the barrier function of human RPMI 2650 cells, a model for nasal epithelial permeability.

Cytotechnology. **65**, 395–406 (2013).

158. Bacteria, (available at http://microbiologyonline.org/about-microbiology/introducing-microbes/bacteria).

159. K. D. Young, The selective value of bacterial shape. *Microbiol Mol Biol Rev*. **70**, 660–703 (2006).

160. P. C. Braga, M. D. Sasso, M. T. Sala, Sub-MIC concentrations of cefodizime interfere with various factors affecting bacterial virulence. *J Antimicrob Chemother*. **45**, 15–25 (2000).

161. M. Wainwright, L. T. Canham, K. Al-Wajeeh, C. L. Reeves, Morphological changes (including filamentation) in Escherichia coli grown under starvation conditions on silicon wafers and other surfaces. *Lett Appl Microbiol*. **29**, 224–227 (1999).

162. R. Mercier, Y. Kawai, J. Errington, General principles for the formation and proliferation of a wall-free (L-form) state in bacteria. *elife*. **3** (2014), doi:10.7554/eLife.04629.

163. R. Koebnik, K. P. Locher, P. Van Gelder, Structure and function of bacterial outer membrane proteins: barrels in a nutshell. *Mol Microbiol*. **37**, 239–253 (2000).

164. H. Nikaido, Outer membrane barrier as a mechanism of antimicrobial resistance. *Antimicrob Agents Chemother*. **33**, 1831–1836 (1989).

165. L. G. Monahan *et al.*, Rapid conversion of Pseudomonas aeruginosa to a spherical cell morphotype facilitates tolerance to carbapenems and penicillins but increases susceptibility to antimicrobial peptides. *Antimicrob Agents Chemother*. **58**, 1956–1962 (2014).

166. T. Horii, M. Kobayashi, K. Sato, S. Ichiyama, M. Ohta, An in-vitro study of carbapenem-induced morphological changes and endotoxin release in clinical isolates of gram-negative bacilli. *J Antimicrob Chemother*. **41**, 435–442 (1998).

167. T. Nishino, S. Nakazawa, Bacteriological study on effects of beta-lactam group antibiotics in high concentrations. *Antimicrob Agents Chemother*. **9**, 1033–1042 (1976).

168. C. Watanakunakorn, M. Hamburger, Induction of spheroplasts of Pseudomonas aeruginosa by carbenicillin. *Appl Microbiol*. **17**, 935–937 (1969).

169. M. Trautmann *et al.*, Antibacterial Activity of Meropenem against Pseudomonas aeruginosa , Including Antibiotic-Induced Morphological Changes and Endotoxin-Liberating Effects. *Eur J Clin Microbiol Infect Dis*. **17**, 754–760 (1998).

170. T. P. T. Cushnie, N. H. O'Driscoll, A. J. Lamb, Morphological and ultrastructural changes in bacterial cells as an indicator of antibacterial mechanism of action. *Cell Mol Life Sci*. **73**, 4471–4492 (2016).

171. J. J. Jackson, H. Kropp, Differences in mode of action of (β-lactam antibiotics influence morphology, LPS release and in vivo antibiotic efficacy. *J Endotoxin Res*. **3**, 201–218 (1996).

172. C. D. Fjell, J. A. Hiss, R. E. W. Hancock, G. Schneider, Designing antimicrobial peptides: form follows function. *Nat Rev Drug Discov*. **11**, 37–51 (2011).

173. T. Dörr, B. M. Davis, M. K. Waldor, Endopeptidase-mediated beta lactam tolerance. *PLoS Pathog*. **11**, e1004850 (2015).

174. P. C. Y. Woo, A. P. C. To, S. K. P. Lau, K. Y. Yuen, Facilitation of horizontal transfer of antimicrobial resistance by transformation of antibiotic-induced cell-wall-deficient bacteria. *Med Hypotheses*. **61**, 503–508 (2003).

175. P. Domínguez-Cuevas, R. Mercier, M. Leaver, Y. Kawai, J. Errington, The rod to L-form transition of Bacillus subtilis is limited by a requirement for the protoplast to escape from the cell wall sacculus. *Mol Microbiol*. **83**, 52–66 (2012).

176. R. Mercier, Y. Kawai, J. Errington, General principles for the formation and proliferation of a wall-free (L-form) state in bacteria.

177. E. A. Marlieke de Kraker, A. J. Stewardson, S. Harbarth, Will 10 million people die a year due to antimicrobial resistance by 2050? *PLoS Med.* **13.11 (2016): e1002184.** (2016).

178. A. Filloux, J.-L. Ramos, Eds., *Pseudomonas Methods and Protocols* (Springer New York, New York, NY, 2014), vol. 1149 of *Methods in Molecular Biology*.

179. P. R. Patel, S. E. Cook, Stability of meropenem in intravenous solutions. *Am J*

Health Syst Pharm. **54**, 412–421 (1997).

180. K. Berthoin, C. S. Le Duff, J. Marchand-Brynaert, S. Carryn, P. M. Tulkens, Stability of meropenem and doripenem solutions for administration by continuous infusion. *Journal of Antimicrobial Chemotherapy*. **65**, 1073–1075 (2010).

181. S. Asif, T. Alam, A. Nawab, S. Naveed, O. Access, Simple UV Spectrophotometric Method Development for Determination of Meropenem in Bulk Form. *RADS Journal of Pharmacy and Pharmaceutical Sciences* (2017).

182. A. S. . Mendez, M. Steppe, E. E. . Schapoval, Validation of HPLC and UV spectrophotometric methods for the determination of meropenem in pharmaceutical dosage form. *J Pharm Biomed Anal*. **33**, 947–954 (2003).

183. M. Lim, M. J. Citardi, J.-L. Leong, Topical antimicrobials in the management of chronic rhinosinusitis: a systematic review. *Am J Rhinol*. **22**, 381–389 (2008).

184. T. A. Davies, W. Shang, K. Bush, R. K. Flamm, Affinity of doripenem and comparators to penicillin-binding proteins in Escherichia coli and Pseudomonas aeruginosa. *Antimicrob Agents Chemother*. **52**, 1510–1512 (2008).

185. P. A. Lambert, Mechanisms of antibiotic resistance in Pseudomonas aeruginosa. *J R Soc Med*. **95 Suppl 41**, 22–26 (2002).

186. Q. Wei, L. Z. Ma, Biofilm matrix and its regulation in Pseudomonas aeruginosa. *Int J Mol Sci*. **14**, 20983–21005 (2013).

187. P. S. Stewart, J. W. Costerton, Antibiotic resistance of bacteria in biofilms. *The Lancet*. **358**, 135–138 (2001).

188. P. A. Suci, M. W. Mittelman, F. P. Yu, G. G. Geesey, Investigation of ciprofloxacin penetration into Pseudomonas aeruginosa biofilms. *Antimicrob Agents Chemother*. **38**, 2125–2133 (1994).

189. M. Tré-Hardy *et al.*, Effect of antibiotic co-administration on young and mature biofilms of cystic fibrosis clinical isolates: the importance of the biofilm model. *Int J Antimicrob Agents*. **33**, 40–45 (2009).

190. S. Diraviam Dinesh, S. Diraviam Dinesh, Artificial Sputum Medium. *Protoc exch*

(2010), doi:10.1038/protex.2010.212.

191. L. Spicuzza *et al.*, Emerging pathogens in cystic fibrosis: ten years of follow-up in a cohort of patients. *Eur J Clin Microbiol Infect Dis*. **28**, 191–195 (2009).

192. R. Amann, B. M. Fuchs, Single-cell identification in microbial communities by improved fluorescence in situ hybridization techniques. *Nat Rev Microbiol*. **6**, 339–348 (2008).

193. W. H. DePas *et al.*, Exposing the Three-Dimensional Biogeography and Metabolic States of Pathogens in Cystic Fibrosis Sputum via Hydrogel Embedding, Clearing, and rRNA Labeling. *MBio*. **7** (2016), doi:10.1128/mBio.00796-16.

194. D. S. Richardson, J. W. Lichtman, Clarifying Tissue Clearing. *Cell*. **162**, 246–257 (2015).

195. J. B. Treweek *et al.*, Whole-body tissue stabilization and selective extractions via tissue-hydrogel hybrids for high-resolution intact circuit mapping and phenotyping. *Nat Protoc*. **10**, 1860–1896 (2015).

196. B. Yang *et al.*, Single-cell phenotyping within transparent intact tissue through whole-body clearing. *Cell*. **158**, 945–958 (2014).

197. A. K. Pragasam, M. Raghanivedha, S. Anandan, B. Veeraraghavan, Characterization of Pseudomonas aeruginosa with discrepant carbapenem susceptibility profile. *Ann Clin Microbiol Antimicrob*. **15**, 12 (2016).

198. C. Rizek *et al.*, Characterization of carbapenem-resistant Pseudomonas aeruginosa clinical isolates, carrying multiple genes coding for this antibiotic resistance. *Ann Clin Microbiol Antimicrob*. **13**, 43 (2014).

199. Expanded Academic ASAP - Document - The epidemiology, pathogenesis and treatment of pseudomonas aeruginosa infections, (available at http://go.galegroup.com.ezproxy.lib.uts.edu.au/ps/retrieve.do?tabID=T002&resultListType=RESULT_LIST&searchResultsType=SingleTab&searchType=AdvancedSearchForm&currentPosition=1&docId=GALE%7CA200668972&docType=Article&sort=RELEVANCE&contentSegment=&prodId=EAIM&contentSet=GALE%7CA

200668972&searchId=R1&userGroupName=uts&inPS=true).

200. J. L. Kuti *et al.*, Microbiological activity of ceftolozane/tazobactam, ceftazidime, meropenem, and piperacillin/tazobactam against Pseudomonas aeruginosa isolated from children with cystic fibrosis. *Diagn Microbiol Infect Dis*. **83**, 53–55 (2015).

201. L. Chen, Y. Wen, The role of bacterial biofilm in persistent infections and control strategies. *Int. J. Oral Sci.* **3**, 66–73 (2011).

202. L. R. Mulcahy, V. M. Isabella, K. Lewis, Pseudomonas aeruginosa biofilms in disease. *Microb Ecol*. **68**, 1–12 (2014).

203. R. L. Henry, C. M. Mellis, L. Petrovic, Mucoid Pseudomonas aeruginosa is a marker of poor survival in cystic fibrosis. *Pediatr Pulmonol*. **12**, 158–161 (1992).

204. J. Haagensen *et al.*, Spatiotemporal pharmacodynamics of meropenem- and tobramycin-treated Pseudomonas aeruginosa biofilms. *J Antimicrob Chemother*. **72**, 3357–3365 (2017).

205. M. H. Alderman, L. R. Freedman, Experimental pyelonephritis. x. the direct injection of e. coli protoplasts into the medulla of the rabbit kidney. *Yale J Biol Med*. **36**, 157–164 (1963).

206. A. Toshkov *et al.*, Experimental pyelonephritis with L-forms of Proteus mirabilis in rats. *Acta Microbiol. Virol. Immunol. Bulg. Acad. Sci*, 6, 35–47. (1977).

207. G. J. Domingue, H. B. Woody, Bacterial persistence and expression of disease. *Clin Microbiol Rev*. **10**, 320–344 (1997).

208. N. Høiby *et al.*, The clinical impact of bacterial biofilms. *Int. J. Oral Sci.* **3**, 55–65 (2011).

209. S. L. Percival *et al.*, A review of the scientific evidence for biofilms in wounds. *Wound Repair Regen*. **20**, 647–657 (2012).

210. C. Winstanley, S. O'Brien, M. A. Brockhurst, Pseudomonas aeruginosa Evolutionary Adaptation and Diversification in Cystic Fibrosis Chronic Lung Infections. *Trends Microbiol*. **24**, 327–337 (2016).

211. R. P. Schleimer, Immunopathogenesis of chronic rhinosinusitis and nasal

polyposis. *Annu Rev Pathol*. **12**, 331–357 (2017).

212. H. Wu, C. Moser, H.-Z. Wang, N. Høiby, Z.-J. Song, Strategies for combating bacterial biofilm infections. *Int. J. Oral Sci.* **7**, 1–7 (2015).

213. R. P. Howlin *et al.*, Low-Dose Nitric Oxide as Targeted Anti-biofilm Adjunctive Therapy to Treat Chronic Pseudomonas aeruginosa Infection in Cystic Fibrosis. *Mol Ther*. **25**, 2104–2116 (2017).

214. Low Dose Nitric Oxide As Adjunctive Therapy To Reduce Antimicrobial Tolerance Of Pseudomonas Aeruginosa Biofilms In The Treatment Of Patients With Cystic Fibrosis: Report Of A Proof Of Concept Clinical Trial | B38. UPDATE IN ADULT CYSTIC FIBROSIS, (available at http://www.atsjournals.org.ezproxy.lib.uts.edu.au/doi/pdf/10.1164/ajrccm-conference.2014.189.1_MeetingAbstracts.A2843).

215. G. G. Zhanel *et al.*, Ceftolozane/tazobactam: a novel cephalosporin/β-lactamase inhibitor combination with activity against multidrug-resistant gram-negative bacilli. *Drugs*. **74**, 31–51 (2014).

216. M. Kolpen *et al.*, Reinforcement of the bactericidal effect of ciprofloxacin on Pseudomonas aeruginosa biofilm by hyperbaric oxygen treatment. *Int J Antimicrob Agents*. **47**, 163–167 (2016).

217. P. K. Taylor, A. T. Y. Yeung, R. E. W. Hancock, Antibiotic resistance in Pseudomonas aeruginosa biofilms: towards the development of novel anti-biofilm therapies. *J Biotechnol*. **191**, 121–130 (2014).

218. S. C. Langton Hewer, A. R. Smyth, Antibiotic strategies for eradicating Pseudomonas aeruginosa in people with cystic fibrosis. *Cochrane Database Syst Rev*, CD004197 (2014).

219. N. Hoffmann *et al.*, Azithromycin blocks quorum sensing and alginate polymer formation and increases the sensitivity to serum and stationary-growth-phase killing of Pseudomonas aeruginosa and attenuates chronic P. aeruginosa lung infection in Cftr(-/-) mice. *Antimicrob Agents Chemother*. **51**, 3677–3687 (2007).

220. The Epidemiology, Pathogenesis and Treatment of Pseudomonas aeruginosa

Infe...: EBSCOhost, (available at http://web.b.ebscohost.com.ezproxy.lib.uts.edu.au/ehost/pdfviewer/pdfviewer?vid=1&sid=5051346f-6e69-4d4a-ab29-f4611589061a%40sessionmgr103).

221. K. Z. Vardakas, G. S. Tansarli, I. A. Bliziotis, M. E. Falagas, β-Lactam plus aminoglycoside or fluoroquinolone combination versus β-lactam monotherapy for Pseudomonas aeruginosa infections: a meta-analysis. *Int J Antimicrob Agents*. **41**, 301–310 (2013).

222. R. Marcus, M. Paul, H. Elphick, L. Leibovici, Clinical implications of β-lactam-aminoglycoside synergism: systematic review of randomised trials. *Int J Antimicrob Agents*. **37**, 491–503 (2011).

223. P. D. Tamma, S. E. Cosgrove, L. L. Maragakis, Combination therapy for treatment of infections with gram-negative bacteria. *Clin Microbiol Rev*. **25**, 450–470 (2012).

224. V. L. D. Siqueira *et al.*, Structural changes and differentially expressed genes in Pseudomonas aeruginosa exposed to meropenem-ciprofloxacin combination. *Antimicrob Agents Chemother*. **58**, 3957–3967 (2014).

225. E. Fuller *et al.*, Beta-lactam resistance in Staphylococcus aureus cells that do not require a cell wall for integrity. *Antimicrob Agents Chemother*. **49**, 5075–5080 (2005).

226. J. H. Merritt, D. E. Kadouri, G. A. O'Toole, *Curr Protoc Microbiol*, in press, doi:10.1002/9780471729259.mc01b01s00.

227. E. Peeters, H. J. Nelis, T. Coenye, Comparison of multiple methods for quantification of microbial biofilms grown in microtiter plates. *J Microbiol Methods*. **72**, 157–165 (2008).

228. M. J. Franklin, C. Chang, T. Akiyama, B. Bothner, New technologies for studying biofilms. *Microbiol. Spectr.* **3** (2015), doi:10.1128/microbiolspec.MB-0016-2014.

229. M.-Y. Chen, D.-J. Lee, J.-H. Tay, K.-Y. Show, Staining of extracellular polymeric substances and cells in bioaggregates. *Appl Microbiol Biotechnol*. **75**, 467–474 (2007).

230. I. K. Delattre *et al.*, Optimizing β-lactams treatment in critically-ill patients using pharmacokinetics/pharmacodynamics targets: are first conventional doses effective? *Expert Rev Anti Infect Ther*. **15**, 677–688 (2017).

231. 2017 Academic Press, Ed., *Antimicrobial Stewardship - Google Books*.

232. G. Jung, H. G. Sahl, Eds., *Nisin and Novel Lantibiotics* (Springer Science & Business Media, 1991).

233. E. Breukink, B. de Kruijff, The lantibiotic nisin, a special case or not? *Biochimica et Biophysica Acta (BBA) - Biomembranes*. **1462**, 223–234 (1999).

234. E. Breukink, B. de Kruijff, Lipid II as a target for antibiotics. *Nat Rev Drug Discov*. **5**, 321–332 (2006).

235. I. Wiedemann *et al.*, Specific binding of nisin to the peptidoglycan precursor lipid II combines pore formation and inhibition of cell wall biosynthesis for potent antibiotic activity. *J Biol Chem*. **276**, 1772–1779 (2001).

236. H. E. Hasper *et al.*, An alternative bactericidal mechanism of action for lantibiotic peptides that target lipid II. *Science*. **313**, 1636–1637 (2006).

237. Expanded Academic ASAP - Document - The expanding role of lipid II as a target for lantibiotics, (available at http://go.galegroup.com.ezproxy.lib.uts.edu.au/ps/retrieve.do?tabID=T002&resultListType=RESULT_LIST&searchResultsType=SingleTab&searchType=AdvancedSearchForm&currentPosition=1&docId=GALE%7CA224840269&docType=Report&sort=RELEVANCE&contentSegment=&prodId=EAIM&contentSet=GALE%7CA224840269&searchId=R1&userGroupName=uts&inPS=true).

238. B. Szomolay, I. Klapper, J. Dockery, P. S. Stewart, Adaptive responses to antimicrobial agents in biofilms. *Environ Microbiol*. **7**, 1186–1191 (2005).

239. D. Field, N. Seisling, P. D. Cotter, R. P. Ross, C. Hill, Synergistic Nisin-Polymyxin Combinations for the Control of Pseudomonas Biofilm Formation. *Front Microbiol*. **7**, 1713 (2016).

240. N. Bagge *et al.*, Pseudomonas aeruginosa biofilms exposed to imipenem exhibit changes in global gene expression and beta-lactamase and alginate production.

Antimicrob Agents Chemother. **48**, 1175–1187 (2004).

241. L. Fernández *et al.*, Adaptive resistance to the “last hope” antibiotics polymyxin B and colistin in Pseudomonas aeruginosa is mediated by the novel two-component regulatory system ParR-ParS. *Antimicrob Agents Chemother*. **54**, 3372–3382 (2010).

242. A. Skiada, A. Markogiannakis, D. Plachouras, G. L. Daikos, Adaptive resistance to cationic compounds in Pseudomonas aeruginosa. *Int J Antimicrob Agents*. **37**, 187–193 (2011).

243. M. Ranieri, Mechanisms of biofilm stimulation by subinhibitory concentrations of antimicrobials. *Curr Opin Microbiol* (2018).

244. G. Orhan, A. Bayram, Y. Zer, I. Balci, Synergy tests by E test and checkerboard methods of antimicrobial combinations against Brucella melitensis. *J Clin Microbiol*. **43**, 140–143 (2005).

245. A. Filloux, J.-L. Ramos, Eds., *Pseudomonas Methods and Protocols* (Springer New York, New York, NY, 2014), vol. 1149 of *Methods in Molecular Biology*.

246. S. L. Chua *et al.*, Selective labelling and eradication of antibiotic-tolerant bacterial populations in Pseudomonas aeruginosa biofilms. *Nat Commun*. **7**, 10750 (2016).

247. L. Yang, M. Nilsson, M. Gjermansen, M. Givskov, T. Tolker-Nielsen, Pyoverdine and PQS mediated subpopulation interactions involved in Pseudomonas aeruginosa biofilm formation. *Mol Microbiol*. **74**, 1380–1392 (2009).

248. E. Banin, M. L. Vasil, E. P. Greenberg, Iron and Pseudomonas aeruginosa biofilm formation. *Proc Natl Acad Sci U S A*. **102**, 11076–11081 (2005).

249. P. K. Singh, M. R. Parsek, E. P. Greenberg, M. J. Welsh, A component of innate immunity prevents bacterial biofilm development. *Nature*. **417**, 552–555 (2002).

250. K. Sauer, A. K. Camper, G. D. Ehrlich, J. W. Costerton, D. G. Davies, Pseudomonas aeruginosa displays multiple phenotypes during development as a biofilm. *J Bacteriol*. **184**, 1140–1154 (2002).

251. M. Al-Holy, M. Lin, B. Rasco, Destruction of Listeria monocytogenes in Sturgeon (Acipenser transmontanus) Caviar by a Combination of Nisin with Chemical Antimicrobials or Moderate Heat. *J Food Prot*. **68**, 512–520 (2005).

252. C. C. Minei, B. C. Gomes, R. P. Ratti, C. E. M. D'Angelis, E. C. P. De Martinis, Influence of Peroxyacetic Acid and Nisin and Coculture with Enterococcus faecium on Listeria monocytogenes Biofilm Formation. *J Food Prot*. **71**, 634–638 (2008).

253. S. L. Gellatly, R. E. W. Hancock, Pseudomonas aeruginosa: new insights into pathogenesis and host defenses. *Pathog Dis*. **67**, 159–173 (2013).

254. D. Lebeaux, J.-M. Ghigo, C. Beloin, Biofilm-related infections: bridging the gap between clinical management and fundamental aspects of recalcitrance toward antibiotics. *Microbiol Mol Biol Rev*. **78**, 510–543 (2014).

255. J. Cryer, I. Schipor, J. R. Perloff, J. N. Palmer, Evidence of bacterial biofilms in human chronic sinusitis. *ORL J Otorhinolaryngol Relat Spec*. **66**, 155–158 (2004).

256. T. F. P. Bezerra, F. G. de M. Padua, E. M. M. S. Gebrim, P. H. N. Saldiva, R. L. Voegels, Biofilms in chronic rhinosinusitis with nasal polyps. *Otolaryngol Head Neck Surg*. **144**, 612–616 (2011).

257. Demonstration of Biofilm in Human Bacterial Chronic Rhinosinusiti...: Ingenta Connect, (available at http://www.ingentaconnect.com.ezproxy.lib.uts.edu.au/content/ocean/ajr/2005/00000019/00000005/art00006).

258. V. Kundoor, R. N. Dalby, Effect of formulation- and administration-related variables on deposition pattern of nasal spray pumps evaluated using a nasal cast. *Pharm Res*. **28**, 1895–1904 (2011).

259. P. Colombo, *Inhalation Drug Delivery: Techniques and Products* (2012).

260. T. S. O. London, in *British Pharmacopeia* (London, UK, 2016), p. Volume V, Appendix XII C.

261. M. Pozzoli *et al.*, in *Application of RPMI 2650 nasal cell model to a 3D printed apparatus for the testing of drug deposition and permeation of nasal products*,

M. Pozzoli et al., Eds. (European Journal of Pharmaceutics and Biopharmaceutics, Europe, 2016).

262. Y. Liu, M. R. Johnson, E. A. Matida, S. Kherani, J. Marsan, Creation of a standardized geometry of the human nasal cavity. *J Appl Physiol*. **106**, 784–795 (2009).

263. P. Dayal, M. S. Shaik, M. Singh, Evaluation of different parameters that affect droplet-size distribution from nasal sprays using the Malvern Spraytec. *J Pharm Sci*. **93**, 1725–1742 (2004).

264. M. Y. Foo, Y.-S. Cheng, W.-C. Su, M. D. Donovan, The influence of spray properties on intranasal deposition. *J Aerosol Med*. **20**, 495–508 (2007).

265. G. J. Zwartz, R. A. Guilmette, Effect of flow rate on particle deposition in a replica of a human nasal airway. *Inhal Toxicol*. **13**, 109–127 (2001).

266. J. D. Schroeter, J. S. Kimbell, B. Asgharian, Analysis of particle deposition in the turbinate and olfactory regions using a human nasal computational fluid dynamics model. *J Aerosol Med*. **19**, 301–313 (2006).

267. K. Matsumoto *et al.*, Japanese Never-Smokers without Asthma.

268. S.-Y. Lee *et al.*, Influence of chronic sinusitis and nasal polyp on the lower airway of subjects without lower airway diseases. *Allergy Asthma Immunol Res*. **6**, 310–315 (2014).

269. Objective Assessment of Lower Airway Involvement in Chronic Rhino...: Ingenta Connect, (available at http://www.ingentaconnect.com.ezproxy.lib.uts.edu.au/content/ocean/ajr/2004/00000018/00000001/art00003).

270. VALIDATION OF ANALYTICAL PROCEDURES: TEXT AND METHODOLOGY Q2(R1).

271. Manufacturing, C. Documentation, Manufacturing, C. Documentation, Nasal Spray and Inhalation Solution, Suspension,.

272. Y. S. Cheng *et al.*, Characterization of nasal spray pumps and deposition pattern in a replica of the human nasal airway. *J Aerosol Med*. **14**, 267–280 (2001).

273. T. Fairlie, D. J. Shapiro, A. L. Hersh, L. A. Hicks, National trends in visit rates and

antibiotic prescribing for adults with acute sinusitis. *Arch Intern Med*. **172**, 1513 (2012).

274. L. Rudmik, Z. M. Soler, Medical therapies for adult chronic sinusitis: A systematic review. *JAMA*. **314**, 926–939 (2015).

275. M. U. Ghori, M. H. Mahdi, A. M. Smith, B. R. Conway, Nasal Drug Delivery Systems: An Overview. *American Journal of Pharmacological Sciences* (2015).

276. B. Sarmento *et al.*, Cell-based in vitro models for predicting drug permeability. *Expert Opin Drug Metab Toxicol*. **8**, 607–621 (2012).

277. Antimicrobial resistance: Tackling a crisis for the health and wealth of nations (2014).

278. S. Shrivastava, P. Shrivastava, J. Ramasamy, World Health Organization releases global priority list of antibiotic-resistant bacteria to guide research, discovery, and development of new antibiotics. *J. Med. Soc.* **0**, 0 (2017).

279. S. de Bentzmann, P. Plésiat, The Pseudomonas aeruginosa opportunistic pathogen and human infections. *Environ Microbiol*. **13**, 1655–1665 (2011).

280. R. B. Cain, D. Lal, Update on the management of chronic rhinosinusitis. *Infect Drug Resist*. **6**, 1–14 (2013).

281. Z. Zhang *et al.*, Clinical factors associated with bacterial biofilm formation in chronic rhinosinusitis. *Otolaryngol Head Neck Surg*. **144**, 457–462 (2011).

282. A. J. Psaltis, E. K. Weitzel, K. R. Ha, P.-J. Wormald, The effect of bacterial biofilms on post-sinus surgical outcomes. *Am J Rhinol*. **22**, 1–6 (2008).

283. I. Brook, Microbiology of chronic rhinosinusitis. *Eur J Clin Microbiol Infect Dis*. **35**, 1059–1068 (2016).

284. A. J. Wood, J. Fraser, S. Swift, S. Amirapu, R. G. Douglas, Are biofilms associated with an inflammatory response in chronic rhinosinusitis? *Int Forum Allergy Rhinol*. **1**, 335–339 (2011).

285. Y.-J. Mao, H.-H. Chen, B. Wang, X. Liu, G.-Y. Xiong, Increased expression of MUC5AC and MUC5B promoting bacterial biofilm formation in chronic rhinosinusitis patients. *Auris Nasus Larynx*. **42**, 294–298 (2015).

286. M. Mantero *et al.*, Once daily aerosolised tobramycin in adult patients with cystic fibrosis in the management of Pseudomonas aeruginosa chronic infection. *Multidiscip Respir Med*. **12**, 2 (2017).

287. L. Y. Chong *et al.*, Saline irrigation for chronic rhinosinusitis. *Cochrane Database Syst Rev*. **4**, CD011995 (2016).

288. M. B. Barshak, M. L. Durand, The role of infection and antibiotics in chronic rhinosinusitis. *Laryngoscope Investig. Otolaryngol.* **2**, 36–42 (2017).

289. O. Ciofu *et al.*, P. aeruginosa in the paranasal sinuses and transplanted lungs have similar adaptive mutations as isolates from chronically infected CF lungs. *J Cyst Fibros*. **12**, 729–736 (2013).

290. A. Folkesson *et al.*, Adaptation of Pseudomonas aeruginosa to the cystic fibrosis airway: an evolutionary perspective. *Nat Rev Microbiol*. **10**, 841–851 (2012).

291. K. L. Whiteson *et al.*, The upper respiratory tract as a microbial source for pulmonary infections in cystic fibrosis. Parallels from island biogeography. *Am J Respir Crit Care Med*. **189**, 1309–1315 (2014).

292. J. Cogen, M. Rosenfeld, Pseudomonas aeruginosa eradication: Finally moving the needle? *J Cyst Fibros*. **16**, 309–310 (2017).

293. K. J. Choi *et al.*, Correlation between sinus and lung cultures in lung transplant patients with cystic fibrosis. *Int Forum Allergy Rhinol*. **8**, 389–393 (2017).

294. M. E. Møller *et al.*, Sinus bacteriology in patients with cystic fibrosis or primary ciliary dyskinesia: A systematic review. *Am J Rhinol Allergy*. **31**, 293–298 (2017).

295. K. Aanæs, Bacterial sinusitis can be a focus for initial lung colonisation and chronic lung infection in patients with cystic fibrosis. *J Cyst Fibros*. **12 Suppl 2**, S1-20 (2013).

296. L. Yang, L. Jelsbak, S. Molin, Microbial ecology and adaptation in cystic fibrosis airways. *Environ Microbiol*. **13**, 1682–1689 (2011).

297. E. E. Smith *et al.*, Genetic adaptation by Pseudomonas aeruginosa to the airways of cystic fibrosis patients. *Proc Natl Acad Sci U S A*. **103**, 8487–8492 (2006).

298. E. Mahenthiralingam, M. E. Campbell, D. P. Speert, Nonmotility and phagocytic resistance of Pseudomonas aeruginosa isolates from chronically colonized patients with cystic fibrosis. *Infect Immun*. **62**, 596–605 (1994).

299. C. Hoboth *et al.*, Dynamics of adaptive microevolution of hypermutable Pseudomonas aeruginosa during chronic pulmonary infection in patients with cystic fibrosis. *J Infect Dis*. **200**, 118–130 (2009).

300. D. Hill *et al.*, Antibiotic susceptabilities of Pseudomonas aeruginosa isolates derived from patients with cystic fibrosis under aerobic, anaerobic, and biofilm conditions. *J Clin Microbiol*. **43**, 5085–5090 (2005).

301. S. J. Dando *et al.*, Pathogens penetrating the central nervous system: infection pathways and the cellular and molecular mechanisms of invasion. *Clin Microbiol Rev*. **27**, 691–726 (2014).

302. K. Patel, D. B. Clifford, Bacterial brain abscess. *Neurohospitalist*. **4**, 196–204 (2014).

303. C.-R. Huang *et al.*, The clinical characteristics of adult bacterial meningitis caused by non- Pseudomonas (Ps .) aeruginosa Pseudomonas species: A clinical comparison with Ps. aeruginosa meningitis. *Kaohsiung J Med Sci*. **34**, 49–55 (2018).

304. Y. C. Chuang, W. N. Chang, C. H. Lu, H. S. Wu, H. W. Chang, Pseudomonas aeruginosa central nervous system infections: analysis of clinical features of 16 adult patients. *Zhonghua Yi Xue Za Zhi (Taipei)*. **62**, 300–307 (1999).

305. B. Capitano *et al.*, Meropenem administered as a prolonged infusion to treat serious gram-negative central nervous system infections. *Pharmacotherapy*. **24**, 803–807 (2004).

306. G. Billings *et al.*, De novo morphogenesis in L-forms via geometric control of cell growth. *Mol Microbiol*. **93**, 883–896 (2014).

307. Y. Briers *et al.*, Intracellular vesicles as reproduction elements in cell wall-deficient L-form bacteria. *PLoS ONE*. **7**, e38514 (2012).

308. W. A. Glover, Y. Yang, Y. Zhang, Insights into the molecular basis of L-form

formation and survival in Escherichia coli. *PLoS ONE*. **4**, e7316 (2009).

309. L. Michailova, V. Kussovsky, T. Radoucheva, M. Jordanova, N. Markova, Persistence of Staphylococcus aureus L-form during experimental lung infection in rats. *FEMS Microbiol Lett*. **268**, 88–97 (2007).

310. B. Mishra, G. Wang, Individual and Combined Effects of Engineered Peptides and Antibiotics on Pseudomonas aeruginosa Biofilms. *Pharmaceuticals (Basel)*. **10** (2017), doi:10.3390/ph10030058.

311. D. Minardi *et al.*, The antimicrobial peptide tachyplesin III coated alone and in combination with intraperitoneal piperacillin-tazobactam prevents ureteral stent Pseudomonas infection in a rat subcutaneous pouch model. *Peptides*. **28**, 2293–2298 (2007).

312. H. Rudilla *et al.*, Synergistic antipseudomonal effects of synthetic peptide AMP38 and carbapenems. *Molecules*. **21** (2016), doi:10.3390/molecules21091223.

313. C. de la Fuente-Núñez *et al.*, D-enantiomeric peptides that eradicate wild-type and multidrug-resistant biofilms and protect against lethal Pseudomonas aeruginosa infections. *Chem Biol*. **22**, 196–205 (2015).

314. L. Grassi, G. Maisetta, S. Esin, G. Batoni, Combination Strategies to Enhance the Efficacy of Antimicrobial Peptides against Bacterial Biofilms. *Front Microbiol*. **8**, 2409 (2017).

315. J. R. Chambers, K. E. Cherny, K. Sauer, Susceptibility of Pseudomonas aeruginosa Dispersed Cells to Antimicrobial Agents Is Dependent on the Dispersion Cue and Class of the Antimicrobial Agent Used. *Antimicrob Agents Chemother*. **61** (2017), doi:10.1128/AAC.00846-17.

316. N. Barraud *et al.*, Involvement of nitric oxide in biofilm dispersal of Pseudomonas aeruginosa. *J Bacteriol*. **188**, 7344–7353 (2006).

317. H. X. Ong *et al.*, “Late-breaking abstract: Sweetening antibiotic treatment for eradication of bacterial biofilm” (European Respiratory Journal 44, European Respiratory Journal 44, 2014).

318. E. Banin, K. M. Brady, E. P. Greenberg, Chelator-induced dispersal and killing of Pseudomonas aeruginosa cells in a biofilm. *Appl Environ Microbiol*. **72**, 2064–2069 (2006).

319. C. N. H. Marques, A. Morozov, P. Planzos, H. M. Zelaya, The fatty acid signaling molecule cis-2-decenoic acid increases metabolic activity and reverts persister cells to an antimicrobial-susceptible state. *Appl Environ Microbiol*. **80**, 6976–6991 (2014).

320. K. R. Allison, M. P. Brynildsen, J. J. Collins, Metabolite-enabled eradication of bacterial persisters by aminoglycosides. *Nature*. **473**, 216–220 (2011).

321. T. K. Wood, Strategies for combating persister cell and biofilm infections. *Microb Biotechnol*. **10**, 1054–1056 (2017).

322. B. W. Kwan, N. Chowdhury, T. K. Wood, Combatting bacterial infections by killing persister cells with mitomycin C. *Environ Microbiol*. **17**, 4406–4414 (2015).

323. N. Chowdhury, T. L. Wood, M. Martínez-Vázquez, R. García-Contreras, T. K. Wood, DNA-crosslinker cisplatin eradicates bacterial persister cells. *Biotechnol Bioeng*. **113**, 1984–1992 (2016).

324. N. Barraud, A. Buson, W. Jarolimek, S. A. Rice, Mannitol enhances antibiotic sensitivity of persister bacteria in Pseudomonas aeruginosa biofilms. *PLoS ONE*. **8**, e84220 (2013).

325. H. X. Ong *et al.*, The effects of mannitol on the transport of ciprofloxacin across respiratory epithelia. *Mol Pharm*. **10**, 2915–2924 (2013).

326. A. Jaques *et al.*, Inhaled mannitol improves lung function in cystic fibrosis. *Chest*. **133**, 1388–1396 (2008).

327. Inhalation of dry-powder mannitol increases mucociliary... - Google Scholar, (available at https://scholar-google-com-au.ezproxy.lib.uts.edu.au/scholar?hl=it&as_sdt=0%2C5&q=Inhalation+of+dry-powder+mannitol+increases+mucociliary+clearance&btnG=).

328. C.-Y. Loo *et al.*, Sweetening inhaled antibiotic treatment for eradication of

chronic respiratory biofilm infection. *Pharm Res*. **35**, 50 (2018).

329. D. C. Cipolla, I. Gonda, Formulation technology to repurpose drugs for inhalation delivery. *Drug Discovery Today: Therapeutic Strategies*. **8**, 123–130 (2011).

330. M. Damm, G. Quante, M. Jungehuelsing, E. Stennert, Impact of functional endoscopic sinus surgery on symptoms and quality of life in chronic rhinosinusitis. *Laryngoscope*. **112**, 310–315 (2002).

331. Outcome of endoscopic sinus surgery for chronic rhinosinusitis patients: a Canadian experience - ProQuest, (available at https://search-proquest-com.ezproxy.lib.uts.edu.au/docview/751170794/fulltextPDF/EE580E3BCA6042 7FPQ/1?accountid=17095).

332. B. M. Woodhouse, K. W. Cleveland, Nebulized antibiotics for the treatment of refractory bacterial chronic rhinosinusitis. *Ann Pharmacother*. **45**, 798–802 (2011).

333. M. Hoggard *et al.*, Chronic rhinosinusitis and the evolving understanding of microbial ecology in chronic inflammatory mucosal disease. *Clin Microbiol Rev*. **30**, 321–348 (2017).

334. J. M. Shin *et al.*, Antimicrobial nisin acts against saliva derived multi-species biofilms without cytotoxicity to human oral cells. *Front Microbiol*. **6**, 617 (2015).

335. S. Maher, S. McClean, Investigation of the cytotoxicity of eukaryotic and prokaryotic antimicrobial peptides in intestinal epithelial cells in vitro. *Biochem Pharmacol*. **71**, 1289–1298 (2006).

336. D. Begde *et al.*, Immunomodulatory efficacy of nisin--a bacterial lantibiotic peptide. *J Pept Sci*. **17**, 438–444 (2011).

337. M. De Kwaadsteniet, K. T. Doeschate, L. M. T. Dicks, Nisin F in the treatment of respiratory tract infections caused by Staphylococcus aureus. *Lett Appl Microbiol*. **48**, 65–70 (2009).

338. R. A. Vaucher, M. L. Teixeira, A. Brandelli, Investigation of the cytotoxicity of antimicrobial peptide P40 on eukaryotic cells. *Curr Microbiol*. **60**, 1–5 (2010).